ALMA MATER STUDIORUM
UNIVERSITÀ DI BOLOGNA

DOTTORATO DI RICERCA IN

SCIENZE E TECNOLOGIE DELLA SALUTE

Ciclo 36

Settore Concorsuale: 03/C2 - CHIMICA INDUSTRIALE

Settore Scientifico Disciplinare: CHIM/04 - CHIMICA INDUSTRIALE

FUNCTIONAL AND STRUCTURAL OPTIMISATION OF ELECTROSPUN SCAFFOLDS FOR THE REGENERATION OF LIGAMENTS AND TENDONS

Presentata da: Amirdhavarshini Padmanabhan

Coordinatore Dottorato

Igor Diemberger

Supervisore

Maria Letizia Focarete

Co-Supervisore

Luca Cristofolini

Giovanna Cenacchi

Esame finale anno 2024

Abstract

This Thesis is presented by the candidate Amirdhavarshini Padmanabhan during her Ph.D. program in Health and Technology at the University of Bologna, Italy. The experimental work discussed in the Thesis took place at the Department of Chemistry "Giacomo Ciamician" and the Department of Industrial Engineering at the University of Bologna in Italy.

Tendons and ligaments are the connective tissues that connect muscles to bones and provide stability and support to joints. Injuries to these tissues are widespread worldwide, affecting millions of people annually and accounting for 15% of all injuries. These injuries can range from sprains to severe tears and ruptures. Current standard treatments for these injuries often have limited repair and, for the most part, do not recover full function, resulting in symptoms such as chronic pain, instability and impaired function. To address these limitations, tissue engineering has emerged as a promising approach in tendon and ligament repair. Electrospinning is a promising and versatile technique to produce nanofibrous scaffolds that mimic the natural extracellular matrix and biomechanical properties of tendons and ligaments. The specific objective of this research work was to optimise the structure and function of electrospun scaffolds for tendon and ligament regeneration. Two critical areas of scaffold optimisation are examined in this research work: the effects of gamma-ray sterilisation on scaffold properties and a novel approach to gradually mineralise an electrospun hierarchical bundle scaffold for enthesis regeneration.

Gamma-ray radiations are one of the most suitable treatments to sterilise electrospun devices, but the amount of irradiation has to be carefully chosen to avoid polymeric nanofibers degradation and changes in biomaterial properties. The first study in the Thesis aimed to investigate the properties of electrospun nanofibrous bundles of poly (L-lactic acid) and collagen, after gamma-irradiation with different doses, to identify the most suitable range of radiations able to minimise their negative effects on the scaffolds' structure and mechanics, while granting effective sterilisation. The first study in the Thesis aimed to investigate the effects of gamma-irradiation on electrospun nanofibrous bundles of aligned nanofibers inspired by tendon/ligament fascicles which were irradiated at three different doses (5, 10, and 25 kGy). The effects of the irradiation were investigated by analysing the scaffold's morphology, physicochemical properties and mechanical properties. The second study in this Thesis was aimed at gradient mineralisation of the fascicle-inspired electrospun bundles for enthesis regeneration. An alternative soaking method was used to deposit minerals in a gradient fashion

to mimic the mineral gradient found in native entheses. Morphological, physicochemical and mechanical characterisation of these mineralised bundles showed that they were ideal candidates for repair of tendon and ligament enthesis.

The research findings contribute to understanding the physicochemical and mechanical properties of optimised scaffolds and discuss their implications in future directions by underlining the potential of optimised electrospun scaffolds in the repair and regeneration of tendon and ligament tissues, promising significant impact on healthcare and patient recovery.

TABLE OF CONTENTS

Chapter 1 Introduction

1.1. Overview of tendon and ligament: anatomy and function

1.1.1. Description of tendons and ligaments

Tendons are specialised connective tissues primarily designed to transmit forces from muscle to bone, facilitating movement.(1) Ligaments, similar in composition to tendons, have distinct structural features suited to stabilising joints.(2) While tendons and ligaments are predominantly composed by Type I collagen and have similar cellular components, their structural organisation and functional roles are distinct.(3) Tendons are designed for strength and efficient force transmission, whereas ligaments are structured for flexibility and joint stability.(3) This fundamental difference is reflected in their respective biomechanical properties and responses to injury and repair.(4) The differences in between a tendon and ligament are highlighted in Table 1.1, and Figure 1.1.

Table1.1. Differences in composition between a tendon and ligament

	Tendon	**Ligament**
Cell type	Tenocytes	Ligamentocytes
Extracellular matrix (ECM)	A complex network of proteoglycans (1-2%) and glycoproteins, including decorin, and fibromodulin interact with collagen fibres, contributing to the tendon's mechanical properties. Type I collagen (75-85%) is arranged in parallel bundles and elastin (0.25-5%) is arranged as a network of random coils. (5)	It contains more elastin (10-15%) than tendons, arranged as a network of random coils, providing joint movement, stability and elasticity. Type I collagen (70-80%) is arranged in a more irregular, woven pattern. (5)
Vascular and neural supply	Tendons have a limited blood supply, a factor in their slow healing process. The neural elements, primarily proprioceptive and nociceptive fibres, play a role in sensing tension and pain.(3)	Like tendons, ligaments have a relatively sparse blood supply, affecting their healing potential. Their neural supply is crucial for proprioception and joint position sense. (3)

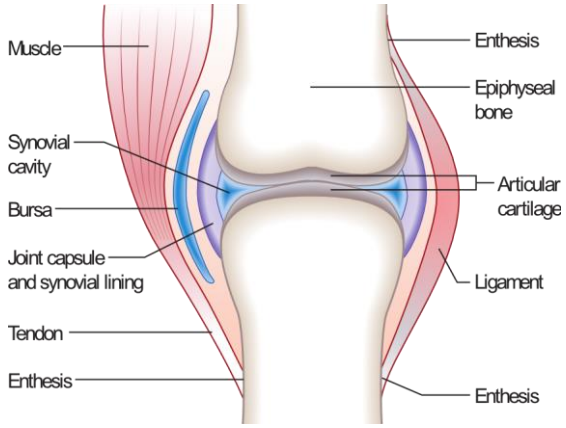

Figure 1.1 Difference between a tendon and a ligament (Adapted without modification from https://en.m.wikipedia.org/wiki/File:Joint.png)

1.1.2. Strength and flexibility

Tendons are known for their tensile strength due to their high collagen content, which is found parallelly arranged, allowing them to withstand the forces generated during muscle contraction. However, tendons also possess a degree of elasticity. This elasticity permits a certain amount of stretch, providing flexibility and the capacity to absorb shock and efficiently transfer muscular energy to the skeletal movement.(7) Ligaments are flexible and yielding to allow movement but become rigid when stressed above a physiological range. This rigidity is crucial for their primary role: stabilising joints by resisting excessive movement to prevent injuries. (8,9)

1.2. Tendon and ligament injuries

1.2.1. Acute injuries

Common injuries to tendons and ligaments are frequent concerns, especially among athletes and physically active individuals. These injuries usually result from overuse, direct injury, or ageing. Acute tendon injuries often result from a sudden, unexpected movement or impact. Examples include ruptures or tears, such as an Achilles tendon rupture often seen in sports. These injuries typically cause immediate swelling, pain, and a loss of function in the affected area.(10,11) Acute ligament injuries are commonly known as sprains. These occur due to a sudden twist or impact that overstretches or tears the ligament, like an ACL tear from a sudden change in direction. Symptoms include immediate pain, swelling, and instability in the joint.(12,13)

1.2.2. Chronic injuries

Chronic tendon injuries, or tendinopathies, develop over time due to repetitive stress and overuse. Common examples include tennis elbow or jumper's knee, which causes stiffness, pain, and weakness in the affected area, often worsening with continued activity.(14,15) Chronic ligament injuries often stem from repeated sprains or inadequate healing of an acute injury. This leads to joint instability, pain, and increased risk of further injury. An example is chronic ankle instability following repeated ankle sprains. (16,17)

1.3. Natural healing process

1.3.1. Intrinsic healing mechanisms: Cellular and molecular processes

The natural healing process of tendon and ligament injuries, both acute and chronic conditions, can be understood through a detailed examination of the intrinsic healing mechanisms and the cellular and molecular processes involved.

Acute Injuries

The initial response to acute tendon or ligament injury involves inflammation. This phase, lasting a few days, is characterised by migrating inflammatory cells, such as neutrophils and macrophages, to the injury site. These cells release cytokines and growth factors that initiate the healing process. Next is the proliferation phase, which involves the proliferation of tenocytes in tendons and fibroblasts in ligaments. The proliferation is stimulated by growth factors like TGF-β (Transforming Growth Factor Beta) and PDGF (Platelet-Derived Growth Factor). This phase is marked by the synthesis of collagen, primarily Type III, which is less organised and weaker than the Type I collagen found in uninjured tendons and ligaments. Over weeks to months, the Type III collagen is gradually replaced by Type I collagen. This remodeling is characterised by a realignment of collagen fibres along the lines of mechanical stress, thereby improving the strength and function of the tendon or ligament. The remodelling is regulated by a balance between matrix metalloproteinases (MMPs), which degrade collagen, and their inhibitors (TIMPs). (18–20)

Chronic injuries

Unlike acute injuries, chronic injuries do not follow the typical healing stages. An absence of inflammatory cells characterises them, and they are often considered a degenerative process

rather than an inflammatory one. There is an increase in the number of tenocytes or fibroblasts, which appear more rounded and less spindle-shaped, indicating a change in phenotype. This change affects the production of extracellular matrix (ECM). The ECM in chronic injuries shows an increased ratio of Type III to Type I collagen, leading to disorganised and mechanically weaker tissue. Additionally, there is an alteration in the balance of MMPs and TIMPs, leading to an abnormal matrix turnover. Chronic tendon injuries often exhibit increased neovascularisation and nerve ingrowth associated with pain in conditions like tendinopathy.

1.3.2. Limitations in natural regeneration

The natural healing process of tendon and ligament injuries, both acute and chronic conditions, also has some inherent limitations. Primarily, these tissues exhibit relatively poor vascularity, significantly obstructing the supply of essential nutrients and oxygen, thus prolonging the healing duration. In acute injuries, the initial inflammatory phase can be excessively protracted, leading to pain and swelling, complicating the healing trajectory. Chronic injuries, often evolving from untreated or recurrent acute trauma, are characterised by the formation of scar tissue, which lacks the original biomechanical properties of healthy tendons or ligament tissue. This can reduce flexibility and strength, increasing the susceptibility to re-injury. Furthermore, the regenerative capacity of these tissues is limited; thus, they often fail to fully regain their pre-injury structure and functionality, leading to persistent weakness and a heightened risk of degeneration.(21)

1.4. Current standard treatments

The current standard treatments for ligament and tendon injuries involve surgical and non-surgical approaches tailored according to the injury's severity, nature (acute or chronic), and specific location.(22) The commonly used approaches are discussed in Table 1.2.

Table 1.2. Surgical and non-surgical approaches to tendon and ligament reconstruction

Methods	Description	Efficacy	Limitation	Ref
NON-SURGICAL APPROACHES				
Rest, Ice, Compression, and Elevation (RICE)	This is often the initial treatment for acute injuries to reduce swelling and pain.	Effective for initial pain and swelling management.	Does not address underlying structural damage.	(23)

Physical Therapy	Rehabilitation exercises are crucial in restoring function, improving strength, and increasing range of motion.	Critical for restoring function and preventing stiffness, especially in enthesis injuries where mobility and strength need to be regained.	It is time-consuming and requires patient compliance; it may not be sufficient for severe injuries.	(24)
Bracing or Splinting	These devices provide support and stability to the injured area during healing.	It provides stability and prevents further injury.	Prolonged use can lead to muscle atrophy and limited effectiveness in treating internal damage.	(20)
Nonsteroidal Anti-Inflammatory Drugs (NSAIDs)	Used to manage pain and reduce inflammation.	Effective for short-term pain relief and inflammation reduction.	Long-term use can have side effects and does not promote tissue healing.	(25)
Corticosteroid Injections	They may be used in cases of severe inflammation, although their long-term use is controversial due to potential tissue weakening.	Quick relief from inflammation and pain.	Potential weakening of the tissue; not recommended for long-term management, especially near the enthesis, due to the risk of further degeneration.	(26)
Extracorporeal Shock Wave Therapy (ESWT)	They are utilised in some chronic tendinopathies like tennis elbow or plantar fasciitis.	Beneficial in chronic tendinopathy by stimulating healing.	Mixed results in efficacy; not universally accepted as a standard treatment.	(27)
Platelet-Rich Plasma (PRP) Injections	This involves injecting a concentrated form of the patient's own platelets to induce healing of injured tendons, ligaments, muscles, and joints.	Potential to enhance healing, especially in enthesis-related injuries.	Lack of standardised protocols; research on long-term efficacy is still ongoing.	(28)
SURGICAL APPROACHES				
Tendon Repair Surgery	Directly repairs the torn tendon; can be open surgery or minimally invasive.	Directly addresses the structural damage; essential for severe tears.	Requires prolonged recovery time; risk of complications; re-tear rates can be significant, especially in enthesis areas where reattachment is complex.	(29)
Ligament Reconstruction	Commonly used for significant injuries such as anterior	Effective for restoring stability, particularly	Graft failure, surgical risks, extensive rehabilitation.	(30)

	cruciate ligament (ACL) tears. This involves replacing the torn ligament with a graft.	in joints with enthesis involvement.		
Arthroscopic Surgery	A minimally invasive technique often used for joint-related tendon and ligament issues.	Less invasive, quicker recovery than open surgery.	Limited to certain types of injuries; may not be suitable for complex enthesis repairs.	(31)
Tenotomy	Involves surgical release of the tendon in chronic tendinopathy resistant to other treatments.	Can provide relief in chronic tendinopathy.	Alters the original anatomy; may lead to weakness.	(32)
Debridement	Surgical removal of damaged tissue to promote healing.	Effective in removing damaged tissue, promoting healing.	Does not address underlying causes of degeneration, particularly in enthesis areas.	(33)

1.5. Challenges in enthesis repair

1.5.1. Importance in tendon and ligament attachment

The enthesis is crucial in attaching tendons and ligaments to bone, representing a critical biomechanical interface in the musculoskeletal system. The primary function of the enthesis is to efficiently transmit mechanical loads from the soft, deformable issues of tendons and ligaments to the rigid structure of the bone. This transmission is essential for movement and the maintenance of joint stability. The enthesis is proficient at distributing mechanical stress over a broad area. This stress distribution is crucial to prevent concentration at a single point, which could lead to injury or tissue degeneration. (34) The enthesis absorbs and dissipates energy, particularly during dynamic activities, thereby protecting the tendon and ligament fibres from damage due to sudden or excessive forces.(35) It provides a seamless structural transition from the compliant tendon/ligament to the stiff bone, accommodating different biomechanical properties and ensuring smooth movement. The enthesis is designed to withstand repetitive mechanical loading, protecting the tendon and ligament from wear and tear.(36,37)

1.5.2. Difficulties in natural and surgical repair

Repairing the enthesis, both natural healing and surgical interventions is markedly challenging due to its distinct anatomical and functional attributes. Characterised by limited blood supply, the enthesis struggles to receive essential nutrients and cells, often culminating in sustained and incomplete healing. This zone, bridging soft tendon/ligament tissues with hard bone, undergoes a specific transition in cell types and extracellular matrix composition, complicating natural regeneration. Furthermore, the enthesis is subject to constant mechanical stress, predisposing it to disruptive healing processes and subsequent scar tissue formation, which lacks the specialised features of the native enthesis, diminishing functionality and heightening re-injury risk. Exacerbating these challenges, the inflammatory response post-injury can be excessive, potentially escalating damage and leading to chronic conditions like tendinopathy or enthesopathy.(38)

From a surgical perspective, mimicking the enthesis's intricate structure and composition presents significant obstacles. The gradient transition from soft to hard tissues is difficult to replicate, frequently resulting in suboptimal biomechanical properties. Maintaining the structural integrity of the repaired enthesis and adjacent tissues is complex, especially given their susceptibility to weakening from injury or degeneration. Moreover, surgical repair may induce uneven stress distribution, risking complications such as bone erosion or re-tear of the tendon/ligament. The formation of adhesions, a standard postoperative occurrence, can impede joint mobility and cause discomfort. Postoperative rehabilitation demands a meticulous approach; premature or excessive loading of the repaired enthesis can lead to repair failure, while insufficient loading may impair tissue quality. Additionally, while promising, emerging regenerative medicine techniques like stem cell therapy or tissue engineering currently face significant hurdles in effectively restoring the original structure and function of the enthesis.(39)

1.6. Role of tendon and ligament tissue engineering

The field of tissue engineering has gained traction over recent decades, driven by advancements in biomaterials, stem cell biology, and bioreactor technologies. This interdisciplinary approach addresses the inherent limitations of natural healing and conventional surgical methods, particularly in repairing complex structures like the enthesis.(40) Tissue engineering

endeavours to regenerate tissues that closely mimic the native structure and function of tendons and ligaments, thereby overcoming the challenges of poor vascularity, scar tissue formation, and inadequate mechanical strength often accompanying traditional treatments. This necessity also stems from several clinical demands.(41) Firstly, the increasing incidence of musculoskeletal injuries necessitates more effective and reliable treatment modalities. Secondly, the growing expectations of patients, especially athletes, for complete functional recovery and rapid return to pre-injury activity levels underscore the need for advanced therapeutic options. Thirdly, the high re-injury rate and long-term complications associated with current treatments highlight the need for innovative solutions that offer more durable and resilient repairs. By harnessing the advances in biomaterials, cellular therapies, and bioengineering, tissue engineering promises to provide solutions that are more anatomically and functionally congruent with the original tissue and tailored to the specific needs and conditions of individual patients.(42)

1.7. Approaches in tendon and ligament tissue engineering

1.7.1. Biomaterials and scaffold design

A pivotal focus in tendon and ligament tissue engineering is developing biomaterials and scaffold designs. These scaffolds serve as three-dimensional structures that support cell attachment, proliferation, and differentiation, crucial for tissue regeneration. Biomaterials used in scaffold fabrication are selected for their biocompatibility, biodegradability, biomechanical properties, and ability to mimic the extracellular matrix of native tendons and ligaments.(43) They range from natural polymers like collagen and silk to synthetic polymers such as polylactic acid (PLA) and polyglycolic acid (PGA) Some examples of the most used biomaterials are given in Table 1.3. The design of these scaffolds is intricately tailored to replicate the unique hierarchical structure of tendons and ligaments, ensuring appropriate mechanical strength and elasticity. Advanced techniques like electrospinning and 3D bioprinting are employed to create scaffolds with precise microarchitecture and porosity, facilitating vascularisation and integration with host tissue. The strategic combination of these biomaterials and scaffold designs is essential in creating an optimal environment for tendon and ligament regeneration, ultimately enhancing the efficacy of tissue-engineered repairs.(44)

Table 1.3. Biomaterials used for electrospinning in ligament and tendon tissue engineering

Origin	**Biomaterials**	**References**
Natural	Collagen	(45)
	Gelatin	(46)
	Silk	(47)
	Chitosan	(46)
	Alginate	(48)
Synthetic	Polycaprolactone (PCL)	(49)
	Polyglycolic acid (PGA)	(50)
	Polylactic acid (PLA)	(51)
	Polyurethane (PU)	(52)

1.7.2. Cell-based and cell-free strategies

In tendon and ligament tissue engineering, two primary approaches are employed: cell-based and cell-free strategies. Some differences between the two approaches have been discussed in Table 1.4.

Table 1.4. Comparison of cell-based and cell-free strategies for application in tendon and ligament tissue engineering.

	Cell-based strategies (53)	**Cell-free strategies(54)**
Core component	Living cells (e.g., Mesenchymal Stem Cells)	Acellular scaffolds and bioactive molecules
Source of Cells/Materials	Stem cells derived from bone marrow, adipose tissue, or tendons/ligaments	Scaffolds made from natural or synthetic materials
Mechanism	Cells differentiate into tendon/ligament cells and produce extracellular matrix	Scaffold provides support and releases growth factors to stimulate healing
Integration with Host Tissue	High, as living cells can integrate and grow with host tissue	Dependent on the body's response to the scaffold and its bioactive cues

Complexity	Higher due to the need for cell harvesting, culturing, and differentiation	Lower, as it eliminates the need for cell manipulation
Immune Response	Potential for immune rejection or complications	Reduced risk of immune reaction as no foreign cells are introduced
Application in Healing	Aims for regeneration of living, functional tissue	Focuses on stimulating the body's healing processes
Challenges	Ensuring cell survival, integration, and proper differentiation	Providing effective recruitment and activation of host cells
Clinical Feasibility	More complex and might require more advanced clinical settings	Potentially more immediately applicable in clinical settings

1.8. Electrospinning for tendon and ligament scaffold fabrication

Electrospinning is a versatile and efficient technique for fabricating nanofibres, widely employed in tissue engineering, including developing scaffolds for tendon and ligament repair. The fundamental principle of electrospinning involves applying a high-voltage electric field to a polymer solution or melt. When the electric force overcomes the surface tension of the polymer solution, a charged jet of the material is ejected from the tip of a needle. As this jet travels towards a grounded collector, it undergoes a process of elongation and solvent evaporation or cooling, resulting in the formation of continuous, ultrafine fibres. These fibres are collected as a non-woven mat with a high surface area-to-volume ratio and porosity, characteristics that are beneficial for cell attachment and proliferation (Fig 1.2). The process parameters, including polymer concentration, voltage, flow rate, and the distance between the needle and the collector, can be finely tuned to control the fibre diameter, alignment, and the overall architecture of the scaffold. This level of control makes electrospinning a highly adaptable technique for creating scaffolds that mimic the native extracellular matrix structure of tendons and ligaments, enhancing their potential for successful integration and regeneration in tissue engineering applications.55,56) Electrospinning offers several distinct advantages in ligament and tendon tissue engineering. One of its primary benefits is the ability to produce nanofibres, which closely mimic the nanoscale architecture of the native extracellular matrix

of tendons and ligaments.(57) This feature facilitates cell adhesion, proliferation, and differentiation, enhancing tissue integration and regeneration. Electrospun fibres' high surface area-to-volume ratio also provides an expansive platform for cell interaction and growth factor delivery, further promoting healing.(58) The versatility of electrospinning allows for incorporating various natural and synthetic polymers, enabling the creation of scaffolds tailored to specific biomechanical and biochemical properties. This adaptability extends to the control over fibre alignment, density, and porosity, which can be optimised to replicate the unique structural characteristics of tendons and ligaments.(59) Furthermore, electrospinning can be combined with other techniques, such as coating with bioactive substances or integration with other biomaterials, to enhance scaffold functionality. These advantages position electrospinning as a potent tool in developing advanced scaffolds for tendon and ligament tissue engineering, offering the potential for improved therapeutic outcomes.(43)

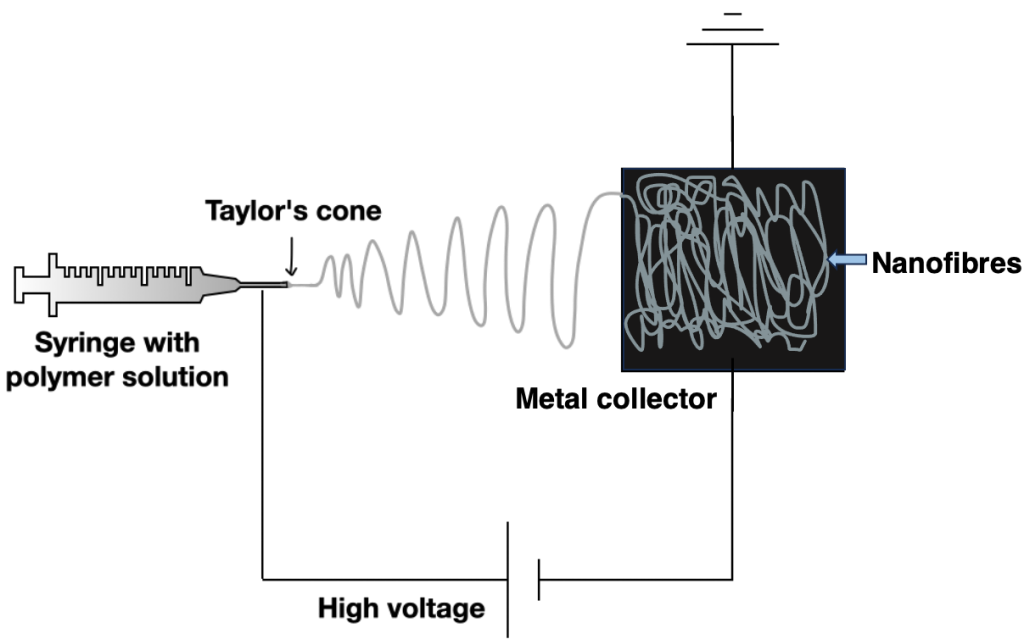

Figure 1.2. Mechanism of electrospinning

1.9. Optimisation of electrospun scaffolds for tendon and ligament regeneration

The optimisation of electrospun scaffolds in tendon and ligament tissue engineering is paramount, as it directly influences the efficacy of tissue regeneration and repair. The types of optimisations can be divided into several sections such as structural (60) (fibre alignment and

diameter, porosity and pore size and material composition), functional (61) (bioactive signalling, gradient mineralisation and mechanical properties), biochemical (62) (surface chemistry and degradation rate), biocompatibility (63) (immunogenicity) and lastly manufacturing optimisation (64) (scalability and reproducibility).

1.9.1. Significance of sterilisation for tendon and ligament tissue engineering

Sterilisation is a fundamental step that significantly impacts the scaffold's transition into clinical use.(65) By effectively eliminating potential microbial contaminants, sterilisation ensures the scaffold meets stringent clinical safety standards, a prerequisite for any medical device or implant. This process must be carefully balanced to maintain the material's structural and functional integrity, ensuring the scaffold retains its desired properties post-sterilisation.(66) Successful sterilisation addresses regulatory and safety concerns and builds clinical trust in the scaffold's use, a crucial aspect when transitioning from laboratory development to patient application. The choice of sterilisation method is essential as it not only ensures the elimination of potential microbial contamination but also significantly influences the physical and biochemical properties of the scaffold. (67)

1.9.2. Significance of mineralisation for tendon and ligament tissue engineering

The significance of mineralisation in tendon and ligament tissue engineering lies in its ability to enhance the bio-functionality and integration of scaffolds, especially for repairing the enthesis, where soft tissue connects to bone. This process plays a crucial role in mimicking the natural transitional zone between tendon/ligament and bone, a critical aspect in the regeneration of these tissues.(68) Mineralisation introduces minerals, such as calcium phosphate compounds, into the scaffold. These minerals are critical components of bone tissue, and their presence in the scaffold helps replicate the bone-like properties necessary for enthesis regeneration. Mineralised scaffolds often exhibit increased biocompatibility and bioactivity. They provide an environment conducive to cell adhesion, proliferation, and differentiation, essential for the successful regeneration of tendon and ligament tissues.(69) The mineral component of the scaffold can enhance its mechanical strength, making it more resilient to the stresses and strains it will encounter in the body. This is particularly important in load-bearing areas where tendons and ligaments operate.(70) Mineralisation is crucial in facilitating the integration of the scaffold with the surrounding bone tissue. This osteointegration is vital for the stability and functionality of the repair, especially at the enthesis. By creating a gradient of

mineralisation, scaffolds can guide tissue regeneration from soft (tendon/ligament) to hard (bone), reflecting the natural enthesis structure.(71) This gradient supports the sequential and organised regeneration of different tissue types. Mineralised scaffolds can stimulate specific cellular responses that are essential for tendon-to-bone healing. For instance, they can promote the activity of osteoblasts (bone-forming cells) at the bone interface while supporting tenocytes (tendon cells) in the soft tissue region.(72)

Together, sterilisation and mineralisation optimisations address two critical aspects of scaffold development: safety and functionality. These optimisations help prevent infection upon implantation and improve the scaffold's ability to support the specific requirements of tendon and ligament regeneration. They address vital clinical concerns and regulatory requirements, paving the way for the scaffold's transition from laboratory innovation to a clinically applicable tool in regenerative medicine, offering new therapeutic avenues for patients suffering from tendon and ligament injuries.

1.10. Objective of thesis

The primary objective of this thesis, "Functional and structural optimisation of electrospun scaffolds for the regeneration of ligaments and tendons" is to develop and refine electrospun scaffold technologies that are specifically tailored for the regeneration of tendon and ligament tissues. This involves two key areas of focus: firstly, sterilisation of the scaffolds to ensure that they are biocompatible and free from microbial contamination without compromising their structural and functional integrity; secondly, implementing gradient mineralisation within the scaffolds to closely mimic the natural enthesis interface closely, thereby enhancing their functionality in enthesis regeneration. Through a combination of experimental and analytical methods, the thesis aims to bridge the gap between laboratory research and clinical application, providing a detailed understanding of how these optimisations can improve scaffold performance and efficacy in regenerative medicine. This research endeavours to contribute significantly to the field of tissue engineering, offering innovative solutions for tendon and ligament injuries, which are prevalent in both athletic and general populations.

1.11. Overview of Thesis chapters

Chapter 1 - This chapter provides an overview of tendon and ligament injuries and the role of tissue engineering in treating them. It outlines the thesis's aims, focusing on the significance of advanced scaffold technologies in regenerative medicine and the expected contributions of this research.

Chapter 2 - Focusing on gamma-ray sterilisation, this chapter reviews its impact on PLLA/Collagen electrospun bundle scaffolds. It presents experimental data to analyse how gamma-ray sterilisation affects scaffold morphology, physicochemical properties, mechanical properties.

Chapter 3 - This chapter explores the advanced in methods and significance of mineralising scaffolds in tissue engineering. It examines various mineralisation methods and their effects on scaffold functionality, the different scaffold modifications that can induce mineralisation and their characterisation techniques.

Chapter 4 - This chapter discusses the gradient mineralisation of PLLA/Collagen electrospun bundle scaffolds to mimic the enthesis. It details the methodology and the gradient mineralisation process and its implications for the scaffolds' properties.

1.12. References

1. Kannus P. Structure of the tendon connective tissue. Scandinavian Journal of Medicine & Science in Sports. 2000;10(6):312–20.

2. Frank CB. Ligament structure, physiology and function. Journal of musculoskeletal & neuronal interactions. 2004;4(2):199-201.

3. Benjamin M, Ralphs JR. Tendons and ligaments--an overview. Histol Histopathol. 1997 Oct;12(4):1135–44.

4. Amiel D, Frank CB, Harwood FL, Fronek J, Akeson WH. Tendons and Ligaments: A Morphological and Biochemical Comparison. Journal of Orthopaedic Research®. 1983;1(3):257-265

5. Goh KL, Listrat A, Bechet D. Hierarchical Mechanics of Connective Tissues: Integrating Insights from Nano to Macroscopic Studies. Journal of biomedical nanotechnology. 2014 Oct 1;10:2464–507.

6. Birch HL. Tendon matrix composition and turnover in relation to functional requirements. International Journal of Experimental Pathology. 2007;88(4):241–8.

7. Winnicki K, Ochała-Kłos A, Rutowicz B, Pękala PA, Tomaszewski KA. Functional anatomy, histology and biomechanics of the human Achilles tendon — A comprehensive review. Annals of Anatomy - Anatomischer Anzeiger. 2020 May 1;229:151461.

8. Dienst M, Burks RT, Greis PE. Anatomy and biomechanics of the anterior cruciate ligament. Orthopedic Clinics of North America. 2002 Oct 1;33(4):605–20.

9. Viidik A. Elasticity and Tensile Strength of the Anterior Cruciate Ligament in Rabbits as Influenced by Training. Acta Physiologica Scandinavica. 1968;74(3):372-380.

10. Snedeker JG, Foolen J. Tendon injury and repair – A perspective on the basic mechanisms of tendon disease and future clinical therapy. Acta Biomaterialia. 2017 Nov 1;63:18–36.

11. Mahieu N, Witvrouw E, Stevens V, Tiggelen DV, Roget P. Intrinsic Risk Factors for the Development of Achilles Tendon Overuse Injury. The American Journal of Sports Medicine. 2006;34(2):226-235.

12. Quatman CE, Quatman-Yates CC, Hewett TE. A 'Plane' Explanation of Anterior Cruciate Ligament Injury Mechanisms. Sports Med. 2010 Sep 1;40(9):729–46.

13. Renström PA, Konradsen L. Ankle ligament injuries. Br J Sports Med. 1997 Mar;31(1):11–20.

14. Järvinen M, Józsa L, Kannus P, Järvinen TLN, Kvist M, Leadbetter W. Histopathological findings in chronic tendon disorders. Scandinavian Journal of Medicine & Science in Sports. 1997;7(2):86–95.

15. Thomopoulos S, Parks WC, Rifkin DB, Derwin KA. Mechanisms of tendon injury and repair. Journal of Orthopaedic Research. 2015;33(6):832–9.

16. Al-Mohrej OA, Al-Kenani NS. Chronic ankle instability: Current perspectives. Avicenna J Med. 2016;6(4):103–8.

17. Bonnel F, Toullec E, Mabit C, Tourné Y. Chronic ankle instability: Biomechanics and pathomechanics of ligaments injury and associated lesions. Orthopaedics & Traumatology: Surgery & Research. 2010 Jun 1;96(4):424–32.

18. Frank C, Schachar N, Dittrich D. Natural history of healing in the repaired medial collateral ligament. Journal of Orthopaedic Research. 1983;1(2):179–88.

19. Józsa L, Kannus P. Histopathological findings in spontaneous tendon ruptures. Scandinavian Journal of Medicine & Science in Sports. 1997;7(2):113–8.

20. Trevino SG, Davis P, Hecht PJ. Management of Acute and Chronic Lateral Ligament Injuries of the Ankle. Orthopedic Clinics of North America. 1994 Jan 1;25(1):1–16.

21. Li ZJ, Yang QQ, Zhou YL. Basic Research on Tendon Repair: Strategies, Evaluation, and Development. Frontiers in Medicine. 2021;8:664909.

22. Kane SF, Olewinski LH, Tamminga KS. Management of Chronic Tendon Injuries. afp. 2019 Aug 1;100(3):147–57.

23. van den Bekerom MPJ, Struijs PAA, Blankevoort L, Welling L, van Dijk CN, Kerkhoffs GMMJ. What Is the Evidence for Rest, Ice, Compression, and Elevation Therapy in the Treatment of Ankle Sprains in Adults? Journal of Athletic Training. 2012 Jul 1;47(4):435–43.

24. Culav EM, Clark CH, Merrilees MJ. Connective Tissues: Matrix Composition and Its Relevance to Physical Therapy. Physical Therapy. 1999 Mar 1;79(3):308–19.

25. Su B, O'Connor JP. NSAID therapy effects on healing of bone, tendon, and the enthesis. Journal of Applied Physiology. 2013 Sep 15;115(6):892–9.

26. Nichols AW. Complications Associated With the Use of Corticosteroids in the Treatment of Athletic Injuries. Clinical Journal of Sport Medicine. 2005 Sep;15(5):E370.

27. Bosch G, de MOS M, van BINSBERGEN R, van SCHIE HTM, van de LEST CHA, van WEEREN PR. The effect of focused extracorporeal shock wave therapy on collagen matrix and gene expression in normal tendons and ligaments. Equine Veterinary Journal. 2009;41(4):335–41.

28. Taylor DW, Petrera M, Hendry M, Theodoropoulos JS. A Systematic Review of the Use of Platelet-Rich Plasma in Sports Medicine as a New Treatment for Tendon and Ligament Injuries. Clinical Journal of Sport Medicine. 2011 Jul;21(4):344.

29. Robertson A, Nutton RW, Keating JF. Current trends in the use of tendon allografts in orthopaedic surgery. The Journal of Bone & Joint Surgery British Volume. 2006 Aug 1;88-B(8):988–92.

30. Yang G, Rothrauff BB, Tuan RS. Tendon and Ligament Regeneration and Repair: Clinical Relevance and Developmental Paradigm. Birth Defects Res C Embryo Today. 2013 Sep;99(3):203–22.

31. Corry IS, Webb JM, Clingeleffer AJ, Pinczewski LA. Arthroscopic Reconstruction of the Anterior Cruciate Ligament. Am J Sports Med. 1999 Jul 1;27(4):444–54.

32. Zancolli EA. THE TRAPEZIOMETACARPAL JOINT: Tenotomy of the Accessory Tendons in Early Osteoarthritis. Hand Clinics. 2001 Feb 1;17(1):13–43.

33. Gohil S, Annear PO, Breidahl W. Anterior cruciate ligament reconstruction using autologous double hamstrings: a comparison of standard versus minimal debridement techniques using MRI to assess revascularisation: A RANDOMISED PROSPECTIVE STUDY WITH A ONE-YEAR FOLLOW-UP. The Journal of Bone & Joint Surgery British Volume. 2007 Sep 1;89-B(9):1165–71.

34. Apostolakos J, Durant TJ, Dwyer CR, Russell RP, Weinreb JH, Alaee F, et al. The enthesis: a review of the tendon-to-bone insertion. Muscles Ligaments Tendons J. 2014 Nov 17;4(3):333–42.

35. Derwin KA, Galatz LM, Ratcliffe A, Thomopoulos S. Enthesis Repair. J Bone Joint Surg Am. 2018 Aug 15;100(16):e109.

36. Benjamin M, Toumi H, Ralphs JR, Bydder G, Best TM, Milz S. Where tendons and ligaments meet bone: attachment sites ('entheses') in relation to exercise and/or mechanical load. Journal of Anatomy. 2006;208(4):471–90.

37. Leong NL, Kator JL, Clemens TL, James A, Enomoto-Iwamoto M, Jiang J. Tendon and Ligament Healing and Current Approaches to Tendon and Ligament Regeneration. J Orthop Res. 2020 Jan;38(1):7–12.

38. Thomopoulos S, Genin GM, Galatz LM. The development and morphogenesis of the tendon-to-bone insertion What development can teach us about healing. J Musculoskelet Neuronal Interact. 2010 Mar;10(1):35–45.

39. Bunker DLJ, Ilie V, Ilie V, Nicklin S. Tendon to bone healing and its implications for surgery. Muscles Ligaments Tendons J. 2014 Nov 17;4(3):343–50.

40. Rodrigues MT, Reis RL, Gomes ME. Engineering tendon and ligament tissues: present developments towards successful clinical products. Journal of Tissue Engineering and Regenerative Medicine. 2013;7(9):673–86.

41. Goh JCH, Ouyang HW, Teoh SH, Chan CKC, Lee EH. Tissue-Engineering Approach to the Repair and Regeneration of Tendons and Ligaments. Tissue Engineering. 2003 Aug 30;9(supplement 1):31–44.

42. Smith L, Xia Y, Galatz LM, Genin GM, Thomopoulos S. Tissue-Engineering Strategies for the Tendon/Ligament-to-Bone Insertion. Connective Tissue Research. 2012 Apr 1;53(2):95–105.

43. Lim WL, Liau LL, Ng MH, Chowdhury SR, Law JX. Current Progress in Tendon and Ligament Tissue Engineering. Tissue Eng Regen Med. 2019 Jun 26;16(6):549–71.

44. Kuo CK, Marturano JE, Tuan RS. Novel strategies in tendon and ligament tissue engineering: Advanced biomaterials and regeneration motifs. BMC Sports Sci Med Rehabil. 2010 Dec;2(1):1–14.

45. Xu Y, Wu J, Wang H, Li H, Di N, Song L, et al. Fabrication of Electrospun Poly(L-Lactide-co-ε-Caprolactone)/Collagen Nanoyarn Network as a Novel, Three-Dimensional, Macroporous, Aligned Scaffold for Tendon Tissue Engineering. Tissue Eng Part C Methods. 2013 Dec;19(12):925–36.

46. Zhang C, Yuan H, Liu H, Chen X, Lu P, Zhu T, et al. Well-aligned chitosan-based ultrafine fibers committed teno-lineage differentiation of human induced pluripotent stem cells for Achilles tendon regeneration. Biomaterials. 2015 Jun 1;53:716–30.

47. Yang C, Deng G, Chen W, Ye X, Mo X. A novel electrospun-aligned nanoyarn-reinforced nanofibrous scaffold for tendon tissue engineering. Colloids and Surfaces B: Biointerfaces. 2014 Oct 1;122:270–6.

48. Lee JY, Chung J, Chung WJ, Kim G. Fabrication and in vitro biocompatibilities of fibrous biocomposites consisting of PCL and M13 bacteriophage-conjugated alginate for bone tissue engineering. J Mater Chem B. 2016 Jan 20;4(4):656–65.

49. Rothrauff BB, Lauro BB, Yang G, Debski RE, Musahl V, Tuan RS. Braided and Stacked Electrospun Nanofibrous Scaffolds for Tendon and Ligament Tissue Engineering. Tissue Eng Part A. 2017 May 1;23(9–10):378–89.

50. Sahoo S, Toh SL, Goh JCH. A bFGF-releasing silk/PLGA-based biohybrid scaffold for ligament/tendon tissue engineering using mesenchymal progenitor cells. Biomaterials. 2010 Apr 1;31(11):2990–8.

51. Sensini A, Gualandi C, Zucchelli A, Boyle LA, Kao AP, Reilly GC, et al. Tendon Fascicle-Inspired Nanofibrous Scaffold of Polylactic acid/Collagen with Enhanced 3D-Structure and Biomechanical Properties. Sci Rep. 2018 Nov 21;8(1):17167.

52. Sharifi-Aghdam M, Faridi-Majidi R, Derakhshan MA, Chegeni A, Azami M. Preparation of collagen/polyurethane/knitted silk as a composite scaffold for tendon tissue engineering. Proc Inst Mech Eng H. 2017 Jul 1;231(7):652–62.

53. Gaspar D, Spanoudes K, Holladay C, Pandit A, Zeugolis D. Progress in cell-based therapies for tendon repair. Advanced Drug Delivery Reviews. 2015 Apr 1;84:240–56.

54. Tamayol A, Akbari M, Annabi N, Paul A, Khademhosseini A, Juncker D. Fiber-based tissue engineering: Progress, challenges, and opportunities. Biotechnology Advances. 2013 Sep 1;31(5):669–87.

55. Xie X, Chen Y, Wang X, Xu X, Shen Y, Khan A ur R, et al. Electrospinning nanofiber scaffolds for soft and hard tissue regeneration. Journal of Materials Science & Technology. 2020 Dec 15;59:243–61.

56. Xue J, Wu T, Dai Y, Xia Y. Electrospinning and Electrospun Nanofibers: Methods, Materials, and Applications. Chem Rev. 2019 Apr 24;119(8):5298–415.

57. Sensini A, Cristofolini L. Biofabrication of Electrospun Scaffolds for the Regeneration of Tendons and Ligaments. Materials. 2018 Oct;11(10):1963.

58. Sensini A, Massafra G, Gotti C, Zucchelli A, Cristofolini L. Tissue Engineering for the Insertions of Tendons and Ligaments: An Overview of Electrospun Biomaterials and Structures. Front Bioeng Biotechnol. 2021 Mar 2;9:645544.

59. Cardwell RD, Dahlgren LA, Goldstein AS. Electrospun fibre diameter, not alignment, affects mesenchymal stem cell differentiation into the tendon/ligament lineage. Journal of Tissue Engineering and Regenerative Medicine. 2014;8(12):937–45.

60. Heidari M, Bahrami H, Ranjbar-Mohammadi M. Fabrication, optimization and characterization of electrospun poly(caprolactone)/gelatin/graphene nanofibrous mats. Materials Science and Engineering: C. 2017 Sep 1;78:218–29.

61. Meinel AJ, Kubow KE, Klotzsch E, Garcia-Fuentes M, Smith ML, Vogel V, et al. Optimization strategies for electrospun silk fibroin tissue engineering scaffolds. Biomaterials. 2009 Jun 1;30(17):3058–67.

62. McCullen SD, Stano KL, Stevens DR, Roberts WA, Monteiro-Riviere NA, Clarke LI, et al. Development, optimization, and characterization of electrospun poly(lactic acid) nanofibers containing multi-walled carbon nanotubes. Journal of Applied Polymer Science. 2007;105(3):1668–78.

63. Ji W, Yang F, Seyednejad H, Chen Z, Hennink WE, Anderson JM, et al. Biocompatibility and degradation characteristics of PLGA-based electrospun nanofibrous scaffolds with nanoapatite incorporation. Biomaterials. 2012 Oct 1;33(28):6604–14.

64. McCullen SD, Stevens DR, Roberts WA, Clarke LI, Bernacki SH, Gorga RE, et al. Characterization of electrospun nanocomposite scaffolds and biocompatibility with adipose-derived human mesenchymal stem cells. International Journal of Nanomedicine. 2007 Dec 1;2(2):253–63.

65. Rediguieri CF, Sassonia RC, Dua K, Kikuchi IS, de Jesus Andreoli Pinto T. Impact of sterilization methods on electrospun scaffolds for tissue engineering. European Polymer Journal. 2016 Sep 1;82:181–95.

66. Valente TAM, Silva DM, Gomes PS, Fernandes MH, Santos JD, Sencadas V. Effect of Sterilization Methods on Electrospun Poly(lactic acid) (PLA) Fiber Alignment for Biomedical Applications. ACS Appl Mater Interfaces. 2016 Feb 10;8(5):3241–9.

67. Bye FJ, Wang L, Bullock AJ, Blackwood KA, Ryan AJ, MacNeil S. Postproduction Processing of Electrospun Fibres for Tissue Engineering. J Vis Exp. 2012 Aug 9;(66):4172.

68. Chen J, Chu B, Hsiao BS. Mineralization of hydroxyapatite in electrospun nanofibrous poly(L-lactic acid) scaffolds. Journal of Biomedical Materials Research Part A. 2006;79A(2):307–17.

69. Zhao W, Li J, Jin K, Liu W, Qiu X, Li C. Fabrication of functional PLGA-based electrospun scaffolds and their applications in biomedical engineering. Materials Science and Engineering: C. 2016 Feb 1;59:1181–94.

70. Ranganathan S, Balagangadharan K, Selvamurugan N. Chitosan and gelatin-based electrospun fibers for bone tissue engineering. International Journal of Biological Macromolecules. 2019 Jul 15;133:354–64.

71. Zhu C, Qiu J, Thomopoulos S, Xia Y. Augmenting Tendon-to-Bone Repair with Functionally Graded Scaffolds. Advanced Healthcare Materials. 2021;10(9):2002269.

72. Di Martino A, Liverani L, Rainer A, Salvatore G, Trombetta M, Denaro V. Electrospun scaffolds for bone tissue engineering. Musculoskelet Surg. 2011 Aug 1;95(2):69–80.

Chapter 2 : Effects of Gamma-ray Sterilisation on Poly (L-lactic acid)/Collagen Electrospun Nanofibrous Bundles for Application in Tendon and Ligament Tissue Engineering

Amirdhavarshini Padmanabhan[a], Alberto Sensini[b], Chiara Gualandi[a], Serafina Pacilio[c,d], Roberta Costa[c,d], Giovanna Cenacchi[c,d], Maria Letizia Focarete[a], Luca Cristofolini[b]

[a]Department of Chemistry, "G.Ciamician", University of Bologna, Italy
[b]Department of Industrial Engineering, University of Bologna, Italy
[c]Department of Neuromotor and Biomedical Sciences, University of Bologna, Italy
[d]Centro di Ricerca Biomedica Applicata, University of Bologna, Italy

Keywords: Poly (L-lactic acid)/Collagen blend; Electrospinning; Tendon and Ligament scaffold; Gamma radiation; Sterilisation;

MANUSCRIPT IN PREPARATION

Graphical Abstract

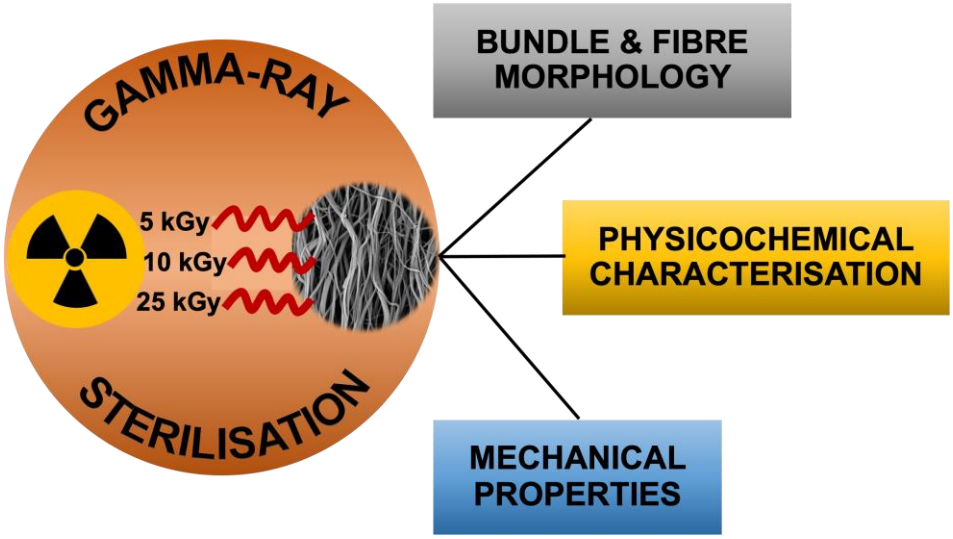

2.1. Abstract

Tendon and ligament tissue engineering require dedicated scaffolds replicating their natural fibrous structure and mechanics of these tissues. Electrospinning is one of the best technologies to produce biomimetic and hierarchical nanofibrous structures for these applications. Before being implanted, electrospun scaffolds must ensure optimal sterility without compromising their structure and mechanical properties. Gamma-ray radiation is one of the most suitable treatments to sterilise electrospun devices, but dosage must be carefully chosen to avoid compromising their structure and mechanical properties. This study investigates the properties of electrospun nanofibrous bundles of poly (L-lactic acid) and collagen blends after gamma-irradiation at different doses (ranging from 5 kGy to 25 kGy) to identify the optimal sterilization condition to minimise negative effects on the scaffolds' structure and mechanical properties while granting effective sterilisation. Bundles of aligned nanofibres were fabricated by electrospinning and crosslinked with N-(3-dimethylaminopropyl)-N′-ethylcarbodiimide hydrochloride (EDC) and N-hydroxysuccinimide (NHS). The scaffolds were then divided into three groups, which were gamma-sterilised at three different doses (5, 10, and 25 kGy). The morphology, thermal, and mechanical properties of the bundles before and after sterilisation were investigated. A smaller decrement in fibres' axial alignment was found for the treatment with 5kGy (-3.1%) and 10kGy (-2.4%) compared to the 25kGy (-11%) one. Thermal analysis revealed that gamma irradiation does not significantly influence the thermal stability of the samples; however, it does enhance the cold crystallisation ability of poly(L-lactic acid) in a dose-dependent manner. This result was attributed to a possible degradation of collagen structure by gamma radiation. Decreasing collagen crosslinking density might induce higher mobility of poly(L-lactic) chains, thus facilitating the cold crystallisation process. The mechanical investigations (tensile tests) demonstrated that the tensile strength of the irradiated bundles is slightly reduced in a dose-dependent manner as compared to the non-irradiated ones. The mechanical properties of the bundles irradiated at 5 kGy were closer to the non-irradiated bundles than the bundles irradiated at 10 kGy and 25 kGy.

2.2.Introduction

In recent years, various scaffolds have been developed to enhance tendon/ligament (T/L) regeneration (1,2). Among the different fabrication techniques explored, electrospinning is undoubtedly one of the most promising (3). Electrospun scaffolds can morphologically and mechanically mimic the entire hierarchical structure of T/L tissue, ranging from the nanoscale to the macroscale (4–8). Several polymers have been electrospun to enhance T/L regeneration, either as plain materials or blended with natural polymers such as the collagen type I (9,10). More recently, promising scaffolds made of poly (L-lactic acid) and collagen blends were developed through electrospinning, resembling the hierarchical structure of T/L in a multiscale fashion (11,10). Poly (L-lactic acid), a synthetic semicrystalline polymer, is known for its wide range of applications in tissue engineering due to its mechanical properties, bioresorbability, and biocompatibility (12). Meanwhile, the inherent properties of biological recognition in collagen are exploited to enhance cell adhesiveness.

Effective sterilisation is crucial in manufacturing scaffolds for implants to create a microbial-free microenvironment, promoting accelerated recovery without infections or rejection upon implantation. Hence, medically approved sterility methods should be considered during scaffold development, especially given clinical translation and future commercialisation. The choice of the proper sterilisation procedure is a critical aspect of polymeric materials, as it depends on their chemical and physical properties (13). Synthetic biocompatible polyesters, such as poly(L-lactic acid), are heat and humidity-sensitive polymers, and commonly used sterilisation protocols involving heat and steam are not suitable, as they may cause hydrolysis and degradation of the polymer, impairing its mechanical properties (13). In particular, in the case of bioresorbable electrospun nanofibres, finding a proper technique that can successfully sterilise the material while preserving its morphology and mechanical and functional properties is even more critical (14). A limited number of studies are available on the effect of the sterilisation protocol on the final electrospun scaffold properties (15–17). In published studies, scaffolds are usually sterilised before cell culture experiments using ethanol (18,19), sometimes in combination with ultraviolet irradiation (20,21). Another sterilisation strategy is using ethylene oxide: although highly effective, it is toxic for operators, and possible residues in the device can impair its outcome (14,22). Moreover, after ethylene oxide sterilisation, electrospun nanofibres have shown modified morphology and mechanical properties (23,24). Gamma rays are the most widely employed form of ionised irradiation used to sterilise bioresorbable electrospun scaffolds (25,26,14,27), thanks to their remarkable penetration ability which is

inversely proportional to the material density (28). Despite being relatively safe for electrospun polymeric fibres, gamma-rays are known to induce chain scission, decreasing polymer molecular weight and negatively impacting the material's thermal and mechanical properties (29,30,26) (14). Gamma-ray irradiation has been shown to slightly increase the crystallinity, Young Modulus, and failure strain of poly (L-lactic acid) electrospun scaffolds (24). In the case of collagen-based biomaterials, gamma rays are considered the most suitable sterilisation method due to the complete lack of residues (31,32). Controversial results regarding the extent of irradiation-induced cross-linking and degradation have been reported for gamma-ray collagen sterilisation. It has been demonstrated that gamma-irradiation induces cleavage of collagen chains, decreases mechanical properties, and increases enzymatic degradation rate (33,34,32,35). However, other studies have suggested that gamma-irradiation at low doses (1.0 kGy) brings about simultaneously chain degradation and cross-linking in fish and porcine gelatin and in collagen, in a protein concentration and irradiation dose-dependent manner (36). The standard sterilisation dose for implantable medical devices is 25 kGy (source: ISO 11137-2:2013). This study aimed to investigate the effect of the irradiation with different gamma-ray doses on poly(L-lactic acid)/collagen electrospun bundles mimicking T/L fascicles to identify a suitable dose capable of limiting changes in the structure and properties of the scaffold.

2.3.Materials and methods

2.3.1. *Materials*

Poly (L-lactic acid) (PLA) (Lacea H.100-E, M_w= 8.4 x 10^4 g/mol^{-1}, PDI=1.7) was purchased from Mitsui Fine Chemicals, Dusseldorf, Germany. Collagen (Type I) (COL) was kindly provided by Kensey Nash Corporation d/b/a DSM Biomedical, Exton, USA. Trifluoroethanol (TFE), 1,1,1,3,3,3-Hexafluoro-2-propanol (HFIP), N-(3-dimethylaminopropyl)-N′-ethylcarbodiimide hydrochloride (EDC) and N-hydroxysuccinimide (NHS) from Sigma-Aldrich (Saint-Louis, USA) were used. A PLA/COL 75/25 (w/w) blend solution was prepared from a 15% (w/v) solution in TFE: HFIP 50:50 (v/v) (10).

2.3.2. Electrospinning

To obtain bundles of axially aligner nanofibres with a diameter in the range of human fascicles (500-650 μm) and fibrils (500-50 nm) (37), a pilot-scale electrospinning machine (Spinbow srl, Bologna, Italy), equipped with a high-speed rotating drum collector (length = 405 mm, diameter = 150 mm; peripheral speed =19.6 m s^{-1}; drum rotations = 2,500 rpm) and with an applied voltage of 22 kV, was used. To detach the nanofibre mats, the drum was covered with a sheet of polyethylene (PE) coated paper (Turconi S.p.A, Italy). The polymeric solution was spun through four metallic needles (internal diameter = 0.51 mm, Hamilton, Romania) via polytetrafluoroethylene tubes (Bola, Germany), using a flow rate of 0.5 mL h^{-1} controlled by a syringe pump (KD Scientific 200 series, IL, United States). The needle-collector distance was set at 200 mm; the sliding spinneret of the machine, where the needles were fixed, had an excursion of 180 mm, with a sliding speed of 1,500 mm min^{-1}. The electrospinning session was set at 2 h at room temperature (RT) and with a relative humidity of 20–30%. After the electrospinning session, the mat was cut in circumferential stripes of 450 mm, wrapped up, and pulled off the drum, obtaining circular bundles of aligned nanofibres.

2.3.3. Sample crosslinking

The collected PLA/COL bundles were crosslinked by immersing them in a solution of 95% ethanol containing EDC and NHS for 24 hours at RT. The bundles were washed in phosphate-buffered saline (PBS) for 30 minutes before rinsing them with distilled water for 2 hours.

2.3.4. Sterilisation treatment

Sterilisation of the crosslinked bundles was carried out by exposing them to gamma irradiation treatment emitted from ^{60}Co source at doses of 5 kGy, 10 kGy, and 25 kGy in air at RT at Sterigenics Italy S.pA (Bologna, Italy). The sterilised bundles were named PLA/COL-5, PLA/COL-10, and PLA/COL-25, respectively. As 25 kGy is the standard dose for medical implantable devices, sample sterility was verified only after sterilisation at 5 kGy and 10 kGy according to ISO 11737-2 by Studio Ambiente s.r.l. (Verona, Italy).

2.3.5. *Assessment of collagen degradation by immersion in water*

To assess COL degradation following the sterilisation treatment, the bundles were washed by immersion in distilled water for 2 hours and dried under a vacuum over P_2O_5, after which their weights were recorded. The weight loss was attributed solely to the dissolution of degraded collagen, as discussed in a previous work (11). After water immersion, the samples are indicated as PLA/COL-5W, PLA/COL-10W, and PLA/COL-25W.

2.3.6. Characterisation techniques

2.3.6.1. Bundle and nanofibres morphology

The diameter of the bundles was determined using an optical microscope (Axioskop, Zeiss, Pleasanton, CA, United States) equipped with a camera (AxioCam MRc, Zeiss, Pleasanton, CA, United States). The bundles' morphology before and after sterilisation was analysed using a scanning electron microscope (SEM) (Phenom Pro-X, PhenomWorld, Eindhoven, Netherlands). The diameters of nanofibres and their distribution were measured using FiJi (38) calculating the mean and standard deviation for a total of 200 measurements acquired on 4 images (magnification = 8000x) for each sample. The nanofibres' orientation was investigated using the Directionality plugin of FiJi. This approach allowed quantifying the number of nanofibres within a given angle range from the axis, using a Local Gradient Orientation method, following a previously validated procedure (10). For each sample, the analysis was performed on 5 images (magnification = 8000x). Each ring-shaped bundle was weighed with a precision balance (MC210P, Sartorius, Gottingen, Germany) and reported as the mean and standard deviation of three measurements. To evaluate the porosity of the bundles, the volume fraction (v) of each specimen was calculated considering the following equation:

$$v = w/(L \cdot A \cdot \rho) \quad (1)$$

where, w is the weight of each specimen, L is the length of the specimen, A is the cross-sectional area of the specimen, $\rho = 0.75 \cdot \rho_P + 0.25 \cdot \rho_C$ is the density of the PLA/COL 75/25 blend (where: ρ =1.28 g/cm^3; ρ_{PLA}=1.26 g/cm^3; ρ_{COL}=1.35 g/cm^3)

The percentage of porosity for each bundle was evaluated using Equation 2:

$$\text{Porosity} = (1 - v) \times 100 \quad (2)$$

2.3.6.2. Physico-chemical characterisation

Thermogravimetric analyses (TGA) were performed on the non-irradiated PLA/COL bundles and bundles after various irradiation doses before and after water treatment. TGA was conducted with a TGA2950 analyzer from TA Instruments by heating 10°C/min in nitrogen gas from RT to 600°C.

Differential Scanning Calorimetry (DSC, TA Instruments Q100 DSC) was performed on non-irradiated PLA/COL bundles and samples after various irradiation doses (5 kGy,10 kGy,25 kGy). The samples were analysed both before and after water treatment. The heating and cooling steps were carried out at a rate of 20°C/min and 10°C/min, respectively, in a nitrogen atmosphere from -60°C to 190°C. Glass transition temperature (T_g), crystallisation temperature (T_c) and melting temperature (T_m) were determined from the heating scan after controlled cooling. Crystallinity degree (χ_c) was calculated for the samples using equation 3:

$$\chi_c(\%) = \frac{\Delta H_m - \Delta H_c}{\Delta H_f \times W_{PLLA}} \times 100 \quad (3)$$

Where ΔH_m is the enthalpy of melting, ΔH_c is the enthalpy of crystallisation, ΔH_f is the heat of fusion of 100% crystallised PLA acid, which is 93.7 J/g (39), W_P is the weight fraction of PLA acid in the scaffold.

2.3.6.3. Mechanical properties

Tensile tests were conducted to compare the stress-strain properties of PLA/COL bundles before and after various irradiation doses. The bundles (n=8 specimens per treatment group) were immersed in PBS for 2 minutes before performing the tensile test. A material testing machine, Model 4465 Instron (Norwood, MA, USA), equipped with ± 100 N load cell from Instron (Norwood, MA, USA), was used. Custom-made capstan grips were used to reduce stress concentrations at the sample ends (10). The testing consisted of a monotonic ramp in displacement control, adjusting the actuator speed for each specimen to impose a strain rate of 10% s^{-1}. The procedure was consistent with the ASTM D1414 standard for determining the physical properties of O-rings. Starting from the load-displacement curves, the following data were computed: failure stress (σ_F), yield stress (σ_Y), Young's modulus (E), failure strain (ε_F), yield strain (ε_Y) unit work to yield (L_Y), unit work to failure (L_F). The force-displacement curves were converted to stress-strain curves using two different approaches:

(i) to describe the macroscopic mechanical behaviour of the specimen, the apparent stress was computed by dividing the force by the macroscopic cross-sectional area measured before the test; the apparent Young modulus and unit works to yield, and failure was thus computed;
(ii) to quantify the net mechanical properties (i.e., removing the effect of porosity), the net stress was also calculated by dividing the apparent stresses by the volume fraction (v) of the specimens; similarly, the net Young's modulus (E), and the unit works were computed.

2.3.7. Statistical analysis

The statistical significance of the effect of sterilisation on the nanofibre diameters (n=200 measurements for each sample category), length of the bundle (n=8 for each sample category), weight of the bundle (n=8 for each sample category), the diameter of the bundle (n=8 for each sample category), porosity (n=8 for each sample category), directionality (n=5 SEM images for each sample category) and mechanical properties (n=8 specimens for each sample category) measured for the non-irradiated and irradiated bundles were analysed using one-way ANOVA followed by Tukey's post-hoc test in GraphPad Prism software (ns $p>0.05$, *$p\leq0.05$, **$p\leq0.01$, ***$p\leq0.001$, ****$p\leq0.0001$).

2.4. Results

2.4.1. Bundle and nanofibres morphology

The surface morphology of electrospun PLA/COL bundles before and after irradiation was investigated by SEM (Figure 2.1.A, B). Results show that bead-free fibres, characterised by smooth surfaces, are obtained both before and after irradiation at various doses (Figure 2.1.A(I-IV) and Figure 2.1.B(I-IV)). The measured diameters of the nanofibres (mean and standard deviation) for PLA/COL were 246.5 ± 67.5 nm, for PLA/COL-5 237.8 ± 63.6 nm, for PLA/COL-10 241.3 ± 80.3 nm and for PLA/COL-25 270.9 ± 67.6 nm (Figure 2.1.E). Statistically significant differences were found between the non-irradiated and irradiated samples at different values of kiloGrays (Table S1). Moreover, the diameter distribution revealed 22.5% of nanofibres in the range of 300-350 nm for PLA/COL-25, which is 13.5% higher compared to that of PLA/COL, 15.5% higher compared to that of PLA/COL-5 and 75% higher compared to that of PLA/COL-10 nanofibres in the same range of diameters.
The porosity of the bundle (mean and standard deviation) for PLA/COL was 64 ± 2.6 %, for PLA/COL-5 was 67.0 ± 2.0 %, for PLA/COL-10 was 65.8 ± 1.7 % and for PLA/COL-25 was

64.1 ± 2.1 %. Statistically significant differences were found between PLA/COL-5 and PLA/COL-25 bundles (Table S1).

The directionality analysis (Figure 2.1.C.) showed that the non-irradiated bundles had 43.3 ± 3.3% of nanofibres within ±12° of their axis (Table 2.1). The bundles irradiated at 5 kGy had 40.2 ± 3% of nanofibres within ±12° of orientation with a mean reduction of 3.1%, and those irradiated at 10 kGy had 40.9 ± 3.1% of nanofibres within ±12° with a mean reduction of 2.4% of aligned nanofibres as compared to the non-irradiated nanofibres. The percentage of aligned nanofibres within ±12° for bundles irradiated at 25 kGy was 32.3 ± 2% with a mean reduction of 11%. The following bundles' diameters were measured: 485 ± 45 μm for PLA/COL, 513 ± 21 μm for PLA/COL-5, 511 ± 30 μm for PLA/COL-10, and 514 ± 40 μm for PLA/COL-25. The length and the weight of the bundles are also reported in Figure 2.1.D(II) and D(III), and the statistical analysis is shown in Table S2.

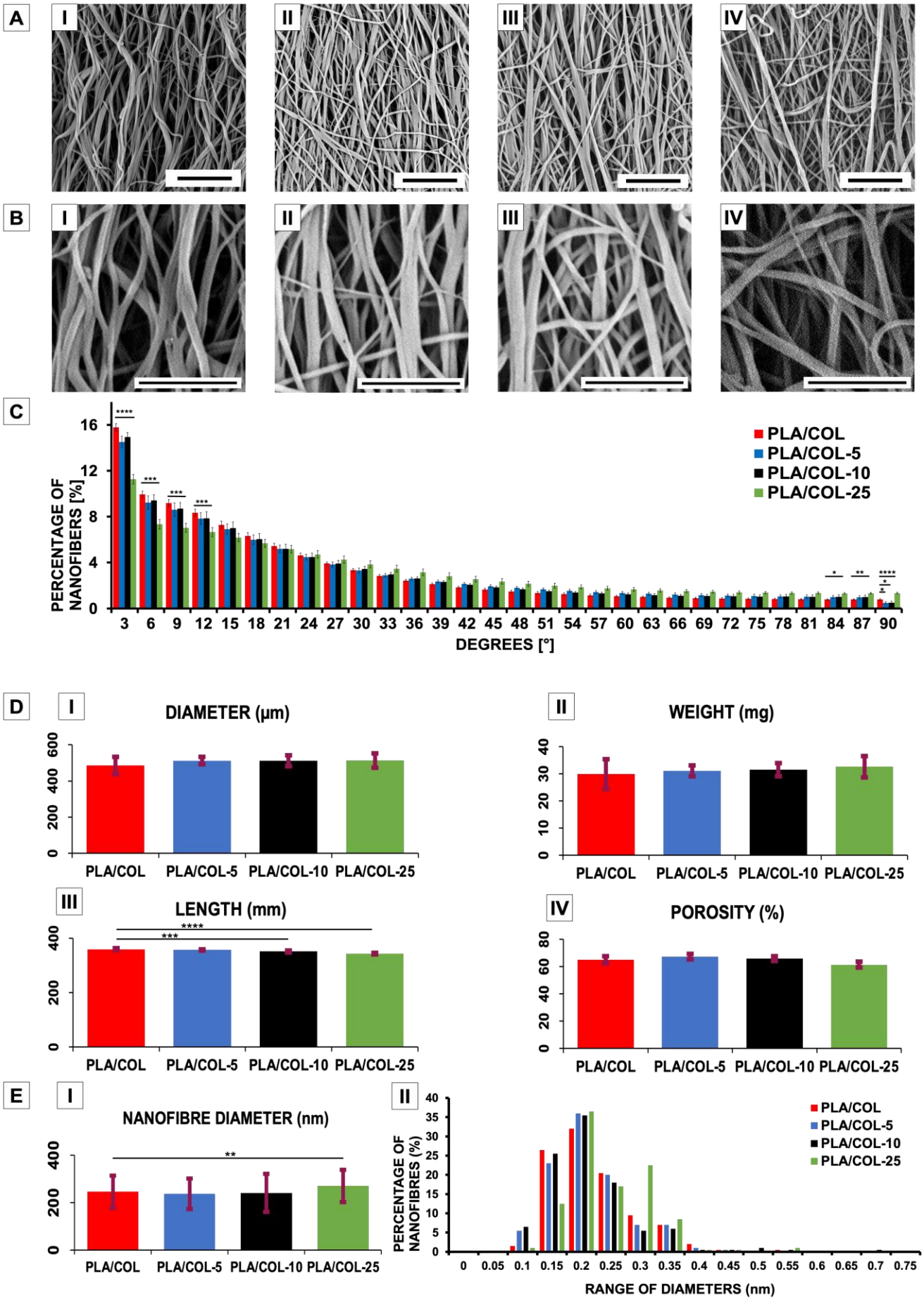
A
I
II
III
IV
B
I
II
III
IV
C
PERCENTAGE OF NANOFIBERS [%]
DEGREES [°]
PLA/COL
PLA/COL-5
PLA/COL-10
PLA/COL-25
D
I
DIAMETER (µm)
II
WEIGHT (mg)
III
LENGTH (mm)
IV
POROSITY (%)
PLA/COL
PLA/COL-5
PLA/COL-10
PLA/COL-25
E
I
NANOFIBRE DIAMETER (nm)
II
PERCENTAGE OF NANOFIBRES (%)
RANGE OF DIAMETERS (nm)

Figure 2.1. SEM images of the nanofibres of (I) PLA/COL, (II) PLA/COL-5, (III) PLA/COL-10, (IV) PLA/COL-25, acquired at different magnifications: (A) 8000x (scale bar = 5 μm); (B) 15000x (scale bar = 3μm). (C) Orientation analysis of the nanofibres in which an angle of 0° corresponds to the longitudinal axis of the specimen while an angle of 90° corresponds to the circumferential direction. The directionality histograms show the distribution in terms of percentage (mean and standard deviation) of nanofibres for the different ranges of angles for the irradiated and non-irradiated samples; (D) Morphological properties of irradiated and non-irradiated bundles: (I) diameter of non-irradiated and irradiated bundles; (II) Weight of non-irradiated and irradiated bundles; (III) Length of non-irradiated and irradiated bundles; and (II) porosity of non-irradiated and irradiated bundles. (E) (I) diameter and (II) distribution of nanofibre diameter in terms of percentage for different ranges of nanofibres of non-irradiated and irradiated bundles. The mean and standard deviation are plotted, and statistical significance is evaluated using one-way ANOVA followed by Tukey's multiple comparisons (ns $p \geq 0.05$, *$p \leq 0.05$, **$p \leq 0.01$, ***$p \leq 0.001$, ****$p \leq 0.0001$).

Table 2.1. Percentage distribution of nanofibres within ±15° from the axis of the bundle

Sample name	Percentage of nanofibres (0-12°)	Alignment reduction (%)
PLA/COL	43.3 ± 3.3%	-
PLA/COL-5	40.2 ± 3%	3.1%
PLA/COL-10	40.9 ± 3.1%	2.4%
PLA/COL-25	32.3 ± 2%	11.0%

2.4.2. Physico-chemical characterisation

The TGA curves of the irradiated and non-irradiated samples are reported in Figure 2.2., whereas the TGA data of all samples are listed in Table 2.2, including data for the bundles after immersion in water. PLA/COL bundles, whether irradiated or not, were characterised by very low weight loss percentages in the temperature range from RT to 150°C (values from 1% to 3%), attributed to loss of adsorbed water. After irradiation, all samples showed a slightly lower thermal stability with the temperature of maximum degradation rate (T_{max}) decreasing by about 15°C, whereas no influence of the irradiation dose was observed. Upon water immersion treatment, no significant changes in T_{max} values were observed (Table 2.2).

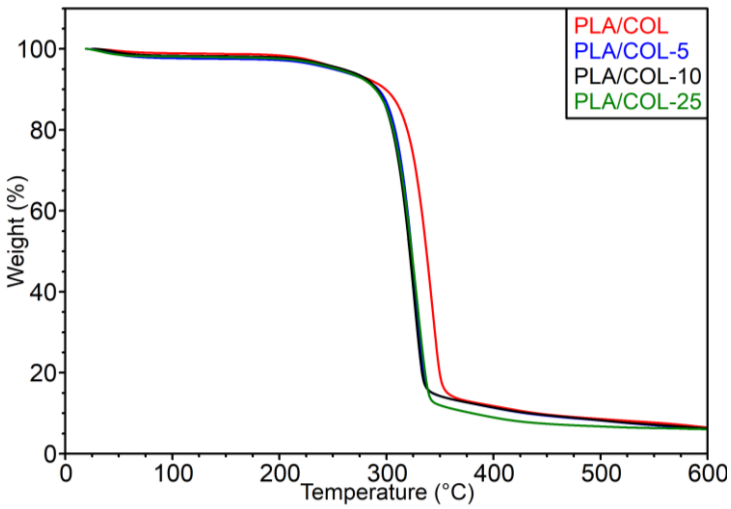

Figure 2.2. TGA curves of PLA/COL and the bundles irradiated with different doses

Table 2.2. TGA data for PLA/COL bundles after irradiation at different doses and irradiated bundles after immersion in water

Sample	**Δ_m% (RT-150°C)**	**T_{max} (°C)**	**Residual weight % (at 600°C)**
PLA/COL	1.3	343	6.4
PLA/COL-5	2.5	328	6.1
PLA/COL-10	1.9	326	6.2
PLA/COL-25	2.1	327	6.5
PLA/COL-5W	2.3	331	6.1
PLA/COL-10W	2.8	325	5.9
PLA/COL-25W	2.4	332	4.4

The calorimetric data of PLA/COL samples before and after gamma-irradiation, together with those of sterilised samples after water immersion, are reported in Figure 2.3. and Table 2.3. The DSC curves (after controlled cooling from the melt) clearly show differences in peak shapes attributed to diversity in the crystallisation ability of the various samples. All samples exhibited a single glass transition, whose T_g values were about 60°C for all samples. A cold crystallisation exothermic peak followed by a melting endothermic peak of almost the same entity (compare ΔHc and ΔHm) was observed for all samples. This result indicates that the melting phenomena that follow the cold crystallisation concern only the crystal phase, attributed to PLA, developed during the heating scan, thus demonstrating that completely

amorphous PLA was obtained after the cold crystallisation DSC scan. No differences in the melting temperature (Tm) were observed for the samples before and after gamma irradiation, whereas the cold crystallisation temperature (Tc) decreased with increasing dose of irradiation, indicating a higher crystallisation ability for irradiated samples, as also demonstrated by the increase in crystallisation and melting enthalpies for these samples. It is also worth noting that the cold crystallisation peaks appear sharper in a dose-dependent manner. No significant differences were observed for irradiated samples after water immersion.

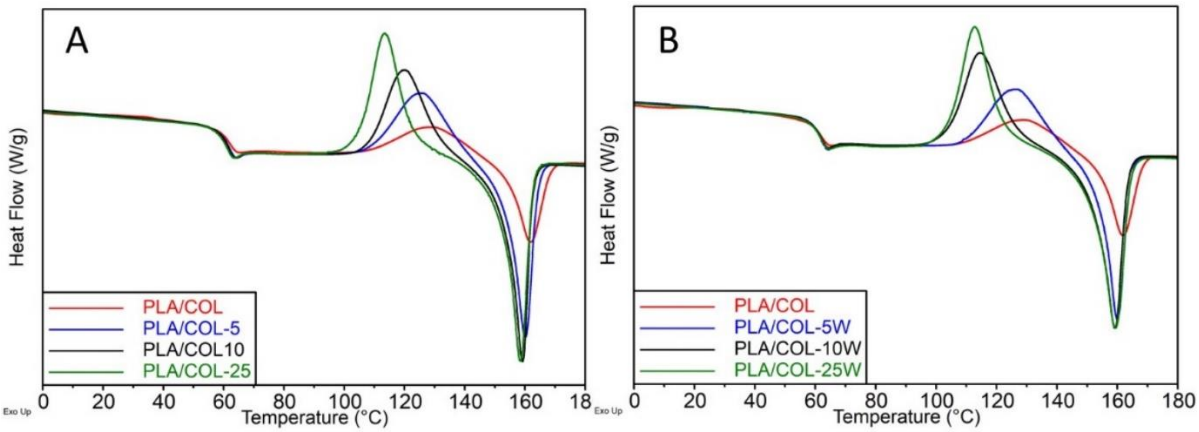

Fig 2.3. (A) DSC curves for irradiated and non-irradiated bundles; (B) DSC curves for irradiated bundles after immersion in water

Table 2.3. Calorimetric data for PLA/COL bundles after irradiation at different doses and irradiated bundles after immersion in water

Sample	**T_g (°C)**	**ΔC_p (J/g°C)**	**T_c (°C)**	**ΔH_c (J/g)**	**T_m (°C)**	**ΔH_m (J/g)**
PLA/COL	61	0.44	130	14	162	14
PLA/COL-5	61	0.49	126	24	160	26
PLA/COL-10	60	0.48	120	26	159	28
PLA/COL-25	60	0.50	113	29	159	31
PLA/COL-5W	61	0.45	127	22	160	24
PLA/COL-10W	61	0.48	115	28	159	29
PLA/COL-25W	61	0.48	113	30	159	31

2.4.3. Mechanical properties

All the stress-strain curves exhibited a non-linear ductile behaviour with a toe region similar to the ones of T/L fascicles (Figure 2.4.A). The apparent yield stress reached its highest values for the PLA/COL-25 (6.6±0.4 MPa) and PLA/COL-10 (6.6±0.4 MPa) bundles, with a slightly lower value for the PLA/COL-5 bundle (6.4±0.3 MPa), indicating that higher irradiation doses resulted in higher apparent yield stresses (Figure 2.4.B). Notably, there were statistically significant differences between the non-irradiated bundles and those irradiated at all three doses (Table S4). The apparent failure stress values decreased for the irradiated bundles PLA/COL-5 (11.3±1.8 MPa) and PLA/COL-25 (11.5±1.3 MPa) as compared to the non-irradiated PLA/COL bundles (15.7±2.1 MPa) (Figure 2.4.C). The highest value for Young's modulus of irradiated bundles was seen in PLA/COL-25 (265±27 MPa), followed by PLA/COL-5 (241±26 MPa) and PLA/COL-10 (238±15 MPa), as compared to the non-irradiated PLA/COL bundles (300±44 MPa) (Figure 2.4.H). Statistically significant differences were found between all the irradiated and non-irradiated bundles (Table S4). The yield strain was highest for PLA/COL-10 (4.11±0.39%) and slightly reduced for PLA/COL-5 (4.04±0.32%) and PLA/COL-25 (3.53±0.38%) (Figure 2.4.D). Failure strain was highest for PLA/COL-10 (48±19 %) and only slightly reduced for PLA/COL-25 (46±7%) and PLA/COL-5 (40±18%) (Figure 2.4.E). The unit work to yield was similar for all the irradiated and non-irradiated bundles (0.010±0.001 J/mm^3) (Figure 2.4.F). The values of apparent unit work to failure were highest for PLA/COL-10 (0.47±0.24 J/mm^3) followed by PLA/COL-25 (0.43±0.10 J/mm^3) and PLA/COL-5 (0.36±0.21 J/mm^3) (Figure 2.4.G). We also calculated the net mechanical properties, avoiding the contribution of the void spaces inside the scaffolds, and they were generally 2.8 to 3 times higher than the apparent ones (Table S3).

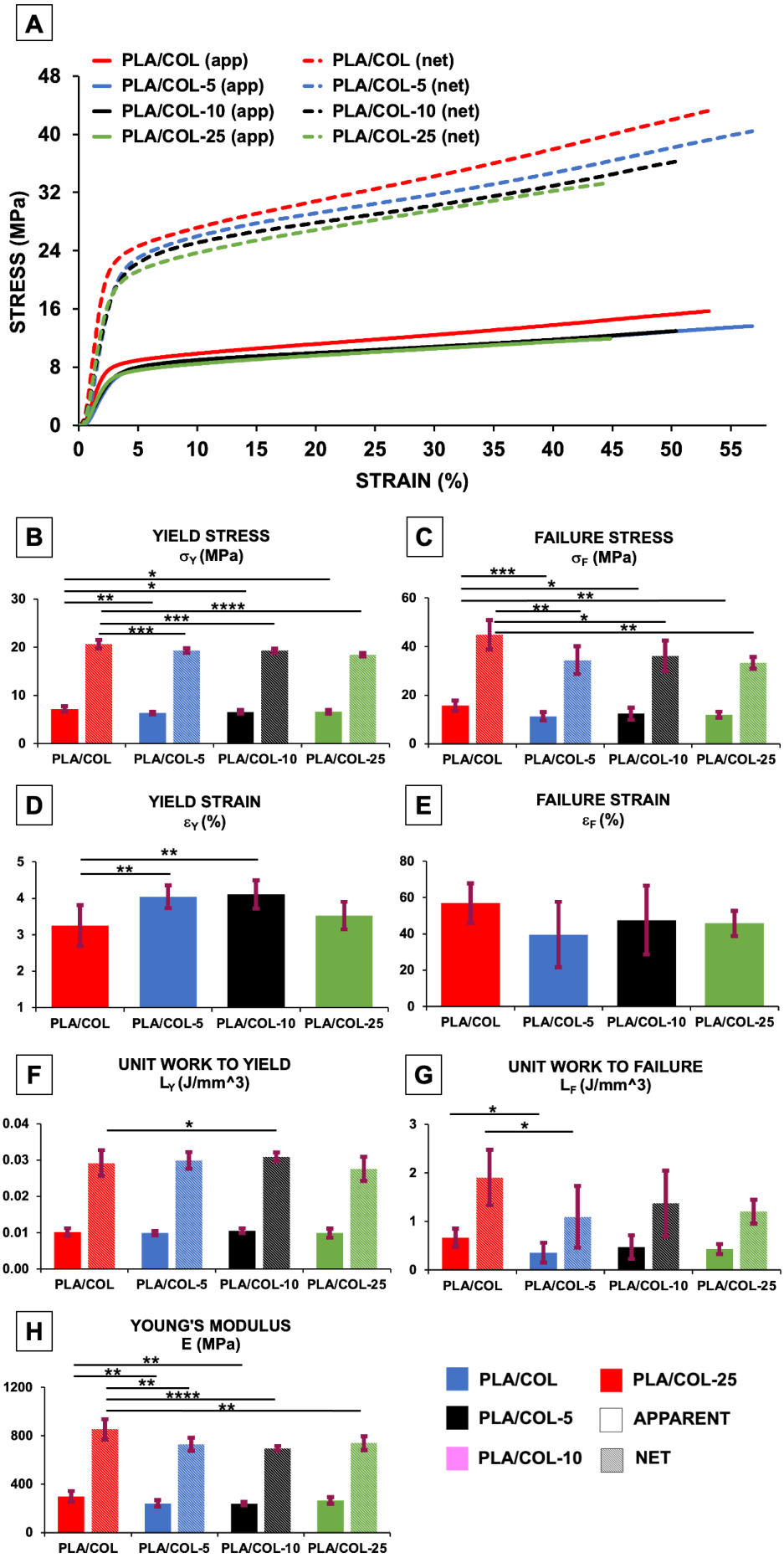
A
PLA/COL (app)
PLA/COL-5 (app)
PLA/COL-10 (app)
PLA/COL-25 (app)
PLA/COL (net)
PLA/COL-5 (net)
PLA/COL-10 (net)
PLA/COL-25 (net)
STRESS (MPa)
STRAIN (%)
B
YIELD STRESS
σY (MPa)
C
FAILURE STRESS
σF (MPa)
D
YIELD STRAIN
εY (%)
E
FAILURE STRAIN
εF (%)
F
UNIT WORK TO YIELD
LY (J/mm^3)
G
UNIT WORK TO FAILURE
LF (J/mm^3)
H
YOUNG'S MODULUS
E (MPa)
PLA/COL
PLA/COL-5
PLA/COL-10
PLA/COL-25
APPARENT
NET

Figure 2.4. (A) Stress-strain curve derived for irradiated and non-irradiated bundles with net and apparent values. Mechanical property indicators as observed for irradiated and non-irradiated bundles during tensile strength testing with net and apparent values – (B) Yield stress; (C) Failure stress; (D) Yield strain; (E) Failure strain; (F) Unit work to yield; (G) Unit work to failure; (H) Young's modulus. The mean and standard deviation are plotted, and statistical significance is evaluated using one-way ANOVA followed by Tukey's multiple comparisons, which are plotted as *p≤0.05, **p≤0.01, ***p≤0.001, ****p≤0.0001

2.5. Discussion

The objective of this study was to analyse the effects of different doses of gamma-irradiation on electrospun PLA/COL electrospun bundles. To this aim, a PLA and COL blend with a composition of 75:25 (w/w) was used to fabricate bundles, according to a previously published method (10), that were crosslinked with EDC/NHS to improve the scaffold's stability and reduce the degradation of collagen. We investigated the changes in morphological, mechanical, chemical, and thermal properties of scaffolds irradiated with gamma radiation at three different doses of 5 kGy, 10 kGy, and 25 kGy.

The electrospun bundles were morphologically characterised by diameter, length, weight, and porosity. There were no significant differences in the diameter and weight of non-irradiated and irradiated bundles. The length of the bundles experienced a shrinkage with an increase in the irradiation dosage, with the highest amount of shrinkage seen in 25 kGy bundles, and these values were statistically significant. The measurements of the irradiated and non-irradiated bundles indicated diameters ranging from 420-570 μm, while the nanofibre diameters fell within the range of 247-271 nm. The slight difference in the diameters can be attributed to the enlargement of the nanofibre's thickness due to their shrinkage in length with increasing dosage (Figure 2.1.E). This increase in diameter, along with the shrinkage in length observed in 25 kGy bundles, implies the bundle's tendency of the Poisson effect. The porosity of irradiated bundles also showed a slight reduction with an increase in dosage of irradiation, showing a statistically significant difference between 5 kGy and 25 kGy, and the bundles showed a significant reduction of porosity when irradiated with 25 kGy.

SEM images of the irradiated and non-irradiated bundles were compared to analyse the alignment of the nanofibres since changes in nanofibre orientation and geometry can alter yield stress, strain, and elastic modulus (40). Nanofibre orientation at 0-12° from the longitudinal axis of the bundle can be considered important for the preferential design to mimic the arrangement of natural collagen fibrils. Therefore, the deviation in the alignment of nanofibres

within 3°, 6°, 9°,12° and 15° from the axis were specifically analysed to determine the effect of gamma-irradiation. At 5 kGy and 10 kGy doses of gamma irradiation, the alignment of nanofibres was observed to be similar to the non-irradiated bundles with minimal variation in orientation, and it is interesting to note that the bundles irradiated at 25 kGy had the largest deviation in alignment compared to the other irradiation doses. Specifically, the percentage of nanofibres within the orientation of 3-18° had reduced the most, and the percentage of nanofibres within 6-30°, 30-45° and 45-90° orientations appeared to be the least varying. This deviation could be the result of shrinkage in the length of the bundles observed after irradiation, which could have increased the diameter of the bundles. In the case of 5 kGy and 10 kGy doses, the percentage of nanofibres was highest within 24° and lowest within 60-90°.

To analyse the changes in thermal stability affected by gamma irradiation, TGA curves derived for bundles irradiated at different doses were compared to non-irradiated PLA/COL. The decrease of T_{max} due to gamma-irradiation was independent of radiation dose and might be associated with the breaking of collagen crosslinks and partial degradation due to chain scission, as reported by (41). Calorimetric data derived from DSC measurements were analysed to see radiation-induced changes in the samples. From Figure 2.3, no significant changes are seen in Tg, whereas irradiated samples exhibited a higher cold crystallisation ability and the formation of a higher amount of crystal phase in a dose-dependent manner which aligns with the decrease in T_{max}. The calorimetric results might be interpreted, in agreement with TGA results, considering that gamma-irradiation could have caused a decrease in collagen crosslinking density that increased the flexibility of the PLA chains facilitating cold crystallisation and a faster rate of crystal formation (higher kinetics of crystallisation) during cooling, which can act as stress concentrators.

Tensile tests were conducted to study the effects of the respective doses on their mechanical properties. The tensile strength of the irradiated bundles is slightly reduced in a dose-dependent manner as compared to the non-irradiated ones. This variation could be the result of chain scission caused by gamma radiation, which caused degradation of collagen as analysed before with TGA and DSC data. The net values of the mechanical properties, not considering the bundle's porosity, result in higher values compared to the apparent ones but with a consistent decrease in the mechanical values. The mechanical properties of the bundles analysed in general did not have a significant variation after 5 kGy, 10 kGy, and 25 kGy dosages of irradiation despite some statistically significant differences between the different samples for different mechanical properties. The mechanical properties of the bundles irradiated at 5 kGy

were closer to the non-irradiated bundles than the bundles irradiated at 10 kGy and 25 kGy. At this stage, we can only conclude that the 5 kGy irradiated bundles exhibited more favourable characteristics when compared to the other categories. It is also interesting to note that the range of the tensile strength of 5 kGy irradiated bundles was similar to that of the human Iliopsoas tendon fascicles, as reported in the literature (42).

2.6. Conclusion

Despite gamma ray sterilisation at 25 kGy being the gold standard for implantable devices, we have found this dose causes detrimental effects on the morphological, physical, and mechanical properties of PLA/COL bundles, which might be attributed to partial degradation of the crosslinked collagen. For this reason, we investigated three doses of gamma irradiation to identify the one that maintains good bundle properties while guaranteeing effective sterilisation. Amongst the three doses of irradiation, 5 kGy had the least effect on the scaffold's properties.

2.7. References

1. Liu S, Al-Danakh A, Wang H, Sun Y, Wang L. Advancements in scaffold for treating ligament injuries; in vitro evaluation. Biotechnology Journal. 2024;19(1):2300251.

2. Lim WL, Liau LL, Ng MH, Chowdhury SR, Law JX. Current Progress in Tendon and Ligament Tissue Engineering. Tissue Eng Regen Med. 2019 Jun 26;16(6):549–71.

3. Xie X, Chen Y, Wang X, Xu X, Shen Y, Khan A ur R, et al. Electrospinning nanofiber scaffolds for soft and hard tissue regeneration. Journal of Materials Science & Technology. 2020 Dec 15;59:243–61.

4. Bosworth LA, Rathbone SR, Bradley RS, Cartmell SH. Dynamic loading of electrospun yarns guides mesenchymal stem cells towards a tendon lineage. Journal of the Mechanical Behavior of Biomedical Materials. 2014 Nov 1;39:175–83.

5. Camarero-Espinosa S, Yuan H, Emans PJ, Moroni L. Mimicking the Graded Wavy Structure of the Anterior Cruciate Ligament. Advanced Healthcare Materials. 2023;12(17):2203023.

6. Laranjeira M, Domingues RMA, Costa-Almeida R, Reis RL, Gomes ME. 3D Mimicry of Native-Tissue-Fiber Architecture Guides Tendon-Derived Cells and Adipose Stem Cells into Artificial Tendon Constructs. Small. 2017;13(31):1700689.

7. Pauly H, Kelly D, Popat K, Easley J, Palmer R, Haut Donahue TL. Mechanical properties of a hierarchical electrospun scaffold for ovine anterior cruciate ligament replacement. Journal of Orthopaedic Research. 2019;37(2):421–30.

8. Sensini A, Gualandi C, Focarete ML, Belcari J, Zucchelli A, Boyle L, et al. Multiscale hierarchical bioresorbable scaffolds for the regeneration of tendons and ligaments. Biofabrication. 2019 Jul 1;11(3):035026.

9. Xu Y, Dong S, Zhou Q, Mo X, Song L, Hou T, et al. The effect of mechanical stimulation on the maturation of TDSCs-poly(L-lactide-co-e-caprolactone)/collagen scaffold constructs for tendon tissue engineering. Biomaterials. 2014 Mar 1;35(9):2760–72.

10. Sensini A, Gualandi C, Zucchelli A, Boyle LA, Kao AP, Reilly GC, et al. Tendon Fascicle-Inspired Nanofibrous Scaffold of Polylactic acid/Collagen with Enhanced 3D-Structure and Biomechanical Properties. Sci Rep. 2018 Nov 21;8(1):17167.

11. Sensini A, Gualandi C, Cristofolini L, Tozzi G, Dicarlo M, Teti G, et al. Biofabrication of bundles of poly(lactic acid)-collagen blends mimicking the fascicles of the human Achille tendon. Biofabrication. 2017 Mar 8;9(1):015025.

12. Armentano I, Bitinis N, Fortunati E, Mattioli S, Rescignano N, Verdejo R, et al. Multifunctional nanostructured PLA materials for packaging and tissue engineering. Progress in Polymer Science. 2013 Oct 1;38(10):1720–47.

13. Dai Z, Ronholm J, Tian Y, Sethi B, Cao X. Sterilization techniques for biodegradable scaffolds in tissue engineering applications. J Tissue Eng. 2016 May 17;7:2041731416648810.

14. Rediguieri CF, Sassonia RC, Dua K, Kikuchi IS, de Jesus Andreoli Pinto T. Impact of sterilization methods on electrospun scaffolds for tissue engineering. European Polymer Journal. 2016 Sep 1;82:181–95.

15. Andrews KD, Hunt JA, Black RA. Effects of sterilisation method on surface topography and in-vitro cell behaviour of electrostatically spun scaffolds. Biomaterials. 2007 Feb 1;28(6):1014–26.

16. Yixiang D, Yong T, Liao S, Chan CK, Ramakrishna S. Degradation of electrospun nanofiber scaffold by short wave length ultraviolet radiation treatment and its potential applications in tissue engineering. Tissue Eng Part A. 2008 Aug;14(8):1321–9.

17. Rainer A, Centola M, Spadaccio C, Gherardi G, Genovese JA, Licoccia S, et al. Comparative study of different techniques for the sterilization of poly-L-lactide electrospun microfibers: effectiveness vs. material degradation. Int J Artif Organs. 2010 Feb;33(2):76–85.

18. Brown BL, Fuerst R. Ethylene Oxide Sterilization of Tissue Culture Media. Science. 1963 Dec 27;142(3600):1654–5.

19. Gualandi C, Govoni M, Foroni L, Valente S, Bianchi M, Giordano E, et al. Ethanol disinfection affects physical properties and cell response of electrospun poly(l-lactic acid) scaffolds. European Polymer Journal. 2012 Dec 1;48(12):2008–18.

20. Evrova O, Kellenberger D, Scalera C, Calcagni M, Giovanoli P, Vogel V, et al. Impact of UV sterilization and short term storage on the in vitro release kinetics and bioactivity of biomolecules from electrospun scaffolds. Sci Rep. 2019 Oct 22;9(1):15117.

21. Łopianiak I, Butruk-Raszeja BA. Evaluation of Sterilization/Disinfection Methods of Fibrous Polyurethane Scaffolds Designed for Tissue Engineering Applications. Int J Mol Sci. 2020 Oct 30;21(21):8092.

22. Holy CE, Cheng C, Davies JE, Shoichet MS. Optimizing the sterilization of PLGA scaffolds for use in tissue engineering. Biomaterials. 2000 Jan 1;22(1):25–31.

23. Kim HL, Lee JH, Lee MH, Kim HH, Kim J, Han I, et al. Direct-current treatment as a safe sterilization method for electrospun biodegradable polymer. Tissue Engineering and Regenerative Medicine. 2011 May;8(3):320–5.

24. Valente TAM, Silva DM, Gomes PS, Fernandes MH, Santos JD, Sencadas V. Effect of Sterilization Methods on Electrospun Poly(lactic acid) (PLA) Fiber Alignment for Biomedical Applications. ACS Appl Mater Interfaces. 2016 Feb 10;8(5):3241–9.

25. Torres-Giner S, Gimeno-Alcañiz JV, Ocio MJ, Lagaron JM. Optimization of electrospun polylactide-based ultrathin fibers for osteoconductive bone scaffolds. Journal of Applied Polymer Science. 2011;122(2):914–25.

26. Bosworth LA, Gibb A, Downes S. Gamma irradiation of electrospun poly(ε-caprolactone) fibers affects material properties but not cell response. Journal of Polymer Science Part B: Polymer Physics. 2012;50(12):870–6.

27. Bhaskar P, Bosworth LA, Wong R, O'brien MA, Kriel H, Smit E, et al. Cell response to sterilized electrospun poly(ε-caprolactone) scaffolds to aid tendon regeneration in vivo. Journal of Biomedical Materials Research Part A. 2017;105(2):389–97.

28. Booth A. Sterilization Validation and Routine Operation Handbook: Radiation. Boca Raton: CRC Press; 2014. 168 p.

29. Skiens WE. Sterilizing radiation effects on selected polymers. Radiation Physics and Chemistry (1977). 1980 Jan 1;15(1):47–57.

30. Takeuchi N, Machigashira M, Yamashita D, Shirakata Y, Kasuga T, Noguchi K, et al. Cellular compatibility of a gamma-irradiated modified siloxane-poly(lactic acid)-calcium carbonate hybrid membrane for guided bone regeneration. Dental Materials Journal. 2011;30(5):730–8.

31. Gorham SD. Collagen. In: Byrom D, editor. Biomaterials: Novel Materials from Biological Sources [Internet]. London: Palgrave Macmillan UK; 1991 [cited 2023 Aug 30]. p. 55–122. Available from: https://doi.org/10.1007/978-1-349-11167-1_2

32. Delgado LM, Pandit A, Zeugolis DI. Influence of sterilisation methods on collagen-based devices stability and properties. Expert Review of Medical Devices. 2014 May 1;11(3):305–14.

33. Sun WQ, Leung P. Calorimetric study of extracellular tissue matrix degradation and instability after gamma irradiation. Acta Biomaterialia. 2008 Jul 1;4(4):817–26.

34. Sullivan DC, Mirmalek-Sani SH, Deegan DB, Baptista PM, Aboushwareb T, Atala A, et al. Decellularization methods of porcine kidneys for whole organ engineering using a high-throughput system. Biomaterials. 2012 Nov 1;33(31):7756–64.

35. Tao M, Ao T, Mao X, Yan X, Javed R, Hou W, et al. Sterilization and disinfection methods for decellularized matrix materials: Review, consideration and proposal. Bioact Mater. 2021 Feb 27;6(9):2927–45.

36. Hara M, Koshimizu N, Yoshida M, Haug IJ, Ulset AST, Christensen BE. Cross-linking and depolymerisation of gamma-irradiated fish gelatin and porcine gelatin studied by SEC-MALLS and SDS-PAGE: a comparative study. J Biomater Sci Polym Ed. 2010;21(6–7):877–92.

37. Kastelic J, Galeski A, Baer E. The multicomposite structure of tendon. Connect Tissue Res. 1978;6(1):11–23.

38. Schindelin J, Arganda-Carreras I, Frise E, Kaynig V, Longair M, Pietzsch T, et al. Fiji: an open-source platform for biological-image analysis. Nat Methods. 2012 Jul;9(7):676–82.

39. Fischer EW, Sterzel HJ, Wegner G. Investigation of the structure of solution grown crystals of lactide copolymers by means of chemical reactions. In: Fischer EW, Müller FH, Kausch HH, editors. Aktuelle Probleme der Polymer-Physik IV. Heidelberg: Steinkopff; 1973. p. 980–90. (Aktuelle Probleme der Polymer-Physik).

40. Pauly HM, Kelly DJ, Popat KC, Trujillo NA, Dunne NJ, McCarthy HO, et al. Mechanical properties and cellular response of novel electrospun nanofibers for ligament tissue engineering: Effects of orientation and geometry. Journal of the Mechanical Behavior of Biomedical Materials. 2016 Aug 1;61:258–70.

41. Faraj K, Brouwer K, Geutjes P, Versteeg E, Wismans R, Deprest J, et al. The effect of ethylene oxide sterilisation, beta irradiation and gamma irradiation on collagen fibril-based scaffolds. Evaluation of biological, physical and chemical parameters. Tissue Engineering and Regenerative Medicine. 2011 Jan 1;8:460–70.

42. Hanson P, Aagaard P, Magnusson SP. Biomechanical properties of isolated fascicles of the Iliopsoas and Achilles tendons in African American and Caucasian men. Annals of Anatomy - Anatomischer Anzeiger. 2012 Sep 1;194(5):457–60.

SUPPORTING INFORMATION

Table S.1. Statistical significance of morphological characteristics evaluated using one-way ANOVA followed by Tukey's multiple comparisons, which are plotted as *p≤0.05, **p≤0.01, ***p≤0.001, ****p≤0.0001

	Diameter (μm)	**Length (mm)**	**Weight (mg)**	**Porosity (%)**	**Nanofibre diameter (nm)**
PLA/COL vs PLA/COL-5	ns p=0.43	ns p=0.34	ns p=0.91	ns p=0.15	ns p=0.59
PLA/COL vs PLA/COL-10	ns p=0.47	*** p=0.00	ns p=0.83	ns p=0.85	ns p=0.88
PLA/COL vs PLA/COL-25	ns p=0.40	**** p=0.01	ns p=0.48	ns p=0.85	** p=0.01
PLA/COL-5 vs PLA/COL-10	ns p=0.99	* p=0.01	ns p=0.99	ns p=0.53	ns p=0.96
PLA/COL-5 vs PLA/COL-25	ns p>0.99	**** p=0.01	ns p=0.85	* p=0.03	**** p=0.01
PLA/COL-10 vs PLA/COL-25	ns p=0.99	**** p=0.01	ns p=0.93	ns p=0.39	*** p=0.01

Table S.2. Statistical significance of directionality of nanofibers evaluated using one-way ANOVA followed by Tukey's multiple comparisons, which are plotted as *p≤0.05, **p≤0.01, ***p≤0.001, ****p≤0.0001

	Within 3°	**Within 6°**	**Within 9°**	**Within 12°**	**Within 84°**	**Within 87°**	**Within 90°**
PLA/COL vs PLA/COL-5	ns p=0.35	ns p=0.42	ns p=0.43	ns p=0.36	ns p=0.53	ns p=0.63	* p=0.01
PLA/COL vs PLA/COL-10	ns p=0.69	ns 0.69	ns p=0.57	ns p=0.42	ns p=0.44	ns p=0.52	* p=0.02
PLA/COL vs PLA/COL-25	**** p<0.00	*** p=0.01	*** p=0.01	*** p=0.01	* p=0.01	** p=0.09	**** p=0.01
PLA/COL-5 vs PLA/COL-10	ns p=0.93	ns p=0.97	ns p=0.99	ns p=0.99	ns p=0.99	ns p=0.99	ns p=0.99

PLA/COL-5 vs PLA/COL-25	** p=0.01	** p=0.01	** p=0.01	** p=0.01	ns p=0.17	ns p=0.09	**** p=0.01
PLA/COL-10 vs PLA/COL-25	*** p=0.01	** p=0.01	** p=0.01	** p=0.01	ns p=0.22	ns p=0.13	**** p=0.01

Table S.3. Mean and standard deviation calculated for net and apparent values of indicators of mechanical properties for non-irradiated bundles (P/C) and irradiated bundles (P/C-5, P/C-10, P/C-25).

		Yield Stress (MPa)		**Failure Stress (MPa)**		**Young's Modulus (MPa)**		**Yield Strain (%)**	**Failure Strain (%)**	**Unit work to yield (J/mm^3)**		**Unit work to failure (J/mm^3)**	
		app	net	app	net	app	net			app	net	app	net
PLA/COL	Mean	7.2	20.6	15.7	44.9	300	854	3.25	57	0.010	0.029	0.66	1.91
	S. D	0.6	0.9	2.1	6.1	44	85	0.56	11	0.001	0.004	0.19	0.57
PLA/COL-5	Mean	6.4	19.3	11.3	34.4	241	730	4.04	40	0.010	0.030	0.36	1.10
	S. D	0.3	0.5	1.8	5.7	26	54	0.32	18	0.001	0.002	0.21	0.64
PLA/COL-10	Mean	6.6	19.3	12.4	36.1	238	697	4.11	48	0.011	0.031	0.47	1.37
	S. D	0.4	0.5	2.5	6.4	15	18	0.39	19	0.001	0.001	0.24	0.68
PLA/COL-25	Mean	6.6	18.5	11.5	33.3	265	739	3.53	46	0.010	0.028	0.43	1.20
	S. D	0.4	0.4	1.3	2.5	27	56	0.38	7	0.001	0.003	0.10	0.24

Table S.4. Statistical significance of mechanical properties evaluated using one-way ANOVA followed by Tukey's multiple comparisons, which are plotted as *p≤0.05, **p≤0.01, ***p≤0.001, ****p≤0.0001

	Yield Stress (MPa)		**Failure Stress (MPa)**		**Young's Modulus (MPa)**		**Yield Strain (%)**	**Failure Strain (%)**	**Unit Work to yield (J/mm^3)**		**Unit Work to failure (J/mm^3)**	
	(app)	(net)	(app)	(net)	(app)	(net)			(app)	(net)	(app)	(net)
PLA/COL vs PLA/COL-5	* p=0.04	**** p<0.001	** p=0.01	** p=0.01	ns p=0.11	** p=0.01	ns p=0.56	ns p=0.43	ns p=0.90	ns p=0.86	ns p=0.09	ns p=0.08
PLA/COL vs PLA/COL-10	* p=0.03	*** p=0.01	* p=0.01	* p=0.01	** p=0.01	**** p<0.01	** p=0.01	ns p=0.58	ns p=0.83	* p=0.01	ns p=0.20	ns p=0.25
PLA/COL vs PLA/COL-25	** p=0.01	*** p=0.01	*** p=0.01	** p=0.01	** p=0.01	** p=0.01	** p=0.01	ns p=0.10	ns p=0.90	ns p=0.99	* p=0.02	* p=0.03
PLA/COL-5 vs PLA/COL-10	ns p=0.99	* p=0.04	ns p=0.97	ns p=0.73	ns p=0.30	ns p=0.48	* p=0.05	ns p=0.99	ns p=0.44	** p=0.01	ns p=0.98	ns p=0.94
PLA/COL-5 vs PLA/COL-25	ns p=0.70	* p=0.04	ns p=0.92	ns p=0.98	ns p=0.42	ns p=0.99	ns p=0.09	ns p=0.83	ns p>0.99	ns p=0.68	ns p=0.90	ns p=0.98
PLA/COL-10 vs PLA/COL-25	ns p=0.75	ns p>0.99	ns p=0.71	ns p=0.92	ns p=0.99	ns p=0.68	ns p=0.99	ns p=0.70	ns p=0.45	* p=0.03	ns p=0.65	ns p=0.77

Chapter 3: Advances in Mineralisation of Electrospun Scaffolds for Tissue Engineering: a Short Review

A.Padmanabhan[a], *M.L.Focarete*[a], *L.Cristofolini*[b]

[a]*Department of Chemistry, "G.Ciamician", University of Bologna, Italy*
[b]*Department of Industrial Engineering, University of Bologna, Italy*

Keywords : Mineralisation; electrospun scaffolds; simulated body fluid;

MANUSCRIPT IN PREPARATION

Graphical abstract

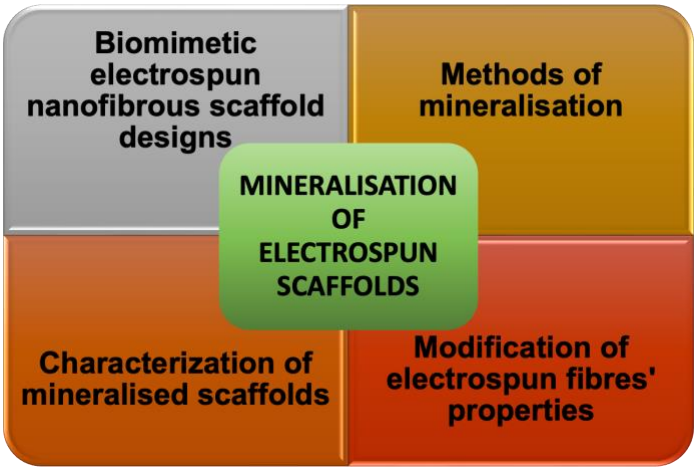

3.1. Abstract

Electrospun scaffolds have gained considerable attention for their applications in musculoskeletal tissue engineering due to their unique nanofibrous structure, controllable porosity, mechanical properties and biocompatibility. The incorporation of minerals into electrospun scaffolds plays an essential role in enhancing their ability to support bone integration and osteoconductivity upon implantation. The objective of this literature review is to present an analysis of the research on the mineralisation of electrospun scaffolds and highlight the different mineralisation techniques used, the types of minerals employed, and their impact on the physical, chemical, mechanical, and biological properties of the electrospun scaffolds. This review aims to contribute to a better understanding of the field and offer valuable guidance for future research and development of advanced mineralised electrospun scaffolds with improved tissue regeneration capabilities.

3.2. Introduction

Electrospinning has emerged as a promising and versatile technique for various tissue engineering applications. Its extensive discussion in several studies highlights the potential of electrospun nanofibrous scaffolds with unique properties such as their ability to mimic the architecture and morphological properties of the extracellular matrix(ECM) of native tissues, providing a high surface area to volume ratio and developing cell-instructive matrices that promote tissue ingrowth and cell migration. The process of electrospinning involves the use of an electrostatic field to draw a polymer solution into a fine fibre. This versatile technique has allowed the development of several types of fibre assemblies, such as nonwoven fibre mesh, aligned fibre mesh, patterned fibre mesh, three-dimensional structures, and sub-micron spring and convoluted fibres.(1)

Electrospun scaffolds have been explored for skin tissue engineering and wound dressing, where the scaffolds create a barrier while promoting the healing process by aiding in the adhesion of keratinocytes and fibroblasts. Electrospun fibres have been investigated in guided nerve regeneration by providing physical cues and delivering neurotrophic factors. The high surface area and porosity of electrospun scaffolds make them suitable for promoting endothelial cell attachment and angiogenesis, which is crucial for vascular tissue engineering. The ability of electrospun nanofibres to mimic the arrangement of collagen fibrils as seen in a cartilage ECM makes it a viable alternative material for the treatment of injured cartilage. Electrospun polymeric matrices have been widely used as biomimetic scaffolds to regenerate musculoskeletal tissues such as bone, tendon, skeletal muscle, and their interfaces.(2)

Synthetic polymers like PCL and natural polymers like collagen have been used in electrospun polymeric scaffolds for bone regeneration, aiming to mimic the native ECM of bone. The porous structures of these scaffolds provide a suitable environment for osteoblast adhesion, proliferation, and mineralisation, while bioactive factors can also be incorporated into the fibres to enhance bone regeneration. Furthermore, the mechanical properties of electrospun scaffolds can be tailored to match those of bone tissue, providing essential support during the healing process. Electrospun scaffolds have also been used to promote the regeneration of tendon and ligament tissues. Aligning the fibres in the scaffold can help guide the orientation of tenocytes, which is crucial for restoring the mechanical properties of tendons and ligaments and also support myoblast adhesion and differentiation. Electrospun scaffolds can be developed to mimic the interfaces between different musculoskeletal tissues, such as the enthesis (bone-

tendon) or myotendinous joint (tendon-muscle) interfaces, promoting gradual transitions of mechanical properties and mineral content while enabling better integration between the different tissue types involved.(3)

Biomimetic mineralisation refers to depositing inorganic minerals to mimic the natural biological process of bone mineralisation found in the ECM of bone to develop scaffolds that mimic the structural aspects of bone and actively promote hydroxyapatite (HA) formation, the major mineral component of bone. (4) Biomimetically mineralised electrospun scaffolds hold significant importance because they enhance osteoconductivity by replicating the mineralisation cues found in native bone tissue by closely resembling the bone ECM. This promotes hydroxyapatite deposition, encourages better cell adhesion, proliferation, and differentiation and improves the scaffold's mechanical properties, making it more suitable for load-bearing applications, which is crucial for successful bone regeneration where the scaffold needs to withstand mechanical stresses. The mineralised surface encourages the deposition of new bone tissue directly onto the scaffold, leading to a stable integration between the scaffold and host bone tissue.(5)

Mineralised electrospun scaffolds can be used in bone defect repair, fracture healing, dental implants, and orthopaedic surgeries, as they can be fabricated to match the specific requirements of the target tissues. In dental regeneration, these scaffolds aid in regenerating dental pulp, periodontal ligaments, and the alveolar bone. These scaffolds can be used in cartilage regeneration by combining mineralised and non-mineralised regions to restore complex structures of the osteochondral interface. For researchers, these biomimetically mineralised scaffolds serve as valuable models for studying the biomineralisation process, understanding the interactions between minerals and cells, and investigating the factors and mechanisms behind mineral deposition on biomaterials. To modulate inflammation at the site of implantation and to prevent infection, mineralised scaffolds can also function as drug delivery systems, allowing the controlled release of therapeutic agents.(6)

3.3. Methods: search strategy and inclusion criteria

A search of relevant literature was conducted to identify studies related to the specified topic. The search was performed in Web of Science, PubMed, and Google Scholar databases from December 2005 to January 2023. The search terms included variations of "mineralisation" and "electrospun scaffolds," along with related keywords. Inclusion criteria encompassed research articles and review papers that studied *in vitro* acellular mineralisation of electrospun scaffolds.

Duplicates were immediately discarded. Studies that addressed only cellular-based mineralisation were excluded. Articles were considered if they studied the effects of acellular and cellular mineralisation. Non-English articles and patents were also excluded. The systematic review of literature on the mineralisation of electrospun scaffolds provides valuable insights into the current state of research, highlights key findings, and identifies gaps in knowledge. The gathered information will aid in advancing the field of tissue engineering by promoting the development of innovative and effective mineralisation strategies for electrospun scaffolds for various applications.

3.4. Results of the literature search

A total of 492 papers were preliminary found from the initial search, after removing duplicates. A total of 178 were considered, after applying the exclusion criteria. The papers selected are reviewed in five main threads: according to (i) the design adopted to develop biomimetic electrospun nanofibrous scaffolds suitable for mineralisation; (ii) the methods used to deliver a mineralisation onto the electrospun scaffolds; (iii) the modifications of the electrospun fibres' chemical-physical and morphological properties to induce mineralisation; (iv) the pre-treatments of electrospun scaffold surfaces to support mineralisation, and (v) the methods to characterise the mineralised scaffolds.

3.5. Biomimetic electrospun nanofibrous scaffold designs suitable for mineralisation

Conventional electrospinning is a well-researched technique to develop nanofibrous scaffolds with optimal porosity and surface area that allows for cellular interaction for various tissue engineering applications, particularly in bone regeneration. However, the random orientation of the nanofibres in these scaffolds limits their ability to mimic the complex hierarchical structure and mechanical properties of native tissues. Advances in electrospinning technology have allowed the fabrication of biomimetic structures with various architectures and properties for musculoskeletal tissue engineering, and the specific design of the scaffold can be tailored to match the requirements of different musculoskeletal tissues. The electrospinning procedures employed to fabricate mineralised scaffolds are reviewed below.

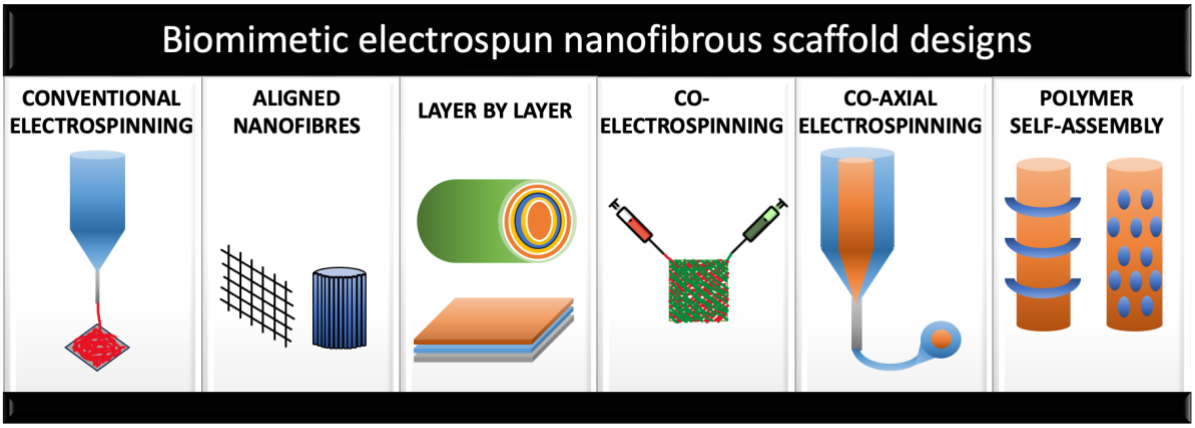

Figure 3.1. Overview of the main designs of biomimetic electrospun nanofibrous scaffold.

3.5.1. Aligned nanofibres

Aligned nanofibres have a fibre arrangement where all the fibres are oriented parallelly along a specific direction. They provide a structured and organised substrate for the mineralisation process by controlling the spatial distribution of minerals. This alignment also mimics the natural bone ECM composed of aligned collagen fibres. Jiang et al. investigated an electrospun scaffold with the fibre orientation changing from random to aligned and consisting of a gradient distribution of BMP-2/hydroxyapatite nanoparticles for its potential to induce interfacial tissue regeneration. Biomimetic mineralisation of this scaffold using 5x SBF to create a second mineral gradient on the surface. The resulting mineral deposits were phosphate deposits gradually distributed along the nanofibre surface and calcium deposits localised to the region with a high content of hydroxyapatite nanoparticles, specifically in the area with random fibre orientation.(7) Li et al. investigated aligned PLGA nanofibres mineralised using an alternate immersion method for their mechanical properties, and the authors reported better elasticity even though the mineralised nanofibres showed slightly decreased tensile strength. An interesting result in this study is the cell cytoskeleton of umbilical cord mesenchymal stem cells cultured on the scaffold that showed alignment and elongation along the fibre axes and a polarised phenotype, suggesting that this type of scaffold can contribute to the matrix-driven cues to form new anisotropic tissue.(8) Kung et al., in their study, examined the mineralisation of PLA-aligned nanofibres and PLA membranes using 10x SBF for 6h and its consequent effect on human adipose-derived stem cell adhesion and proliferation. The cells on the mineralised aligned nanofibres expressed more alkaline phosphatase and osteocalcin activity than those cultured on the membranes. Also, they showed elongation along the direction of alignment.(9) Aligned PLA/PLGA nanofibres were surface-modified with glutamic acid peptide to investigate their effect on calcium phosphate deposition and osteogenic differentiation of rat

marrow stromal cells since ECM proteins containing amino acid sequences abundant in glutamic acid facilitate the mineralisation process. To increase the diffusion of calcium and phosphate ions within the nanofibres and achieve a favourable calcium phosphate to fibre ratio, Karaman et al. employed a bilayer technique where one layer of PLA/PLGA scaffold was mineralised using SBF and a new layer of PLA/PLGA nanofibres were electrospun on top of the apatite coating. This procedure was continued for 5 bilayers, achieving calcium phosphate to fibre ratios as high as 200%, falling between the ratios found in cancellous (160%) and cortical (310%) bones. The extent of osteogenic differentiation and mineralisation in marrow stromal cells correlated with the amount of calcium phosphate deposited on the fibres before cell seeding. The gradual increase in the expression of osteogenic markers such as osteopontin, alkaline phosphatase (ALP), osteocalcin, and type 1 collagen was associated with higher calcium phosphate deposition.(10)

3.5.2. Layer by layer

Bilayered scaffolds, unlike traditional scaffolds, have been shown to functionally resolve the requirements of both bone and cartilage in a single structure using a sandwich-like or stratified design of a composite layered morphology. Yunos et al. employed this strategy in their study to produce stratified PDLLA scaffolds coated on Bioglass® derived foams to mimic the osteochondral interface). The scaffold showed a high affinity for chondrocyte attachment and proliferation. The fibres' surface roughness was reportedly 13 times higher than their previous study that incorporated PDLLA fibres into 2D Bioglass® pellets for bioactive bone scaffolds. The authors reported a reduced HA deposition with increased thickness of the PDLLA fibrous layer when immersed in SBF for 7 days. Therefore, the authors controlled the thickness of the scaffold at 150 μm to prevent HA deposition on the chondral side of the scaffold.(11,12) Another exciting application of the electrospinning technique is the fabrication of scaffolds made of concentric layers. To mimic the cortical bone structure, which is a tightly packed unit of osteons oriented parallel to the axis of the bone, Andric et al. developed a technique to fabricate cortical bone scaffolds by rotating a core collection of PGA microfibres using a custom setup and utilising it further to collect concentric layers of electrospun PLLA/gelatin nanofibres. The authors reported successful mineralisation using 10x SBF and suitable attachment and differentiation of MC3T3-E1 cells after 28 days of cell culture. The authors also fabricated another scaffold to mimic the dual structural organisation of natural bone with

cortical and trabecular regions. The inner core comprises electrospun sheets of PEO fibres surrounded by individual osteon-like scaffolds made of PEO.(13) Bian et al. have fabricated a similar multi-level hierarchical structure that mimicked this motif by rolling aligned mineralised collagen electrospun nanofibres and arranging these bundles from nano-level to macro-level to form a composite scaffold. However, these scaffolds had insufficient compressive strength after mineralisation and did not mimic the non-uniform motifs of natural bone.(14)

Guided bone regeneration is used to regenerate bone in areas with insufficient bone volume, often due to periodontal disease, tooth extraction, or implant placement. Guided tissue regeneration is a technique that promotes various periodontal tissues, including gingival tissue, periodontal ligament, and cementum. In some instances, combining them in a single scaffold may be beneficial to ensure the restoration of both bone and periodontal tissues. Rad et al. studied the effects of increasing the concentration of β-TCP nanoparticles in a two-layered scaffold. One side of the scaffold contained PCL/PGS/Chitosan for tissue regeneration and PCL/PGS/β-TCP for bone regeneration.(15) Zheng et al. have employed a layer-by-layer coating of cationic collagen and anionic chondroitin sulphate sequentially to form a precursor matrix for apatite mineralisation on PCL scaffolds modified with polydopamine.(16) In another study, PCL scaffolds containing chondroitin sulphate and bioactive glass at various concentrations were layered from an increasing to decreasing order of both composites from one direction to another using agarose as a hydrogel filler to fabricate a 3D hybrid scaffold with a gradient mineral deposition for cartilage regeneration.(17) PCL nanofibres were also layered onto calcium phosphate-modified gelatin scaffolds by electrospinning them one after the other on the same collector, modulating their mechanical properties while enhancing bioactivity. Rajzer et al. reported that these scaffolds had better pore size distribution than individual gelatin or PCL scaffolds.(18)

3.5.3. Coaxial electrospinning

Coaxial electrospinning is a variation of the conventional electrospinning technique, which uses two or more concentric nozzles to produce hybrid nanofibre scaffolds. Pathamanapan et al. have used this technique to fabricate nanofibres with an inner core layer of PVA containing oregano extract and mesoporous silica nanoparticles and an outer shell layer of PCL blended with collagen and hydroxyapatite. This study investigated the scaffold's biocompatibility, cell attachment, and proliferation owing to its sheath layer made of a natural polymer and the core

layer built of hydrophilic polymer incorporated with hydroxyapatite nanoparticles that refine the osteogenic abilities of the scaffold.(19) He et al. developed a novel hierarchically structured nanofibre scaffold from PCL and gelatin using template-assisted electrospinning. This scaffold was studied after mineralisation in simulated body fluid (SBF) for 2,4 and 7 days, and the results highlighted the osteoimmunomodulatory functions of the scaffold, which in turn promoted the recruitment and differentiation of bone mesenchymal stem cells. When implanted *in vivo* in rats to repair an alveolar bone defect, the scaffold exhibited accelerated bone regeneration as compared to a combination of commercial Bio-Gide and Bio-Oss membranes.(20) Xie et al. fabricated a submicron bioactive glass tube by coaxial electrospinning of PVP, tetraethyl orthosilicate and triethyl phosphate as the shell layer and heavy mineral oil in the core. Transmission electron microscopy (TEM) was used to visualise the submicron hollow bioactive glass tubes that resulted from removing the PVP and heavy mineral oil post-electrospinning via calcination at 600°C for 5h. Both the inner and outer sides of the tubes had mineral deposits after incubation in SBF for different time intervals, and the larger surface area that came into contact with the SBF solution accelerated the mineralisation rate. An important application of this type of scaffold is controlled drug and protein release. Therefore, the authors investigated the release of bovine serum albumin (BSA) and lysozyme loaded onto these scaffolds. The loaded BSA had a delayed release, and the bioactivity of the released lysozyme was maintained at 90.9%, making these scaffolds a promising strategy for topical drug or gene delivery.(21) Kang et al. incorporated mesoporous bioactive glass nanospheres into a core/shell scaffold of PEO/PCL to act as carriers of fibroblast growth factor (FGF18), known for its osteogenic and angiogenic properties. This integration enhanced the apatite-forming ability and mechanical properties of the scaffold when compared to the ones without the nanospheres. Furthermore, cytochrome C, a model protein, was used to load two growth factors (FGF2 and FGF18) into the scaffold, one in nanospheres and the other in the core shell of the fibre. Cytochrome C assay investigated its release rate in a 6-week in vivo study performed on rat calvarium defects. The FGF2-FGF18-loaded fibre scaffolds demonstrated a significant increase in bone formation with augmented bone volume and density.(22) These results were similar to those of other studies conducted using mesoporous silica, where it was employed as either the shell layer for nanofibres by physical absorption after surface treatment or by directly incorporating it into the nanofibres. These studies also reported the controlled release characteristics of bioactive molecules from the nanofibre core

and shell, along with its ability to enhance apatite coating when incubated in SBF as compared to nanofibres without the integration of mesoporous silica.(23),(24)

3.5.4. Co-electrospinning

This specialised electrospinning technique involves the simultaneous electrospinning of two or more different polymer solutions to create composite nanofibres with combined properties. The resulting scaffold can have tailor-made properties by adjusting the composition of the polymer solutions. Samavedi et al. have fabricated a graded electrospun mesh containing nano-hydroxyapatite/PCL and poly(ester urethane) urea elastomer to mimic the ligament-bone interface to capture its intricate mechanical and chemical gradients. Tensile tests of these meshes showed a gradient of tensile modulus along its length, and the gradient was more pronounced upon treatment with 5x SBF for 2h.[13] Torricelli et al. employed co-electrospinning to fabricate a PLLA and gelatin scaffold crosslinked with genipin to mimic the cartilage-bone interface. These scaffolds had mechanical properties intermediate to pure PLLA and gelatin and varied as a function of the PLLA content.[14]

3.5.5. Polymer self-assembly

In the context of biomimetic mineralisation, the arrangement of nanoscale minerals within the organic fibre matrix is of vital significance. This arrangement directly impacts achieving precise organic-inorganic interfaces and mineral concentrations. These factors influence hybrid materials' mechanical characteristics, degradation patterns, and biocompatibility. Chen et al. demonstrated that block copolymer self-assembly and a one-dimensional polymer nucleation process can precisely control the orientation of mineral crystals and their spatial distribution at the nanoscale level. The authors electrospun PCL nanofibres and induced crystallisation of the ionic block copolymer PCL-b-PAA to form a nanofibre "shish-kebab" structure with ionic PAA periodic nanodomains that mediated hydroxyapatite growth when incubated in 2x SBF. This mineral growth was along the c-axis parallel to the kebab surface due to the geometrical confinement between two adjacent PCL-b-PAA lamellar crystals that allowed for precisely controlled mineral growth.(27) Jing et al. used this principle to fabricate PCL/chitosan scaffolds with controlled copolymer crystallisation. These scaffolds also showed similar controlled mineralisation when incubated in 2x SBF. The authors also incorporated this protocol in another study using PCL/nanohydroxyapatite scaffolds with similar results.(28,29) In specific ways, this self-assembly can be attributed to phase separation since these two

phenomena are not mutually exclusive. Xu et al., in their study, employed automatic phase separation and crystallisation of PLA and chitosan to design “island-like” nanosized topographic modifications of chitosan on PLA nanofibres. The authors demonstrated that these modified scaffolds showed good mineralisation ability and balanced out the hydrophobicity and hydrophilicity of the fibres.(30) In a recent study, Liu et al. developed a bionic periosteum in a shish kebab structure with PCL nanofibres loaded with calcium-binding peptide that had to mimic the microenvironment of periosteum. This peptide, composed of a negatively charged heptaglutamate domain (E7) from the E7-BMP-2 protein, was combined with calcium ions from a tricalcium phosphate sol (TCP sol) through electrostatic interactions. They prolonged the release of E7 peptide and BMP-2 and encouraged the formation of mineral deposits on the bionic periosteum. The scaffold’s in vitro and in vivo evaluation showed excellent osteogenic abilities, resulting in vascularised bone formation.(31)

3.6. Methods of Mineralisation

The effectiveness of electrospun scaffolds is significantly influenced by the method of mineralisation employed. Diverse mineralisation techniques, such as biomimetic deposition using simulated body fluid, electrospraying, electrochemical deposition, supersaturated mineralising solutions and alternated soaking method each impart unique characteristics to the scaffold, affecting its mechanical strength, biocompatibility, and osteoconductivity. Therefore, an optimal mineralisation method tailored for each scaffold is imperative to ensure the desired biological response and structural properties, ultimately enhancing the scaffold's efficacy in bone tissue engineering applications.

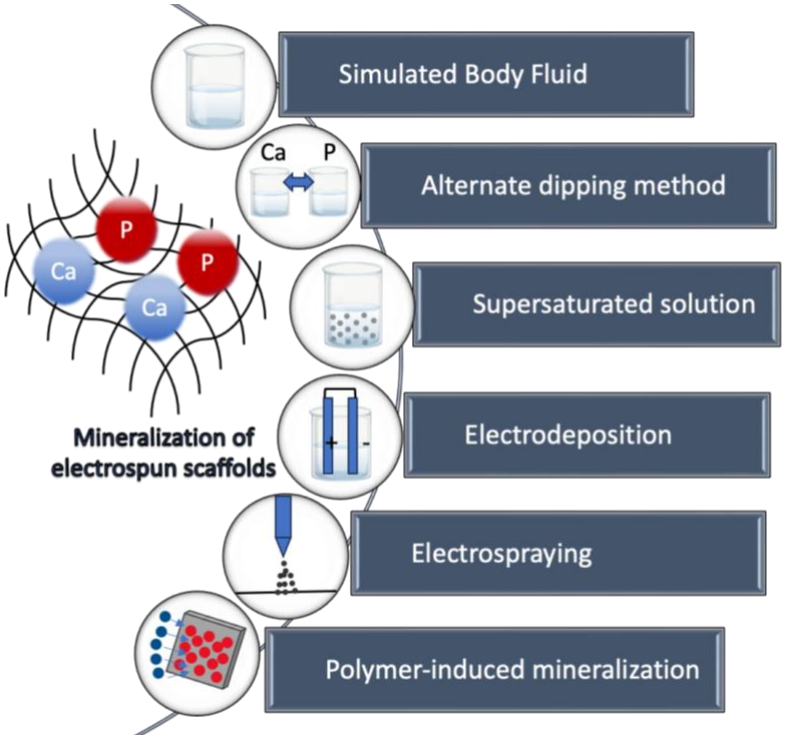

Figure 3.2. Different types of mineralisation techniques

3.6.1. Simulated Body Fluid

To recreate the ionic environment that resembles the bone mineralising conditions in the human body and to evaluate the bone-binding ability of a biomaterial by its potential to form apatite, Kokubo et al. developed a solution designed to mimic the ionic composition and pH of the human blood plasma called as the simulated body fluid or SBF in 1987. It typically contains ions, such as calcium, phosphate, magnesium, and carbonate, essential for forming mineralised tissues. When incubating a biomaterial in the SBF, the ions in the solution precipitate and form a layer of apatite, simulating the natural mineralisation process.(32) However, Kim et al. in 1999 reported that the apatite layer deposited by SBF had a slightly different composition than the inorganic part of the bone in that the apatite layer had lower HCO_3^- and higher Cl^- concentrations.(33) Consequently, in 2003, Oyane et al. published their study of several different formulations of SBF having ionic concentrations either equal to or closer to that of blood plasma to identify the optimum ionic concentration for *in vitro* bioactivity assessment of biomaterials and biomimetic apatite formation.(34) In 2007, the International Organisation for Standardisation (ISO) published the corrected SBF or conventional SBF (c-SBF) as a solution for assessing bioactivity of implant materials *in vitro*, further updating it in 2012 and 2014.(35),(36) Table 3.1 lists the reagents of the c-SBF as described by Kokubo and Takadama

along with the exact order of dissolving the reagents to avoid precipitation of apatite in the solution.

Table 3.1. The reagents to prepare 1L conventional SBF (35)

Order	**Reagent**	**Name**	**Amount**
1	NaCl	sodium chloride	8.035g
2	$NaHCO_3$	sodium bicarbonate	0.355g
3	KCl	potassium chloride	0.225g
4	$K_2HPO_4.3H_2O$	potassium phosphate dibasic trihydrate	0.231g
5	$MgCl_2.6H_2O$	magnesium chloride hexahydrate	0.311g
6	1.0M HCl	1M hydrochloric acid	39ml
7	$CaCl_2$	calcium chloride	0.292g
8	Na_2SO_4	sodium sulphate	0.072g
9	Tris	tris (hydroxymethyl aminomethane	6.118g
10	1.0M HCl	1M hydrochloric acid	0-5ml

Table 3.2. Ionic concentrations of human blood plasma, original SBF and conventional SBF (35)

Ion	**Human blood plasma (mM)**	**Original SBF (mM)**	**Conventional SBF (mM)**
Na^+	142.0	142.0	142.0
K^+	5.0	5.0	5.0
Mg^{2+}	1.5	1.5	1.5
Ca^{2+}	2.5	2.5	2.5
Cl^-	103.0	148.8	147.8
HCO_3^-	27.0	4.2	4.2
HPO_4^{2-}	1.0	1.0	1.0
SO_4^{2-}	0.5	-	0.5

Yilmaz et al., in their review, have discussed in detail the various types of modifications in the composition of SBF since its first formulation until 2020 and their purposes in different areas of biomedical research. In their study, (37) Li et al. employed a higher concentration of SBF (10x SBF) to accelerate apatite deposition on electrospun PCL scaffolds coated with gelatin. The use of a higher concentration of SBF tended to reduce the time taken to precipitate apatite on scaffolds and also to avoid the use of Tris and HEPES buffers in the SBF solution, which form soluble complexes with Ca^{2+} ions that reduce its concentration in the solution. The short incubation time was also particularly significant for degradable biopolymers.(38) Cai et al. employed supersaturated 5x SBF to accelerate the mineralisation of PLLA/gelatin scaffolds. However, the high concentration of HCO_3^- in the solution was seen as a problem since its decomposition could release CO_2 gas, which would increase the pH of the solution, and this

unstable pH could result in the deposition of homogenous precipitates. Therefore, to maintain the stability of the pH of the solution, the authors employed continuous CO_2 bubbling while mineralising the scaffolds, which resulted in the formation of carbonated calcium-deficient hydroxyapatite.(39)

The use of SBF to precipitate apatite on scaffolds has shown promise for biomimetic crystallisation, and the concentration of HCO_3^- has been extensively studied to understand its effects on the ability of the SBF solution to form homogeneously nucleated apatite particles. However, a few reviews have emphasised the importance of heterogeneous nucleation for simulating the *in vivo* bioactivity of bone formation.(40),(41) Homogenous and heterogenous apatite crystallisation refers to two different processes which form HA. Homogenous nucleation involves the formation of crystals directly from a homogenous solution, where the solute concentration is uniform throughout. The ionic components of the solution simply come together to form HA crystals without needing specific surfaces or templates to guide them, leading to a random distribution of crystal growth throughout the scaffold. Due to the metastability of the solution, introducing any piece of foreign body would inevitably induce mineralisation, even without the chemical or biological requirements specific to an implant material. Homogenous nucleation occurs rapidly due to the supersaturation of the mineralising solution, and researchers use this process in *in vitro* mineralisation studies. On the other hand, heterogeneous nucleation occurs when crystals form on pre-existing surfaces, such as nucleation sites, other mineral crystals, organic molecules, or functional groups on biomaterials, often following a specific pattern of deposition dictated by the template arrangement that results in controlled crystal growth. Researchers have used this type of crystallisation in developing implantable biomaterials with controlled mineralisation patterns.

3.6.2. Supersaturated solutions

In their study, Yang et al. employed a supersaturated mineralising solution on chitosan/PVA scaffolds containing $CaCO_3$. The authors performed mineralisation by placing the scaffold in a 50 mL beaker containing $CaCl_2$ powder and then placing the first beaker in a 250 mL beaker containing KH_2PO_4, followed by filling the beaker with distilled water until the liquid level covered the top of the smaller inner beaker at pH 3.6 and 25°C. Upon mineralisation, the scaffolds were rinsed with distilled water and placed in 1 M NaOH solution for 6 h. The authors postulated that the $CaCO_3$ particles in the nanofibres acted as nucleation points for the mineralisation process to produce homogenous island crystals of stable calcite and some

vaterite.[1,2] The authors also used this mineralisation solution in another study that employed chitosan/PVA scaffolds with and without N-carboxyethyl. In this case, polyanionic additive PAA was added to the solution setups to incorporate carboxylic groups onto the scaffold surface. This additive ensured the homogenous distribution of mineral deposits on the surface of scaffolds, and the authors reported that the concentration of PAA in the mineralising solution can aid in the controlled growth and distribution of the mineral phase.(43) Liu et al. used PAA as a $CaCO_3$ crystal growth modifier to deposit calcite thin film coatings composed of nanoneedles on CA nanofibres. The authors crystallised the $CaCO_3$ using a slow gas-liquid diffusion technique with $CaCl_2$ and NH_4HCO_3, resulting in calcite networks composed of microtubes after removing the CA nanofibres from the CA/$CaCO_3$ scaffolds.(44) Torricelli et al. in their study had utilised another slightly supersaturated calcium phosphate solution obtained by dissolving $CaCl_2.2H_2O$, $Na_3PO_4.12H_2O$, and $NaHCO_3$ to mineralise a co-electrospun PLLA/gelatin scaffold. The samples were incubated in the calcifying solution for 6h at 37°C, which resulted in the formation of spherical aggregates of poorly crystalline apatite with a Ca/P ratio of 1.45.(26)

3.6.3. Alternative dipping method

Ravichandran et al introduced a novel technique to mineralise electrospun PLLA/PBLG/Collagen nanofibres in their study. This technique is called the calcium phosphate dipping method, wherein the scaffold is immersed alternatively in 0.5 M $CaCl_2$ and 0.3 M Na_2HPO_4 multiple times to induce mineral deposition on the surface of the scaffold, which acts as bioactive macromolecules. The resulting apatite formation demonstrated a strong affinity for the adhesion and differentiation of adipose stem cells.(45) The same method was used by Gandhimathi et al to mineralise PCL/PAA/Collagen scaffolds and PLACL/SF/AA/TC scaffolds in their studies, which facilitated the adhesion, proliferation, and mineralisation of mesenchymal stem cells.(46),(47)

In another study, the authors Arafat et al. used the dipping method to create nucleation points of $CaHPO_4$ on the surface of PEG nanofibres by immersing the scaffold in 0.2 M $CaCl_2$ and 0.2M K_2HPO_4 alternatively for three cycles. The coated scaffolds were then mineralised using aqueous solutions of 0.1 M $CaCl_2$, 0.1 M H_3PO_4, 0.1 M Na_2CO_3, and 0.1 M CH_3COOH at pH 9 and titrated with NaOH. This study's XRD and FTIR results showed that the mixture of aqueous solutions deposited carbonated hydroxyapatite precisely.(48) This type of carbonated hydroxyapatite, which is another essential biological component of bone tissues apart from

hydroxyapatite, was found to be used in another study conducted by Liao et al., where the authors compared PLGA scaffolds and collagen scaffolds to investigate the importance of surface functional groups in the process of mineralisation.(49) Rajzer et al. have also reported similar results in their study incorporating carbonated hydroxyapatite into PLDL and PAN nanofibres that showed increased mineralisation potential and provided stability during the carbonisation process.(50,51)

When glutaraldehyde crosslinked gelatin scaffolds were coated alternatively with $CaCl_2$ and Na_2HPO_4, Zhao et al. reported that the minerals formed on the glutaraldehyde solution-treated scaffolds were smaller than the minerals formed on the glutaraldehyde vapour-treated ones, suggesting that glutaraldehyde solution crosslinking of gelatin scaffolds made them less rigid, thereby postulating more carboxyl groups on the surface, that improved nucleation and crystallinity of HA, but limited its size.(52)

Apart from the commonly used $CaCl_2$ and Na_2HPO_4 solutions, $Ca(NO)_3$ and $(NH_4)_2HPO_4$ solutions have also shown promising results, as demonstrated by Thien et al. In this study, the authors mineralised chitosan nanofibrous scaffolds alternatively using 0.3M $Ca(NO)_3$ and 0.18M $(NH_4)_2HPO_4$ for 4 cycles. The chitosan scaffolds were also incubated in SBF to compare the deposition of minerals in both methods. The alternative dipping method and SBF-treated scaffolds showed equally effective deposition of minerals, proving that the HA deposition from both techniques is equally biomimetic, except that the former only took three h. In contrast, the latter took 6 days to coat the scaffold with minerals.(53),(54)

3.6.4. Electrodeposition

Electrodeposition is another mineralisation technique initially used on metallic substrates, which involves the application of an electrical potential between two electrodes while immersing the scaffold in a solution containing mineral ions. At an optimised voltage, the scaffold surface becomes charged and attracts the mineral ions from the surrounding solution, leading to their deposition. He et al. introduced this technique to rapidly generate a versatile calcium phosphate coating on the surface of PLLA nanofibres. They compared the deposition rate, chemical composition, and mineral morphology to the mineral deposits of SBF. The authors reported that the electrodeposition method reduced the mineralisation time from ~2 weeks to 1 hr to achieve the same amount of mineralisation as SBF. The electrodeposition method made it possible to control the chemical composition and morphology of the calcium phosphate by varying the electric potential and electrolyte temperature, which resulted in a

tuneable composition of dicalcium phosphate dihydrate and hydroxyapatite; however, SBF only deposited low crystalline hydroxyapatite.(55,56)

Taylor et al. fabricated a three-dimensional trabecular scaffold with PLLA, PDLA, gelatin and nano-powder hydroxyapatite, which was then mineralised using electrodeposition with varying parameters (voltage, time and direction of mineralisation). The process involved placing a platinum wire (negative lead) through the cylindrical scaffold's centre and a silicon electrode (positive lead) around the scaffold. The authors submerged this arrangement in SBF at pH 4.4 and applied 5V,10V, and 15V voltages to the electrodes. Alizarin red staining assay confirmed maximum mineralisation at the voltage of 5V for 2 h.(57)

3.6.5. Electrospraying

This technique involves the generation of fine droplets from a liquid solution under the influence of an electric field that can be employed to deposit minerals onto scaffolds, enabling their uniform distribution, which is crucial for achieving consistent mechanical properties and bioactivity throughout the scaffold structure. Nedjari et al. employed an electrostatic template-assisted deposition of hydroxyapatite onto electrospun nanofibres collected on a micropatterned collector, introduced as an innovative method for precisely controlling the electrospray deposition of microparticles onto a substrate. This approach involved creating an electrostatic template by electrospinning a thin layer of fibres onto a collector with micro patterns such as hexagons, bars, blocks and mazes at the bottom. The electrospun fibres formed a template with regions of attraction and repulsion as they trapped charges over the recessed areas of the collector. During the subsequent electrospraying process, this electrostatic template guided the accurate deposition of the mineral particles. The authors integrated these scaffolds into a biochip featuring 21 wells and utilised them for studying MG-63 cell proliferation and mineralisation.(58)

3.6.6. Polymer-induced mineralisation

Polymer-induced mineralisation is an intrinsic mineralisation process in which a polymer itself contains ions or functional groups that facilitate the nucleation and growth of minerals, typically in a controlled manner. The presence of the predetermined nucleation sites allows for precise control over the location and rates of mineral deposition. Calcium silicate, a commonly used bone substrate known for its excellent bioactivity, promotes hydroxyapatite formation on the scaffold surface when calcinated at high temperatures. However, it is necessary to optimise

the calcination temperature, which influences the scaffold's degradation rate and bone formation behaviours. Du et al. investigated the properties of calcium silicate electrospun nanofibres after sintering them at 800°C, 1000°C and 1200°C. The nanofibres showed higher crystallinity and slower degradation rates with increased calcination temperature. Upon mineralisation in SBF for 5 days and α-MEM containing 10% foetal bovine serum for 7 days, the nanofibres displayed maximum mineral deposition with the fastest mineral nucleation and growth rate when calcined at 800°C.(59)

Chitosan is known for its bone-forming abilities; however, grafting anionic groups on its backbone to mimic the non-collagenous phosphoproteins can provide a negatively charged surface and act as *in situ* nucleation sites during mineralisation. Phosphorylation of chitosan to graft anionic groups has gained attention for its biochemical involvement in the mineralisation process, and several studies have reported the advantages of using phosphorylated chitosan for enhancing mineralisation and inducing osteoblast differentiation. One such study by Datta et al. analysed the mineralisation potential of N-methylene phosphonic chitosan electrospun nanofibres and hydrogel when soaked in SBF for 3 days. The electrospun nanofibres showed significant mineral deposition compared to the gels owing to the nanofibres' high surface area and the phosphonic groups' chelating tendency to attract calcium ions to the surface of the fibres. (60) Further, the authors conducted another study to analyse the mineralising potential of a synthetic analogue of non-collagenous phosphoproteins, i.e., partially phosphorylated polyvinyl alcohol (PPVA) fabricated as nanofibres and films. This PPVA nanofibre scaffold showed more homogenous mineralisation than the films due to the high surface area with phosphate groups as surface nucleation sites. However, the authors reported that PPVA induced changes in the physicochemical properties of the polymer by altering intermolecular hydrogen bonds and charge distribution, which made it more challenging to fabricate into electrospun nanofibres.(61) Another related study by Jie et al. revealed that phosvitin, a phosphoprotein found in egg yolk, promoted the transformation of DCPD to HA by accelerating nucleation when incubated in SBF.(62) These results were similar to the study by Liang et al., where the authors used layer-by-layer assembly of chitosan and phosvitin on cellulose nanofibres that drastically improved mineralisation.(63)

Like chitosan, gelatin also shows a high affinity for calcium ions, which makes it one of the most commonly used biomaterials to mimic the mineralisation of bone. Choi et al., in their research, studied the CaP crystal-forming ability of gelatin and its consecutive apatite formation in SBF by introducing Ca^{2+} and PO_4^{3-} ionic precursors in the electrospinning

solution. The aim of producing CaP crystals with precursors was to induce apatite formation on the external surface and on the inner layers of the scaffold to mimic the natural bone. The gelatin scaffolds with precursors were placed in counterion solutions ($CaCl_2$ and Na_2HPO_4) to induce crystal formation. Upon further mineralisation with SBF, the scaffolds containing Ca^{2+} precursors showed overall mineralisation in the inner and external surfaces owing to the higher affinity of calcium ions to the carboxyl groups on gelatin. The authors employed a similar approach by combining gelatin with PHBV at different ratios and reported that the increase in PHBV content increased the apatite formation. Although, in this case, only PO_4^{3-} were used as precursors, and due to an increased ratio of PHBV, which caused phase separation between the polymer and the precursor, the PO_4^{3-} interaction with gelatin was high following immersion in counterion solution of $CaCl_2$ leading to bead like aggregates on the scaffold surface that helped accelerate mineralisation in SBF.(64),(65),(66) However, Suslu et al. demonstrated that treatment of PHBV scaffolds with surfactants such as dodecyl trimethyl ammonium bromide, 12-hydroxysteric acid and sodium dodecyl sulphate has allowed for a uniform suspension of HA particles in its fibres, especially by carrying them towards the nanofibre surface with increased osteoblastic metabolic activity. These surfactants also activated the precipitation rate of apatite, which, in turn, affects the crystallinity percentage of the nanofibres.(67)

Polyamide-6, a synthetic polymer, shows structural and molecular similarity to collagen but has significant limitations, such as hydrophobicity and slow degradation. Pant et al., in their study, modified polyamide-6/lactic acid nanofibres using a bioactive plasticiser component containing calcium ions without disturbing the internal structure of the fibres. TEM images of the nanofibres displayed a core-shell structure with polyamide- 6 in the core and lactic acid in the shell. The electrospun scaffolds were soaked in 0.1M $Ca(OH)_2$ solution for 5 min, which resulted in a point-bonded fibrous structure due to the plasticiser effect of lactic acid, which then converted into calcium lactate. The authors reported that the core-shell structure of the fibres electrospun from a homogenous mixture of low and high-molecular-weight polymer was due to the varying blending ratio and molecular weights of the components of the electrospinning solution. Consequently, when mineralised using SBF for 10 days, the scaffold showed accelerated deposition of calcium compounds due to the partial dissolution of calcium lactate and the subsequent release of calcium ions, which acted as nucleation sites.(68) A similar study was also conducted by Hwang et al. using PCL/cellulose acetate nanofibres that supported these results by simultaneously regenerating calcium lactate and cellulose when treated with $CaOH_2$.(69)

Pant et al. have also demonstrated a similar improvement in mineral deposition in nylon-6/chitin butyrate core-shell electrospun scaffold fabricated similarly. The CaP deposition, in this case, was explained by the chitin butyrate bioactivity since it is the shell layer of the fibre.(70) Liao et al. developed a more straightforward process for directly incorporating calcium lactate in PCL/zein scaffolds using a two-nozzle electrospinning approach that increased the hydrophilicity of the scaffolds. The calcium ions provided a nucleation site for the deposition of calcium compounds, consequently enhancing the mineralisation in SBF compared to pure PCL scaffolds.(71) Polyphosphazene is a polymer class with a flexible backbone formed by alternate phosphorus and nitrogen atoms. Nykanen et al. fabricated an electrospun scaffold from cyclic phosphazenes and polyphosphazenes bearing 4-hydroxy-L-proline methyl ester and L-proline methyl ester that enhanced its bioactivity. After incubation in SBF for 48h the scaffold showed flower-like apatite formations with Ca/P ratios from 1.5 to 1.6.(72)

3.7. Modification of electrospun fibres' physico-chemical and morphological properties to enhance mineralisation

Modifying the properties of electrospun fibres to facilitate and promote mineralisation is an interesting area of research focusing on tailoring nanofibre properties to promote mineral deposition. These modifications can influence hydrophilicity, fibre electroactivity, porosity, fibre diameter, and surface roughness, affecting the deposition and growth of minerals on the nanofibres. It can also induce hydroxyapatite nucleation and bioactive ionic release on the surface, which aids in the mineralisation of the scaffold. These modifications are done pre-electrospinning or post-electrospinning based on their ability to affect the scaffold properties for optimal mineralisation. Coating of functional layers on electrospun scaffolds represents a valuable strategy to enhance its mineralisation by not only improving the scaffold's bioactivity but also by providing a surface that interacts favourably with calcium and phosphate ions that consequently facilitates the integration of the scaffold within the host tissue, promoting cell adhesion, proliferation, and differentiation. These modifications allow for precise control over the mineralisation process, ensuring the development of biomimetic scaffolds with specific modifications of properties without modifying the chemical structure of the underlying bulk material.

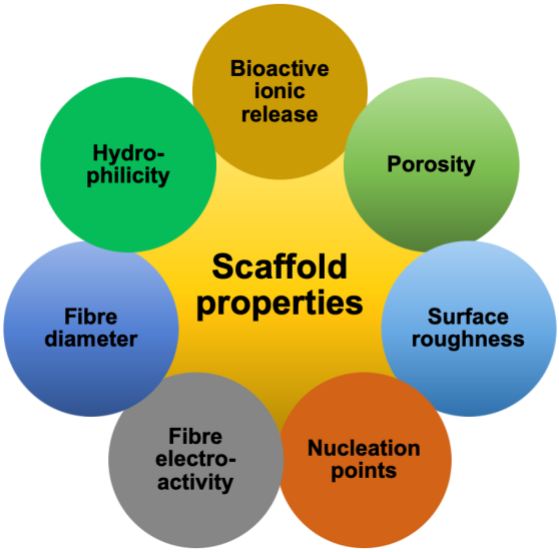

Figure 3.3. Physico-chemical and morphological properties of electrospun scaffold

3.7.1. Modifications of fibre hydrophilicity

Ngiam et al., in their study about the fabrication of nano-hydroxyapatite on PLGA nanofibrous scaffolds, demonstrated the difference in the mineral deposition on scaffolds that contained collagen and those without it. The authors have reported that the mineralisation of PLGA nanofibres increased its hydrophobicity, but the mineralisation of PLGA/collagen scaffold showed a significant increase in its hydrophilicity. The lack of strong hydrogen bonding between the mineral deposits and PLGA could explain this. The extent of HA formation on the surface was evident in the collagen-containing fibres based on the reported SEM, TGA and AFM results. These results suggest that collagen is a good template for nucleation of HA.(73) PCL scaffold fibres have also been incorporated with collagen while being co-electrospun simultaneously with PVP to improve hydrophilicity of the scaffold that facilitated Ca deposition when incubated in SBF. This study, conducted by Choubar et al., proved that the addition of collagen and PVP to the PCL scaffolds is a promising technique for developing an ECM-mimicking scaffold with a suitable microenvironment for cell adhesion, proliferation and differentiation while also enhancing the scaffold's mechanical properties, biodegradation ratio, water absorption and hydrophilicity.(74) Li et al. reported similar results when incorporating nanohydroxyapatite particles into the PLGA fibres pre-electrospinning. (75)

PHB is a natural macromolecule polyester whose degradation by-products are resorbable by the human body. However, it has shortcomings, such as brittleness, slow degradation rate and hydrophobicity, that limit its usage. Mohammadalipour et al., in their study, have incorporated lignin, another commonly used natural polymer in the field of tissue engineering, along with

PHB to overcome its mechanical and biological weaknesses. The resulting electrospun fibres were ribbon-like with a reduced diameter, increasing the scaffold's porosity. The authors used the Taguchi design to optimise the fabrication process to obtain a hybrid PHB/lignin scaffold at 6 wt% lignin with augmented hydrophilicity and biological properties that showed improved Ca/P ratio when immersed in SBF for 7 and 28 days as compared to scaffolds without lignin.(76)

To fabricate mechanically enhanced, carbon nanostructure functionalised electrospun scaffolds with increased hydrophilicity, Xu et al. have studied the effect of functionalising PLA scaffolds with coffee-ground-derived quantum dots (QD). The QD-modified PLA membranes showed increased hydrophilicity owing to their oxygen-rich functional groups from water contact angle analyses. This addition also enhanced the mineralisation of the scaffolds when incubated in 2X SBF for 1 week at 6.8 pH as compared to non-functionalised PLA scaffolds.(77)

Zein is an alcohol-soluble hydrophobic protein derived from corn, which contributes to water resistance when incorporated into a hydrophilic scaffold-like gelatin. This addition balances the scaffold's overall hydrophilicity, reducing swelling and enhancing resistance to solvent-induced damage. Deng et al. investigated its effects on mineralisation at various concentrations in combination with gelatin when fabricated as electrospun scaffolds, crosslinked with glucose and incubated in 10x SBF for different intervals. After morphological characterisation of the mineralised scaffolds, the authors reported that pure gelatin scaffolds showed the highest amount of mineral deposition with flaky apatite morphology, and the Ca/P ratio suggested the apatite layer was dicalcium phosphate dihydrate. On the other hand, the scaffolds containing zein at higher ratios indicated the formation of octacalcium phosphate. The authors reported that the mineralisation kinetics in pure gelatin scaffolds and gelatin/zein scaffolds were modified by zein because of the difference in the hydrogen bonds, influencing the crystal size, morphology and degree of mineralisation.(78) Yao et al. have reported similar results in their study using zein nanofibrous scaffolds functionalised using acetic acid to introduce carboxylic groups on the surface.(79) Zhang et al. incorporated a layer of apatite on zein nanofibrous scaffolds without any functionalisation but used a supersaturated 10x SBF to mineralise the scaffolds.(80)

Higher bioactive substances in polymeric scaffolds could accelerate regeneration and enhance recovery, especially if the bioactive composite has anti-osteoporotic, anti-microbial and anti-inflammatory characteristics for treating critical-sized bone defects due to trauma or osteosarcoma. *Cissus quadrangularis* is an example used in Ayurvedic medicine for centuries as a "bone setter". Parvati et al. have used this herbal therapeutic drug in PLLA scaffolds at

high weight percentages to study its effect as a biomaterial. Upon mineralisation in SBF for 14 days and consequent alizarin staining to measure calcium deposition, the scaffolds showed increased mineral content with an increase in the weight percentage of the herb. The authors also reported a rise in hydrophilicity, which explains the increase in mineralisation.(81) Calcium-containing PVA scaffolds also have a similar mineralisation effect in alternate immersion techniques by producing a continuous crystalline HA layer, although in this case, the calcium ions aided in the nucleation of the minerals.(82) Enayati et al. have used cellulose nanofibres along with HA nanoparticles as fillers in electrospun PVA scaffolds to increase their hydrophilicity and, thereby, their mineralisation in 1.5x SBF.(83) However, Si et al. incorporated nano cellulose and hydroxyapatite in PCL scaffolds to address the concern of mechanical strength that usually arises in cellulose nanofibres, and they also showed similar mineral nucleation effects when incubated in SBF.(84)

Kim et al., in their study, incorporated a bone interface scaffold with a compositional gradient fabricated by layering pure gelatin nanofibres with gelatin nanofibres containing different ratios of hydroxyapatite (20, 40 and 60 wt%). The authors used a hydroxyapatite formulation achieved by combining aqueous solutions of calcium nitrate and ammonium hydrogen phosphate, separately dissolved with gelatin powder and mixed dropwise while keeping a constant pH of 10 at 40° C. SEM images showed uniform nanofibres of the diameter 200-400nm for the 20% and 40% hydroxyapatite compositions, but non-continuous beaded fibres for the 60%. The authors concluded that this strategy of electrospinning nanocomposites would eliminate the limitations experienced in the conventional method of depositing apatite crystals post-electrospinning. They also reported that this method offers the advantage of fabricating a scaffold with multiple layers of varying amounts of hydroxyapatite while addressing the challenges of producing uniform nanofibres with a hydroxyapatite concentration of over 40%. (85)

Apart from proteins, peptides also constitute a promising biomolecule that can enhance biomineralisation because they can form three-dimensional structures that specifically support the growth of minerals. Self-assembling peptides such as P_{11}-4 and P_{11}-8 oligopeptides are amphiphilic as they mimic the phosphoserine-rich motifs observed in mineralisation-related proteins. Gharaei et al. and Araujo et al. have used this oligopeptide coated over PCL electrospun scaffolds in various concentrations to identify the samples with the highest mineralisation content after incubating in SBF under shaking conditions for up to 4 weeks. The results of both the studies based on elemental analysis and X-ray diffraction analyses proved

that the concentration of P_{11}-4 peptide absorbed onto the PCL scaffold influenced its mineralisation potential proportionally by increasing the scaffold's hydrophilicity and nucleation points for attachment of the mineralising ions from the SBF.(86),(87)

Synthetic peptides have also been beneficial to increase calcium phosphate deposition and regulate its crystal structure. Ohkawa et al. have incorporated a synthetic peptide constructed from O-phospho-L-hydroxyproline (Hyp(PO_3H_2) residues into gelatin fibres. Upon calcium phosphate deposition using an alternate immersion technique, the authors reported that mineralisation resulted in crystalline octacalcium phosphate transforming into hydroxyapatite. The authors reported that the phosphoryl groups of the synthetic peptides affected both the crystalline phase and the amount of calcium deposition, depending on the position of the phosphoryl groups in the repeating sequence of the polypeptides.(88)

Adsorption of carboxymethyl cellulose onto regenerated cellulose scaffolds in the presence of $CaCl_2$ increased its hydrophilicity by increasing the number of carboxylate groups on the fibre surface, as demonstrated by Rodriguez et al. The authors treated the regenerated cellulose scaffolds in CMC for 24h at 37°C) or 2h at 80°C) along with 0.1 NaOH. When mineralised with SBF for 1 week, both types of treated scaffolds showed a pearl-on-string arrangement of amorphous Ca/P indicated by XRD analyses with almost no difference in crystal structure or growth between the two types of treated scaffold.(89) However, in their study, Yamaguchi et al. demonstrated that the carboxymethylation process can control the size and concentration of HA precipitation and increase NaOH concentration.(90) Li et al. have used a layer-by-layer assembly technique to coat gelatin on electrospun PCL scaffolds to mimic the bone ECM closely. The authors coated the PCL scaffolds with poly(styrene sulfonate, sodium salt) and gelatin as a bilayer until the scaffold surfaces had five bilayers with gelatin as the outermost layer. Poly(styrene sulfonate, sodium salt) is a negatively charged polyelectrolyte that can immobilise positively charged gelatin onto the scaffold surface to avoid the crosslinking of gelatin along with the cytotoxicity caused by the chemicals employed during crosslinking. Calcium phosphate was deposited on the gelatin-covered fibres by mineralisation in 10x SBF for 2h. The authors have reported that the uniform distribution of mineral deposits was possible due to the increased hydrophilicity and introduction of -COOH and -NH_2 groups of gelatin.(38) Another non-toxic method for crosslinking gelatin is through the use of microbial transglutaminase, which also significantly improved its mechanical properties, as demonstrated by Taylor et al.(91)

3.7.2. Influence of fibre diameter

Nitya et al. reported that the use of halloysite-based nanoclay in PCL scaffolds significantly impacted its mineralisation properties, i.e., a uniform increase in diameter was observed at higher ratios of nanoclay compared to pure PCL scaffold. This observation is in contrast with another study by Dehkordi et al. that used Layered Double Hydroxide (LDH), a brucite-based nanoclay, to fabricate bioactive electrospun PCL scaffolds at concentrations varying from 0.1-10 wt%, following the same protocol. This study identified that an optimal ratio of PCL: LDH of 1 wt% enhanced its mechanical properties and protein absorption along with mineralisation compared to the scaffolds with other concentrations of LDH, and the fibres experienced a decrease in average diameter at this weight concentration. Other studies have also reported that a reduced fibre diameter can improve mineralisation potential due to an increased surface area. The authors attributed the difference in the fibre diameter to the increased electro-spinnability of the brushite-containing scaffolds and the reduced mobility of the PCL chain experienced during fibre formation, which resulted in thinner fibres. In the former case, the halloysite-based scaffold might have experienced a higher viscosity of polymer solution due to its smaller particle size than brushite nanoclay, resulting in a thicker fibre diameter. (92),(93)

LDH nanoparticles are also an anionic type of nanoclay with positively charged layers, which present a unique layered crystal structure interleaved with charge-balancing anions and water molecules. Therefore, their incorporation into electrospun scaffolds provides specific functionalities such as increased hydrophilicity and drug delivery. Baradaran et al. reported that incorporating magnesium/aluminium layered double hydroxide microsphere aggregates in PCL scaffolds increased their hydrophilicity, but Mg^{2+} ions prevented matrix mineralisation and calcium deposition. (94)

Liao et al., in their study, have employed a comparison between two types of PLGA scaffolds with different fibre dimensions, one with thin fibres (97.5 ± 38.9 nm) and another with thick fibres (319.9 ± 118.1 nm), to investigate the influence of fibre diameter on apatite nucleation and growth. Upon mineralisation of these scaffolds with aqueous solutions of $CaCl_2$, H_3PO_4, and CH_3COOH, the thin fibres had a considerable amount of apatite growth almost throughout the scaffold's surface but with large aggregations as compared to the thick fibres that were unable to promote nucleation and crystal growth due to the reduced amount of surface area.(49)

On the contrary, Zhang et al. have mineralised electrospun PLGA scaffolds containing multi-walled carbon nanotubes using 1.5x SBF even though the modified fibres experienced an increase in diameter due to the high aspect ratio of the carbon nanotubes, which means they

have a large surface area compared to their volume. However, multi-walled carbon nanotubes are known to enhance a scaffold's mechanical and electrical properties, which could have contributed to the increased mineral deposition on the fibres along with the increased surface area that facilitated the formation of apatite growth.(95) In their study, He et al. compared the mineralisation effects of PLLA scaffolds with varying polymer concentrations using electrodeposition and incubation in 1.5x SBF. The authors reported that with the increase in the diameter of the nanofibres, the mineral deposition during electrodeposition also increased. The authors hypothesised that fibres of larger diameters provided a larger surface area on individual fibres, allowing for the development of more stable mineral nuclei and the growth of larger mineral particles, leading to an increased deposition rate. However, the fibres mineralised in 1.5x SBF experienced a slower deposition rate since the nucleation sites on the fibres equally compete for the calcium and phosphate ions, which led to a non-directional uniform coating with a smaller crystal size. For mineralisation using SBF, smaller diameter fibres with larger total surface area would be preferable, leading to a faster mineral deposition.(56) PEG was incorporated into PCL nanofibres to reduce its hydrophobicity and toxicity, as studied by Tiwari et al. The authors have employed an electrospinning/netting technique to fabricate a heterogenous scaffold with a blend of PCL primary fibres with PEG nano-nets. These nano-nets accelerated the nucleation of calcium phosphate deposition when incubated in SBF by drastically improving the scaffold's hydrophilicity.(96)

3.7.3. Modifications of fibre electroactivity

Electrospun scaffolds of PCL and hydroxyapatite with a conductive polyaniline coating were fabricated by Rajzer et al. using simple ink-jet printing along with conventional electrospinning to stimulate faster mineral deposition. Although this study proves that the conductive layer on the scaffold does not affect its mineralisation when incubated in1.5x SBF for 2 weeks as compared to the scaffold that does not have the conductive layer, it is not clear if the conductivity of the polyaniline layer improves the mineral deposition in quantity and speed due to its ability to stimulate ion transport and deposition.(97)

Jeong et al. developed a conductive nanofibrous electrospun PCL scaffold by coating it with a hydrogel containing graphene oxide and PVP and crosslinking them through gamma irradiation. This conductive scaffold showed increased mineral deposits upon immersion in SBF, owing to graphene oxide, a well-known amphiphilic.(98)

Polypyrrole is another biocompatible polymer known for its electrical conductivity. Jing et al., in their study, have attempted to study the effect of electrical stimulation (75mV/mm, 3h per day) on the mineralising potential of PPY-coated PLLA fibres when immersed in 5x SBF until 36h. The authors reported an accelerated apatite deposition on the PPY-coated fibres due to the ionic adsorption on the rough surface of PPY, which acted as nucleation sites for the mineral deposits.(99)

3.7.4. Enhancing HA nucleation

Silver nanoparticles and simvastatin-incorporated PCL scaffolds containing cellulose acetate have been studied for their mineralisation potential by Ko et al. using SBF for 1,2 and 3 weeks of incubation. The study revealed that the mono-dispersion of Ag nanoparticles in the scaffold accelerated mineralisation owing to their high surface area to volume ratio, which increased the absorption and retention of the mineral ions from the SBF as analysed by SEM and EDS. The simvastatin drug release from the scaffold also aided this process, acting as nucleation points on the fibre surface rapidly depositing minerals on the scaffold.(100)

Ashraf et al. conducted a study with Ag and titanium dioxide nanoparticles. They investigated the adverse toxic effects of unreduced Ag nanoparticles in cellulose nanofibres, as reported from the drop in cell viability after 6 days of incubation with fibroblasts, proving that optimising the concentration of Ag nanoparticles is mandatory to build an efficient scaffold without adverse reactions to the surrounding tissues. It might be interesting to note that the mineralisation of this scaffold using SBF for 15 days was independent of the concentration of both nanoparticles.(101)

Lignin is known for its compatibility with polar polymers such as PCL, which promotes a miscible structure that can overcome the shortcomings of polymers when used separately. Wang et al., in their study, investigated a novel property of lignin, i.e., to mediate interfacial mineralisation. PCL electrospun scaffolds containing lignin at different concentrations (10-50 wt %) were fabricated and soaked in 1.5 SBF solution for 5 days, which resulted in a uniform coating of mineralisation on the surface of the scaffold due to the high availability of phenolic hydroxyl and aliphatic hydroxyl groups that donated reactive sites for the calcium and phosphate ions. The blank PCL scaffolds showed no traces of particulates.(102)

Several studies have reported using silk fibroin to enhance the nucleation of mineral ions while also improving the scaffold's hydrophilicity. It contains two vital proteins – sericin and fibroin- with low immune rejection. Shanmugavel et al. employed silk fibroin in their study to regulate

the incorporation of aloe vera in PCL scaffolds, consequently improving the scaffold's mineralisation potential.(103) Pascu et al. had similar effects when they incorporated silk fibroin with PHBV scaffolds to improve the balance in the electrospinning dynamic that was changed by including nanohydroxyapatite particles.(104) Panda et al. used electrospun eri-tasar silk fibroin for its hydrophilicity and the ability to induce osteogenesis with its amino acid sequences.(105) Luo et al. also investigated the ability to induce osteogenesis by providing biochemical cues to cultured cells in PCL/silk fibroin scaffolds. The authors coupled these scaffolds with polyglutamate acid and BMP-2 peptide, which improved binding with mineralised crystals and enhanced the expression of osteogenic genes compared to PCL scaffolds.(106) Gao et al. observed that adding tussah silk fibroin to PLGA nanofibres accelerated its mineralisation and improved its mechanical properties.(107) M13 bacteriophage is known for its integrin binding and calcium binding sites. It can also impart biochemical cues, but it has some limiting factors in that it is mechanically weak and processing extensively. To address these concerns, Lee et al. fabricated an electrospun PCL scaffold containing M13 bacteriophage and alginate. In SBF, these scaffolds formed homogenous mineral coatings owing to the negative phages on the surface that could attract the calcium ions and, consequently, the phosphate ions.(108)

Another similar study by Junka et al. used BSA coated on decellularised ECM cultured on PCL scaffolds to act as a calcium-binding biomolecule. The decellularised ECM and BSA-coated PCL scaffolds were incubated in 2x SBF for 7 days after activating the surface with 1 M Ca^{2+}($CaCl_2$) and 1 M PO_4^{3-}(Na_2HPO_4) for 30 s. The concentration of the bio-deposited calcium, as calculated using a calcium liquicolor assay kit (CPC), showed a high value for the samples with BSA and decellularised ECM coating as compared to the samples without either BSA or ECM, thus proving that this dual coating is synergistic to mineralisation with specific effects on size and distribution of the CaP crystals.(109)

Interestingly, Cheng et al. smashed electrospun mats into short nanofibres to develop a composite aerogel where these short nanofibres acted as nucleation points for HA deposition. The authors have used a hybrid silk fibroin/chitin electrospun scaffold, smashed into smaller pieces and incorporated into an ethylene glycol diethyl ether/silk fibroin aerogel at various ratios. This coating showed enhanced mechanical properties and uniform homogenous deposition of HA crystals when immersed in 30 mL of SBF for 7 days at 37°C as evaluated by SEM images.(110) Chitin whisker is the by-product of acid hydrolysis of chitin, and its incorporation in electrospun scaffolds has also shown improvement in composite mechanical

properties, as demonstrated by Pangon et al. The scaffolds in this study were electrospun using PVA, chitosan and chitin whiskers. When incubated in 10x SBF, the scaffolds showed remarkably improved mechanical properties while maintaining their biocompatibility and biodegradability due to the crystalline nature of chitin whiskers.(111) Zeolite is another such nanocrystalline composite used by Jazi et al. in their study to improve the bioactivity in PLGA scaffolds.(112)

Biocompatible organic silane agents such as 3-glycidoxypropyltrimethoxysilane (GPTMS) have been used as a hydrophilic coating on electrospun nanofibres to induce deposition of hydroxyapatite layer on its surface. In their study, Ghorbani et al used a combination of GPTMS and PVA to coat the surface of polyaniline nanofibres activated by oxygenated plasma treatment. This type of hybrid organic-inorganic scaffold has not only shown to provide a stable surface coating by crosslinking the hydrophilic functional groups of the polymer, but also the SiOH and SiOSi functional groups found in the structure of GPTMS acted as nucleation sites for the deposition of apatite layers by attracting calcium ions as seen in this study.(113)

Tannic acid is another surface coating used in the study by Zheng et al. to incorporate nucleation sites for Ca^{2+} ions for accelerated hydroxyapatite deposition on silk fibroin scaffold. The resulting hybrid scaffold displayed enhanced mechanical properties due to conformational changes in the random coils β sheets triggered by the tannic acid molecules) compared to the unmodified scaffolds. Upon mineralisation using 1.5x SBF, the modified scaffold showed uniform and continuous growth of minerals after 7 days of incubation.(114)

Among the various functional changes that Bioglass® induces on a nanofibre surface, introducing nucleation sites is essential and tends to be the most common reason for its use as a hybrid coating material. Silanol groups on the surface of the fibres act as nucleation sites for the deposition of minerals, followed by the calcium ions released from the Bioglass® coating that reacts with the phosphate ions in the SBF to precipitate HA-like material on the surface. Gao et al., in their study, have tested the effect of Bioglass® coating on PVA scaffolds and gelatin scaffolds separately, fabricated using a combination of sol-gel processing and electrospinning for their potential to form mineralisation *in vitro* using SBF.(115,116)

Catecholamines are molecules characterised by a catechol nucleus, a benzene ring with two hydroxyl groups and an amine group. In the human body, they represent a particular group of neurotransmitters and hormones such as dopamine, norepinephrine and epinephrine. Specifically, in mineralisation, catecholamines can modify the behaviour of collagen in the ECM by forming strong coordination bonds with metal ions such as Ca^{2+} with the help of the

catechol functional groups. Therefore, they act as nucleation sites for calcium phosphate mineral deposition and regulate the growth of the crystals. Ghorbani et al., in their study, have demonstrated that the catecholamine moieties in polydopamine coated on polyurethane/graphene oxide nanofibres have played a key role in enhancing mineralisation in SBF by accumulating Ca^{2+} ions at the interface through electrostatic interactions and acting as nucleation sites for HA.(117) Dhand et al. used two different catecholamines, dopamine and norepinephrine, along with $CaCl_2$ in collagen nanofibres which were then mineralised by incubating in $(NH_4)_2CO_3$ to precipitate $CaCO_3$ on the scaffold surface. The authors reported that divalent cations in the electrospinning solution triggered the oxidative polymerisation of the catecholamines, which led to the formation of a collagen network with welded or soldered joints, i.e., fibres were no longer distinct. The authors negated this process by using a crosslinking method to stabilise collagen while mineralising the fibres.(118)

Another strategy to induce gradient mineralisation is surface modification of electrospun scaffold with gelatin grafts. By varying the grafting concentration at different places on the scaffold, it is possible to control the nucleation and growth of HA on the fibres. Cui et al. and Zou et al. employed gelatin grafting on PDLLA nanofibres in their studies to induce the formation of nonstoichiometric nanostructured HA. After introducing free amino groups on the surface of the PDLLA scaffold through aminolysis, the authors used glutaraldehyde treatment to convert these free amino groups into aldehyde groups. The amount of gelatin grafts and amino groups were quantified using kinetic equations as a function of aminolysis time. The scaffolds were analysed with SEM and XRD after mineralisation in 1.5x SBF for 2,4 and 6 days. The results showed that the regions grafted with gelatin and incubated in SBF for 4 and 6 days showed increasing amounts of mineral coatings, and their crystal size, as calculated with Scherer's formula, decreased with an increase in gelatin content. The authors reported using this strategy to control the size of HA crystal formation to 10-20 nm, similar to the apatite found in bone. The increase in mineralisation content was due to the abundant supply of coordination sites available for calcium ions, which also limited the size of the HA crystals. Zou et al. also employed a similar technique in another study with gelatin grafting on PDLLA nanofibres followed by mineralisation with SBF, which was then dissolved in THF and electrospun again to fabricate blended electrospun composite fibres. These HA/PDLLA scaffolds were employed to study *in vivo* to promote bone healing of femoral defects. Zou et al. also employed the gradient mineralisation of gelatin-grafted PDLLA scaffolds to the load plasmid DNA contents as they have a higher affinity for calcium phosphate. The authors reported that scaffolds with plasmid DNA gradient loading content can achieve target protein

expression and identical autocrine and paracrine signalling compared to native tissue, which in turn can aid in regulating the release of growth factors in scaffolds. This controlled growth factor release is considered vital for supporting the growth of interfacial tissue regeneration.(119),(120),(121) Lu et al. fabricated PDA-coated, doxorubicin, and lamellar HA-loaded PLGA scaffolds and investigated drug release for simultaneous prevention of tumour recurrence along with bone regeneration. This scaffold also showed good bioactivity after mineralisation in SBF owing to the PDA coating, even though doxorubicin and PLGA are hydrophobic and lack sites for nucleation.(122) A similar study conducted with amoxicillin and HA-loaded PCL scaffolds showed that the interaction between the drug and HA compromised the mechanical properties after mineralisation, compared to the common trend where the tensile strength usually increases after mineralisation. This interaction also modified the drug release pattern, reducing the initial rapid release or burst effect in drug-loaded scaffolds.(123) While incorporating drugs into scaffolds can benefit specific applications, its adverse effects on scaffold properties are also critical factors.

3.7.5. Bioactive ionic release

Serio et al., in their study, used PLLA electrospun scaffolds incorporated with bioactive silica-based glass particles to investigate its potential to form apatite coating when immersed in SBF for 21 days on an oscillating tray in an incubator. The large quantities of deposited minerals showed typical cauliflower-like morphology attributed to the bioactive ionic release of calcium, phosphate and silica from the glass particles, which acted as building blocks for hydroxyapatite formation.(124)

Doping hydroxyapatite with other trace elements to replace calcium has been researched widely for its effects on the scaffold's properties and mineralisation potential. Each of these dopants brings unique characteristics that can influence the mineralisation process and the resulting properties of the scaffolds. Wang et al. and Shi et al., in their studies, entrapped poly(acrylic acid) modified Zn-doped calcium phosphate nanoparticles in PLGA scaffolds, which resulted in enhanced mineralisation in SBF. Zn is an indispensable trace element in bone regeneration and is known to improve bioactivity in nanofibrous scaffolds. The authors reported that the presence of Zn led to the formation of amorphous calcium phosphate and enhanced the osteogenic differentiation of rADSC cells cultured on the scaffolds by monitoring its ALP activity.(125,126) Weng et al., in their study, incorporated strontium-doped HA into polydopamine-coated PCL scaffolds. Upon mineralisation with 10x SBF that contained

strontium and calcium ions, the scaffolds showed accelerated mineralisation within 1 day, and its degradation and release of ions took up to 28 days. The mechanical properties were also 6 times higher as compared to pristine PCL fibres.(127)

Another silica-based functional additive is silica-doped vaterite, developed by Obata et al., which was electrospun along with PLLA to prepare flexible porous scaffolds in their study. Vaterite is one of the three crystalline calcium carbonate ($CaCO_3$) versions. When immersed in SBF, its most unstable polymorph can also be induced to transform into valuable biominerals such as hydroxyapatite. The authors have justified silica use because it can stimulate osteogenic processes in cells when used in trace amounts, similar to Bioglass®. Vaterite was employed to release calcium ions upon degradation of the thin PLLA layer, which can help accelerate the mineralisation process. The vaterite was doped with silica to prevent the loss of flexibility caused in the scaffold due to the coordinate bonds formed by the calcium ions with carboxy groups on the PLLA surface. The carboxy groups formed amide bonds with amino groups in the siloxane phase and coordinated with calcium ions released from the vaterite on the scaffold surface by adding silica.(128) Wakita et al. have also reported similar findings in their study conducted on siloxane-PLA-vaterite electrospun scaffolds.(129) Apart from using bioactive glass as particles, Konyali et al. have also investigated the effects of bioactive glass fibres incorporated into PCL scaffolds. Upon mineralisation in SBF, both types of bioactive glass were observed to enhance mineral deposition. However, the calcium-phosphate-based material formation was higher in bioactive glass particle-containing samples than in glass fibre-containing samples. The particle-containing scaffolds also reported a higher degradation rate and an increased release of silicium ions, which explains the higher calcium phosphate deposits.(130) These results were supported by another study by Deliormanli et al. that employed bioactive glass fibres to investigate their mineralisation as a function of immersion time in SBF and fibre concentration.(131)

In their study, Kim et al. produced hollow vaterite microspheres by introducing CO_2 gas to an aqueous mixture of $CaCl_2$ and NH_4OH in the presence of dopamine. These microspheres were then electrospun along with PCL to fabricate composite bone scaffolds. Upon immersion in SBF for 48 h, the nanofibres showed a lath-like hydroxyapatite formation. The authors also fabricated hybrid scaffolds of PCL coated with dopamine and $CaCO_3$ microspheres, showing untransformed calcite crystals on the surface.(132) Cao et al. had similar results when employing $CaCO_3$/casein microspheres in PCL scaffolds.(133) The use of CO_2 along with $Ca(OH)_2$ in mineralising $CaCO_3$ containing PVA/chitosan scaffolds were also investigated by

Sambudi et al.(134) Rezk et al. in their study have used beta-tricalcium phosphate and simvastatin to fabricate functional composite nanofibre scaffolds and investigated its mineralisation potential in SBF. Beta-tricalcium phosphate is known to release calcium and phosphate ions, and their release provides a local concentration of ions that can enhance mineralisation. The mineralised scaffolds showed a uniform distribution of apatite-like layers after 14 days of immersion in SBF.(135)

Elsayed et al. have used CaCO3-incorporated gelatin electrospun scaffolds to fabricate calcified gelatin scaffolds for dental applications. The calcification occurred as a consequence of immersing the CaCO3-containing gelatin scaffolds in PBS, which caused the swelling and degradation of the fibres, thereby releasing calcium ions onto the surrounding PBS. The authors conclude that the apatite growth found after 4 weeks of immersion in PBS was due to $CaCO_3$ in the fibres that acted as nucleation sites for the calcium ions in PBS primarily released from the scaffold. The swelling also enhanced the deposition by creating hydroxyl groups on the surface of the fibres.(136) Another unique enamel matrix protein that was reported useful in controlled-release electrospun scaffolds for dental applications is amelogenin.(137) COOH-functionalised nanodiamond particles (COOH-NDPs) induced homogenous mineralisation when incorporated into gelatin nanofibres. Introducing COOH-NDPs into fish gelatin nanofibres in concentrations ranging from 0.25% to 1% did not significantly alter the capacity for mineralisation in SBF, as seen from detailed microstructural and spectroscopic investigations. Interestingly, under Ca/P alternate immersion conditions, TEM analysis confirmed the selective development and firm attachment of nano-apatite crystals near COOH-NDPs-embedded fibre regions.(138) One study also specifically investigated a strategy to fabricate calcium-containing gelatin nanofibre electrospun using non-toxic solvents such as ethanol, which were mineralised using phosphate solutions. The authors reported the formation of minerals in various morphologies and combinations by modifying reaction parameters such as temperature, pH, reaction rate, and ions in the mineralisation solution.(139)

Zhao et al. investigated the effects of adding carboxymethyl chitosan to polyethylene oxide electrospun scaffolds and its apatite-forming potential when soaked in 5x SBF until 16 h. Carboxymethyl chitosan is a polysaccharide derivative of chitosan that has been reported to release calcium ions, enhancing the nucleation of mineral ions from SBF. Further, carboxymethyl chitosan also aided the growth of apatite through its functional carboxyl groups, making the surface more bioactive.(140)

Choi et al. incorporated PHBV/gelatin scaffolds with PO_4^{3-} ions by adding 16 w/v% of 0.2 M K_3PO_4 to the polymer solution before electrospinning. When immersed in 0.2 M $CaCl_2$ solution

for 20 mins at 37°C, the electrospun scaffold formed CaP crystals on the fibre surface. Upon immersing in SBF for 3 days, the scaffolds showed a layer of apatite formed with the help of the fine CaP crystals and its partial dissolution in the local environment that caused the supersaturation of Ca^{2+} and PO_4^{3-} and consequently its precipitation on the fibre surface.(66) Incorporation of $CaCl_2$ in PU nanofibres also has a similar effect on ionic release as studied by Nirmala et al. The addition of the $CaCl_2$ salt resulted in reduced fibre diameter, forming ultrafine mesh-like nanofibres with a large surface-area-to-volume ratio and interconnected porosity. Upon immersion in SBF, a monotonic increase in apatite crystal size was seen with an increase in $CaCl_2$ concentration.(141)

Biomineralisation in living organisms involves the deposition of inorganic crystalline components onto an organic matrix consisting of proteins, primarily differentiated into collagenous and non-collagenous. The presence of proteins in the organic matrix controls the nucleation, growth and geometry of the crystals deposited. Afza et al. have incorporated BSA into their electrospun PCL scaffolds containing hydroxyapatite nanoparticles and studied the attachment of BSA to hydroxyapatite through molecular dynamic simulation to amplify the absorption of calcium phosphate during mineralisation. The study concluded that the attachment between BSA and hydroxyapatite nanoparticles produced non-smooth broken fibres, which amplified the Ca/P atomic ratio when immersed in SBF for 7 days compared to the scaffolds with only BSA.(142) In reverse order, a mineral coating on electrospun scaffolds can also help bind proteins to fabricate bi-functional scaffolds. Lee et al., in their research, have engineered a bi-functional interface on a mineralised electrospun PCL/gelatin scaffold by introducing a fusion protein comprising fibronectin 9-10 domain-containing osteocalcin ($FN_{III9\text{-}10}$ – OCN) to promote stem cell adhesion, growth and osteogenic differentiation. The anchoring mechanism for this protein was employed through hydroxyapatite mineralisation on the scaffold surface using 2x SBF for 4 days and 1x SBF for 2 days. The stable binding between the protein and mineral surface was highly selective and facilitated by the molecular recognition of OCN to the apatite crystal lattice. After culturing mesenchymal stem cells on the fibres with and without the protein link, the authors observed a significant level of cell adhesion and distribution, and after 2-3 weeks, enhanced expression of osteogenic genes and proteins was exhibited.(143)

3.7.6. Effects of porosity

In solid nanofibres, the surface area available for the precipitation of mineralising ions is much less than in porous nanofibres. In their study, Zhu et al. used acetone to increase porosity in electrospun PLLA nanofibres containing hydroxyapatite nanoparticles. The scaffolds were immersed in acetone for 5 minutes at room temperature before incubating in 5x SBF for 6 h. The resulting porous nanofibres were 3 times bigger in diameter and showed accelerated apatite coating owing to the solution's infiltration rate.(144) Rodriguez et al. incorporated a computer-aided design approach involving CO_2 laser ablation to achieve controlled microporosity of a cellulose acetate scaffold with controlled microarchitecture. Upon mineralisation, the porous scaffolds showed slight variations in atomic composition, i.e., the C and Mg were 1.4 and 1.6 times higher, respectively, compared to the non-porous scaffolds. The inner pore surface had 1.7 times more Ca and P concentrations, and the EDX data showed a higher Ca/P ratio for the porous scaffolds.(145) Lee et al. fabricated PLLA scaffolds with lactic acid, which contains negatively charged -COOH groups that induce the strong repulsion of spinning jets, resulting in the fabrication of low-density, high-porosity, fluffy scaffolds. The mineralisation potential of the PLLA/lactic acid scaffolds was investigated by incubating in SBF as compared to a PLLA mat without lactic acid, and the authors reported that the large pore size of the spongy scaffolds allowed the SBF solution to enter into the pores and the surface functional groups assisted in the nucleation of HA thereby enhancing mineralisation.(146) In one exciting study by Sun et al., PLLA/PCL/silk fibroin three-dimensional scaffolds were fabricated by dynamic liquid support electrospinning that resulted in nanoyarn scaffolds. Dynamic Liquid Support Electrospinning (DLSE) is an advanced technique that collects electrospun fibres on a liquid support or dynamic liquid layer during electrospinning. This approach aims to overcome some limitations of traditional electrospinning methods and offers unique advantages for fabricating complex and functional nanofibre structures; in this case, the fibres had a smaller diameter, resulting in higher porosity than scaffolds without silk fibroin. The nanoyarn scaffold was mineralised using an alternate immersion method using 6 cycles and aided in good proliferation and osteogenesis of cells cultured on it.(147) Another similar technique, called the wet-electrohydrodynamic jet process, was employed by Kim et al. to develop a controlled macroporous PCL scaffold by direct electrospinning of the polymer melt onto an ethanol solution. These scaffolds were then plasma treated before mineralising in SBF for 7 days, resulting in a homogenous layer of mineral coating without significantly affecting the scaffold's porosity.(148) Using a porogen to fabricate fast-dissolving fibre fractions results in scaffolds with adjustable pore sizes, as demonstrated by Mi et al., where the authors used NaCl crystals

to produce rectangular pores polyurethane scaffolds. In this study, the authors used different solvents to fabricate different pore morphologies.

Similarly, PHBV scaffolds with PEO porogen at various concentrations were fabricated by Lyu et al. The PEO parts were later dissolved in SBF and water, which created a synergistic effect between pore formation and calcium deposition. The authors reported that the pore size increased with an increase in PEO concentration and that the pore size in the films was more extensive than that in nanofibres, which ranged from 70 to 120 nm.(149,150)

3.7.7. Effects of surface roughness

Curcio et al had incorporated a thin film coating of bioactive glass-ceramic material supplemented with manganese ions on hybrid PDLLA/gelatin electrospun scaffolds in their research to investigate its ability to induce mineralisation when immersed in SBF for 28 days. This study's microscopic and spectroscopic results showed a densely packed layer of nanocrystalline HA completely covering the sample's surface. In contrast, the samples not coated with the thin film had no apatite deposition, concluding that scaffolds with this coating type that change the fibres' morphology by increasing its roughness represent a promising strategy for complex osteochondral tissue development.

Another study by Yunos et al, also conducted on PDLLA fibres to increase its surface roughness, implemented deposition of the electrospun PDLLA fibres on 45S5 Bioglass® sintered discs to fabricate a bioactive bone scaffold. The surface of the PDLLA coated Bioglass® pellets were then characterised using white light interferometry before and after mineralisation in SBF until 4 weeks to investigate the surface topography induced by fibres and its characteristic surface roughness values. The resulting values of surface texture showed a significant increase, and consequently, higher mineralisation and cell adhesion were observed after SBF treatment and cell culture with MC3T3 cells.(11)

3.8.Pre-treatment of electrospun scaffold surfaces to support mineralisation

Synthetic polymer nanofibres, in general, are hydrophobic and do not carry polar functional groups such as -COOH, -OH, and -NH_2 in abundance to attract mineralising ions. In order to facilitate the homogenous integration of calcium, phosphate and other ions to the fibres, the hydrophobicity of the polymers needs to be reduced by introducing functional groups to the fibre surface. Functionalising polymeric fibres can also be a powerful strategy to introduce

nucleation points on their surface to enhance the geometry of the resulting calcium phosphate minerals and their rapid homogenous deposition. Three types of functionalising treatments have been found commonly in the literature: chemical, physical and physicochemical.

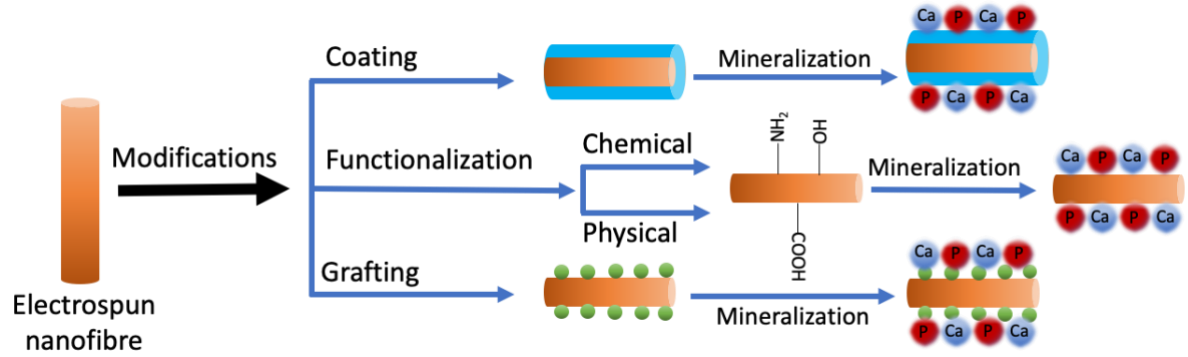

Figure 3.4. Different types of modification of electrospun scaffolds to support mineralisation

Chemical functionalisation

Functionalisation of electrospun fibre surfaces through chemical methods induces irreversible changes to the polymer's backbone by breaking chains at specific sites or groups. Hydrolysis and aminolysis are the most widely used chemical treatments before the mineralisation of electrospun scaffolds to enable rapid and homogenous deposition of minerals.

3.8.1. Hydrolysis

Hydrolysis involves the breakage of chemical bonds on the polymeric chain caused by the acid or base used for the treatment. This forms carbon radicals that react with OH^- to form functional groups. The hydrolysis treatment of PCL electrospun scaffolds using sodium hydroxide (NaOH) in an ultrasonic bath for 40 minutes was employed by Luickx et al to induce reactive groups on the fibre surface that acted as nucleation sites for the deposition of a thin layer of calcium-deficient apatite (CDHAp). Before immersion in NaOH solution, the PCL scaffolds were dipped in ethanol, demonstrating that this technique preserved the scaffold's porosity, which is critical for this type of chemical treatment. The treated scaffold showed increased hydrophilicity, as proved by the WCA measurements.(151) A similar result was reported by Savalyeva et al in their study that employed an ultrasonic bath of $CaCl_2$ on PCL scaffolds followed by mineralisation with $CaCO_3$ coatings.(152)

Luickx et al in another study used ultrasonic assisted hydrolysis with demineralised water for 3s to functionalised PDLLA scaffolds that showed optimised rapid deposition of a thin

homogenous layer of slightly carbonated calcium deficient apatite or a combination of apatite and dicalcium phosphate dihydrate based on the variation in time and concentration of the mineralising solutions. The treated scaffolds exhibited increased osteoblast viability, adhesion and proliferation when seeded with MC3T3-E1 cells after 7 days of culture.(153)

Phosphorylation of electrospun scaffolds is another interesting technique to hydrolyse cellulose nanofibres, as shown by Li et al in their study using a solution mixture of phosphoric acid (20ml), ethanol (20ml), hexanol (25ml) and phosphorus pentoxide (62.5g) for 72h. In this study, the authors have demonstrated that a small number of phosphate groups, as measured by the spectrophotometric method of molybdenum blue, when introduced to the surface of the nanofibres, enhanced the scaffolds' ability to interact with Ca^{2+} ions through coordination bonds to form Ca-P nuclei. Although the phosphorylation reaction caused degradation of the cellulose nanofibres, as seen from the viscosity molecular weight of treated and non-treated nanofibres, the authors concluded that the nanofibre mat was still mechanically robust as a scaffold material. (154)

Hydrolysis through silicification using silicic acid solution, as shown by Ha et al to improve crystal formation and increase nucleation sites for apatite-like material deposition on polyvinyl acetate nanofibres, has proved effective in increasing calcium and phosphorous content on the surface of the nanofibres upon soaking in SBF.(155)

NaOH treatment on carbonised nanofibres typically introduces hydroxyl groups on the fibre surface by cleaving carbonyl, carboxyl or ester groups. This increases the scaffold's hydrophilicity and introduces nucleation points for attaching mineralising ions on the fibre surface.(156) Samadian et al, in their study, have incorporated this hydrolysis method to functionalised electroactive carbonised nanofibres derived from electrospun polyacrylonitrile nanofibre via heat treatment. This carbonised and surface-activated nanofibre scaffold was then subjected to biomimetic mineralisation by immersion in SBF for 12, 24, 48, and 72 hrs at 37°C. The resulting mineralised scaffolds showed a homogenous deposit of minerals and superhydrophilicity as shown by water contact angle measurements before and after mineralisation to be 133.5°±0.6° to 0°, respectively. However, the toxicity of the mineralised scaffolds was significantly higher for the ones treated for 48 h in SBF.(157)

One of the earlier studies by Chen et al using PLLA scaffolds showed the effects of using 0.5 M NaOH for different time intervals (5,10, and 30 min) and its consequent mineralisation in SBF for 2 and 4 weeks. The resulting mineralised PLLA scaffolds treated in NaOH until 30 mins showed increased degradation due to hydrolysis. The scaffolds hydrolysed for only 5

mins and incubated in SBF for 14 days showed homogenous mineralisation and comparatively less degraded nanofibres. The authors also investigated the effects of adding 50 μm/mL of citric acid or poly-L-aspartic acid to the SBF as an anionic functional group to control the nucleation and growth of minerals.(158) Following this study, Yu et al investigated the mineralisation potential of PCL scaffolds after hydrolysis in 2N NaOH, incubated at 24°C for 12h while being stirred. The authors have utilised the alternate dipping method to induce CaP nucleation on the fibre surface and incubate in SBF for 21 days to deposit a mineral coating. TEM analysis of the mineralised scaffold showed the mineral coating to be crystalline apatite. The authors have also reported a significantly increased response of MC3T3-E1 cells cultured on the mineralised scaffold, which shows osteogenic stimulations by studying its gene expression.(159)

Cellulose is a natural polymer found in plants and is considered biocompatible and biodegradable. Cellulose acetate, while also biodegradable, might have slightly different properties due to the presence of acetyl groups. Regenerating cellulose from cellulose acetate restores the natural polymer, making it more suitable for biomedical applications. One of the most common methods for regenerating electrospun cellulose acetate scaffolds is saponification (alkaline hydrolysis) with NaOH/ethanol. Joshi et al. investigated the mineralisation potential of regenerated cellulose when electrospun along with PCL. The scaffolds showed uniform deposition throughout the matrix, which the authors have reported to be due to the improved wettability after regeneration treatment and the availability of hydroxyl groups on the surface that assisted HA nucleation. The authors have also employed a gas foaming technique with sodium borohydride on regenerated cellulose scaffolds that produced hydrogen gas in the pores of the scaffold, resulting in a three-dimensional cellulose sponge. When mineralised in SBF, the fibres in the sponge were found to be entirely covered by mineralisation, which the authors have reported to be due to the anionic borate groups absorbed onto the surface during the gas foaming, which may have bound with Ca^{2+} to nucleate calcium phosphate growth on the scaffold.(160,161) The authors also reinforced cellulose with nylon 6 fibres, which showed accelerated calcium deficient mineralisation in SBF due to the hydroxyl groups from the cellulose chains.(162) Kim et al incorporated calcium hydroxide in situ of a three-dimensional multi-layered PCL/cellulose scaffold by a modified gas foaming approach and investigated its mineralising capacity after incubating in SBF for 10 days. The modified nanofibres showed the depth of calcium-based particles, which enhanced

mineralisation as the calcium incorporation resulted in a faster uptake of phosphate anions, leading to hydroxyapatite nucleation.(163)

3.8.2. Aminolysis

Aminolysis is another diversely used functionalisation technique that involves the addition of hydroxyl, carboxyl and amino groups to the surface of the nanofibre, thereby reducing the hydrophobicity of the electrospun scaffold. However, it is not as common as hydrolysis due to its limitations in that its efficiency is reduced on polymers with high crystallinity, and aminolysis is mainly used for functionalising films rather than nanofibres due to the surface instability caused by the treatment.(164)

In an attempt to clarify the effects of carboxyl, hydroxyl and amino groups, their densities and cooperation with each other in the process of mineralisation, Cui et al conducted a study with PDLLA electrospun nanofibres functionalised with these groups prior to mineralising them in 2x SBF. The PDLLA fibres contained carboxyl, amino/carboxyl hydroxyl/carboxyl and amino/hydroxyl/carboxyl in different samples. XPS analysis was used to quantify the densities of the total chemical groups on the fibres, around 0.9 nmol/cm^2. With SEM, FTIR and XRD analyses of the mineralised scaffolds, the authors reported that the scaffold containing higher amounts of carboxyl groups, a combination of hydroxyl/carboxyl in the ratio 3/7, a combination of amino/hydroxyl/carboxyl in the ratio 2/3/5 were found to be favourable for hydroxyapatite nucleation and growth in SBF that resulted in higher content and lower crystal size. The authors also suggested that the formation of hydroxyapatite on the surface of fibres was controlled by the charge density of the groups and their interaction among ionic and polar groups present on the fibre surface.(165)

Zou et al used the same method to fabricate functionalised PDLLA fibres to study their degradation behaviours during up to 1 year of incubation in degradation media. The functionalised PDLLA fibres with and without the presence of calcium phosphate deposits were studied before and after hot-press treatment. Amongst types of samples, the hot-pressed composites of non-mineralised fibres showed the most negligible degradation due to their dense structure, small pore size and fusion of fibres due to the hot-press treatment. However, after hot-press treatment, mineralised fibres showed a higher degradation rate due to their quicker and stronger water uptake. As discussed by the authors in this study, the degradation mechanisms can prove helpful in the design of electrospun composite scaffolds with controlled biodegradation.(166)

Cui et al also incorporated free amine groups onto the surface of the electrospun PDLLA nanofibres by immersing them in 0.02g/ml of 1,6-hexanediamine solution in isopropanol for 10 mins in another study. The aminolysed mat was coated with chitosan, a hydrophilic polymer, to control the amount of hydroxyapatite formed on the mat upon immersion in SBF. The amount of chitosan-coated on the surface was controlled by the aminolysis time, and this increased the wettability of the nanofibre surface as shown in their WCA measurements of 0°. The study also demonstrates a mathematical strategy to understand the growth kinetics of HA formed on the surface as a function of the amount of chitosan-coated on the nanofibre surface. The resulting kinetic model shows the correlation between the amount of aminolysis time, the amount of chitosan-coated and the amount of HA formed on the surface.(167)

In an attempt to altogether avoid using surface treatments that may affect the mechanical integrity of the scaffold to functionalise the nanofibres, especially that of hydrophobic polyester scaffolds, Liu et al fabricated a series of polyurethane block copolymers containing PHB as the hard segment and PEG as the soft segment of a mineralisable bone scaffold through electrospinning. The resulting copolymer blend showed higher surface and bulk hydrophilicity as seen from WCA measurements and had low to no crystallinity as seen from their DSC measurements upon mineralisation in 10x SBF followed by 2.5x SBF for 12 h each, a controlled and continuous growth of minerals were observed with SEM. The authors report that the PEG segment in the copolymer acted as nucleation points for the growth of calcium minerals.(168)

Another interesting study conducted by Raic et al employed the use of BSA electrospun nanofibres to investigate its effects on cell adhesion and mineralisation potential. BSA is a natural polymer, and the authors introduced primary amine groups on its surface to mimic the chemical composition and fibrous architecture of ECM in bone tissue by treating the fibres with ethylenediamine solution containing *N*-(3-dimethylaminopropyl)-*N′*-ethylcarbodiimide hydrochloride, which made the fibres cationised. Upon mineralisation in SBF and Ca^{2+}/HPO_4^{2-} solution for 21 days, the cationised BSA fibres were found to have better deposition than the non-treated nanofibres. However, when mesenchymal stem cells were cultured on the mineralised fibres, the osteogenic induction was lower in the cationised scaffolds than in the non-cationised fibres. However, the osteogenesis was found to be higher on the non-mineralised cationised scaffold in comparison to the mineralised ones. The authors hypothesised that this could be the effect of the surface charge on the cationised BSA fibres and its influence on cell functions and that the hydroxyapatite layer was causing hindrance to

the MSC differentiation that was otherwise observed to be enhanced on the cationised fibres.(169)

As an alternative to natural proteins, wool keratin is another biocompatible polymer with many carboxyl or carbonyl groups, which also aids in the chelation of Ca^{2+} ions, leading to efficient mineral nucleation. Li et al developed a strategy to introduce hydroxyapatite and keratin into PLLA nanofibres. The authors observed that upon mineralisation, the growth of mineral deposits on nucleation sites provided by keratin were tiny crystals with different directions on the surface. Moreover, the supply of calcium ions from the SBF solution to the HA nucleation sites was reduced due to their capture by the carboxyl and carbonyl groups from keratin chains. This inhibited HA growth along a particular axis, as reported by the authors.(170)

Physico-chemical functionalisation

The functionalisation strategies that involve physical and chemical changes in the electrospun scaffold surface to enhance functionality, surface characteristics and bioactivity can be considered physicochemical changes. By integrating physical altercations, such as surface activation and surface roughness and chemical altercations, such as the introduction of functional groups or reactive sites, the resulting scaffold offers a synergistic platform for optimised mineral deposition, cell-material interactions and tissue regeneration.

3.8.3. Plasma treatment

Plasma treatment involves subjecting an electrospun scaffold to a low-temperature plasma discharge that releases highly energetic ions, electrons, and reactive species to interact with the fibre surface that, introduces functional groups, aids in the crosslinking of polymers and modifies surface roughness. The high-energy species can also lead to chemical changes, such as the breaking and reforming of chemical bonds, which may enhance the scaffold's wettability and cell adhesion. Lao et al have employed the use of air plasma treatment on PLGA nanofibres to introduce carboxyl, hydroxyl and amino groups to the polymer matrix that, in turn, can enhance the electrostatic and hydrogen binding of collagen to the surface without causing denaturation of its triple helix structure since there are no organic solvents used. The scaffolds were treated with radio frequency power of 400 W for 15 min before incubation in 1mg/mL collagen at 4°C. After collagen immobilisation, the PLGA scaffold was mineralised with 5x SBF for up to 9 days. The authors reported that the hydrophilic groups introduced by the plasma

treatment acted as nucleation sites for the mineral deposits on PLGA nanofibres, which showed significant mineralisation. However, the PLGA nanofibres coated with collagen showed a different morphology of minerals with a faster mineralisation rate owing to the polar groups on collagen that acted as nucleation sites.(171)

Ivanova et al have implemented the use of low-temperature plasma to study the mineralisation behaviour of $CaCO_3$ deposited on PCL scaffolds by improving its wettability and permeability. The plasma processing was done in O_2^-, NH_3^- and Ar^- atmospheres to introduce highly reactive chemical groups such as O^- and N^- on the scaffold. After plasma treatment for 120 s under a pressure of 30 Pa, mineralisation of the PCL scaffolds was done by precipitating $CaCO_3$ particles from a mixture of saturated $CaCl_2^-$ and $Na_2CO_3^-$ solutions. The authors reported that in the O_2^- atmosphere, the PCL scaffolds were coated with vaterite phase, which was smoother than the coating formed in NH_3^- and Ar^- atmospheres. Using high-resolution micro-computed tomography, the authors found that $CaCO_3$ nucleation occurred much deeper into the scaffold in O_2 plasma than in the other two conditions.(172) Kim et al also used low-frequency oxygen plasma on PCL scaffolds to enhance hydrophilicity and water absorption by increasing surface oxygen content that, in turn, improved the deposition of hydroxyapatite when incubated in SBF.(148)

3.9. Characterisation of mineralised scaffolds

A thorough characterisation of mineralised scaffolds is essential to ensure their quality, biocompatibility, mechanical properties, and regenerative potential. This knowledge informs the design, fabrication, and selection of scaffolds for tissue engineering and other biomedical applications, ultimately leading to more successful clinical translation.

3.9.1. Surface characterisation

3.9.1.1. Scanning electron microscope (SEM)

SEM is a valuable tool for characterising mineralised scaffolds. It offers detailed insights into their surface morphology, microstructure, mineralisation, and cell interactions. By using SEM, researchers can better understand the properties and performance of mineralised scaffolds, contributing to advancing tissue engineering and biomaterials research.

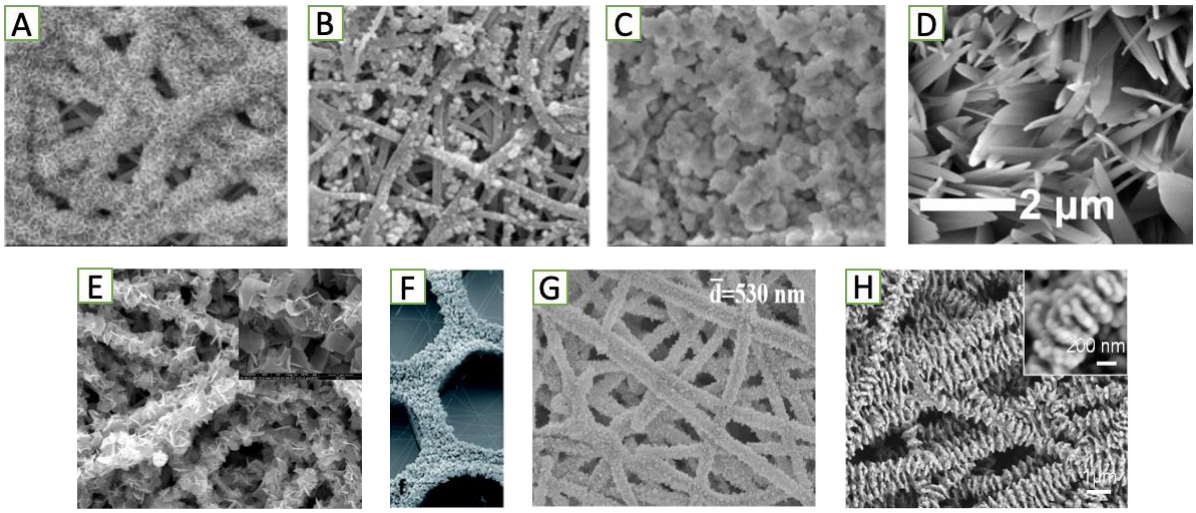

Figure 3.5. Different types of morphology observed in scaffolds mineralised using different techniques. (A) PLGA nanofibre mineralised using concentrated SBF method for 3h; (B) PLGA nanofibre mineralised using supersaturated calcification solution method for 3h ; PLGA nanofibre mineralised using alternate soaking method for 3h ((A-C) adapted from Meng et al. (173), reproduced with permission); (D) PLLA nanofibre mineralised using electrodeposition method (adapted from He et al. (55), reproduced with permission); (E) Carboxymethyl cellulose treated cellulose scaffolds mineralised with PBS containing magnesium, calcium and PAA for 7 days (adapted from Rodriguez et al. (145), reproduced with permission); (F) PCL fibres electrospun on a honeycomb template and mineralised by electrospraying HA (adapted from Nedjari et al. (58), reproduced with permission); (G) Sintered calcium silicate nanofibres mineralised by soaking in a α-MEM containing 10% FBS for 7 days (adapted from Du et al. (59), reproduced with permission); (H) PCL nanofibre electrospun into shish kebab structure mineralised using 10x SBF for 3 days (adapted from Chen et al. (27), reproduced with permission).

3.9.1.2. Transmission electron microscope (TEM)

TEM is another powerful visualisation tool similar to SEM. It can be used to analyse the detailed internal structures of scaffolds, including the nanoscale details of individual mineral crystals within the scaffold. It can show cellular ultrastructure, nanoparticles, and nanoscale features of the scaffold's mineralisation. In TEM, a thin sample section (ultrathin, around 50-100 nm) is prepared and placed under the path of an electron beam, and the electrons that are transmitted through the sample are captured on a digital detector. This makes the sample preparation for TEM very extensive.

3.9.1.3. Atomic Force Microscopy (AFM)

AFM analysis of mineralised scaffold can provide information on surface topography by allowing high-resolution imaging of the scaffold's surfaces to help visualise the distribution,

size and shape of mineral deposits, including their arrangement. Raic et al utilised this technique to investigate the surface roughness induced by the cationisation and mineralisation of BSA nanofibres. This data was then further used to study the effect of surface roughness on mesenchymal stem cell adhesion to the scaffold.(169) A similar study was conducted by Jaiswal et al to analyse the change in surface topography after coating PLLA scaffolds with gelatin, which showed small granular patterns and, after mineralisation, larger granular patterns. This data was attributed to the efficient nucleation of hydroxyapatite on gelatin.(174)

3.9.1.4. Synchrotron Micro CT imaging

Apart from the standard SEM imaging that helps visualise the surface mineral content on a sample, Synchrotron Micro CT imaging can be used to study the internal deep structures of the scaffold to visualise pore distribution, mineral deposition, and material interfaces. It provides exceptionally high-resolution using X-ray-generated synchrotron radiation while keeping the sample intact. Ivanova et al have used this method to study the internal characteristics of PCL scaffold and the influence of O_2 plasma on the calcification process.(172)

3.9.1.5. White light interferometry

White light interferometry is a powerful, non-destructive, high-resolution surface characterisation technique for electrospun scaffolds made of thin films and mats. Its mechanism involves splitting a broadband light source into two beams, one reflecting off the sample surface and the other travelling through the reference surface. Upon recombining these beams, the interference patterns are analysed to measure surface characteristics such as roughness, height variations, and thickness precisely. In the context of mineralised scaffolds, the surface topography measurements can provide information about the quality and uniformity of the crystals formed. Quantifying data, such as roughness (*Rms*), can be done using dedicated software attached to the instrument.(11)

3.9.1.6. Water Contact Angle (WCA)

This characterisation technique provides information about the wettability of a surface. It involves measuring the angle formed between a droplet of water and the surface of a solid material, which measures the hydrophilicity of a scaffold surface. Mineralisation of scaffold surfaces is often known to increase their hydrophilicity. PLGA scaffold with aligned nanofibres

mineralised using an alternate immersion method was analysed by Li et al for an increase in hydrophilicity after the mineral coating, which also consequently affected the cell adhesion and facilitated cell elongation.(8) Water contact angle and water absorption are data that provide insights into the interaction between a scaffold's surface and water. In a study conducted by Sani et al, the water contact angle of PCL/chitosan/HA scaffolds was measured to be reduced with an increase in the chitosan content grafted onto the PCL. However, the water absorption was found to be reduced, which the authors reported was due to the low porosity of the fibres caused by the agglomeration of HA nanoparticles.(175)

3.9.1.7. Elemental composition

Determining elemental constituents within a mineralised electrospun scaffold provides a comprehensive understanding of the mineral apatite coating, which contains three major elements – calcium, phosphorus and oxygen—the difference in their ratios results in various depositions commonly identified under the calcium orthophosphate family. Table 3.3 presents the list of various types of calcium phosphates and their ratios used as composites or precipitated in mineralising solutions as found in the literature.

Table 3.3 List of calcium phosphates and their Ca/P ratios (176)

Compound	**Chemical formula**	**Ratios**	**Ref**
Dicalcium phosphate dihydrate (DCPD)	$CaHPO_4.2H_2O$	1.0	(62,173)
Octacalcium phosphate (OCP)	$Ca_8(HPO_4)_2(PO_4)_4.5H_2O$	1.33	(62)
β-Tricalcium phosphate (β-TCP)	$\beta\text{-}Ca_3(PO_4)_2$	1.5	(15)
Amorphous calcium phosphate	$Ca_xH_y(PO_4)_z \cdot nH_2O$, n = 3 – 4.5; 15 – 20% H_2O	1.2-2.2	(89)
Calcium-deficienthydroxyapatite (CDHA)	$Ca_9(HPO_4)(PO_4)_5(OH$	1.5-1.67	(162)
Hydroxyapatite (HA)	$Ca_{10}(PO_4)_6(OH)_2$	1.67	

Energy dispersive spectra or EDS or EDX is the most commonly used analysis technique to identify the composition of mineral coatings on electrospun scaffolds. It is performed in the SEM, which focuses an electron beam on the sample while detecting the X-ray emitted by the sample due to the electron interactions. It is collected on a detector to identify the elements since each peak is characteristic of a specific element. Meng et al compared the mineral coatings formed by three mineralisation techniques – SBF, alternate immersion and a supersaturated calcification solution containing CH_3COOH, $CaCl_2$ and H_3PO_4. All three

methods yielded mixed coatings of DCPD, OCP and HA. However, the main component of minerals from the SBF method was DCPD and HA for the other two methods. The authors reported that the morphologies and Ca/P components did not influence the adhesion, proliferation and activity of MG63 cells cultured on them.(173)

Inductively Coupled Plasma-Atomic Emission Spectroscopy (ICP-AES) is another analytical technique used to determine the elemental composition of a sample by measuring the intensity of light emitted from excited atoms in an inductively coupled plasma source. It can be used to assess the degree of mineralisation along with its bioactivity, as shown by Rad et al and Wakita et al.(15),(129) Elemental analysis of a submicron hollow bioactive glass tube mineralised with SBF was investigated by Xie et al which revealed that the percentage of Si and O atoms decreased on the scaffold with increased incubation time in the SBF solution while Ca and P were found to increase indicating the bioactive ionic release from the glass tube which enhanced mineralisation.(21)

3.9.1.8. Fourier Transform Infrared (FTIR) spectroscopy

FTIR was often used alongside EDX analysis to provide information about the crystal structure, mineral phase, and chemical composition of mineral deposits. It has also found useful applications in identifying the functional groups present on the surface and their relative abundance for a quantitative analysis. This technique involves using infrared rays that are emitted from a source and absorbed by the sample molecules. The absorbed infrared energy causes the molecules to vibrate and stretch, changing their dipole moments—the change in dipole moments results in the absorption of specific wavelengths of infrared light. The FTIR instrument measures the intensity of absorbed light at different frequencies, generating an absorption spectrum. The analysis of these intensities or peaks is usually compared with the infrared spectra for its identification. In the study conducted by Fu et al, mineralised PCL-PEG-PCL copolymer scaffolds were analysed using FTIR compared with the non-mineralised scaffolds to identify absorption bands of the deposited apatite. The peaks at 605 cm^{-1}, 564 cm^{-1} and 1032 cm^{-1} corresponded to PO_4 vibrations. The relative intensity of these peaks increased with an increase in mineralisation time, indicating an increase in HA deposition.(177) Some studies were also able to throw light on the bonding between a composite and hydroxyapatite using these data. Chitosan contains active surface functional groups, which was observed in the vibrational shift of the carbonate group at 1450 cm^{-1} to 1389 cm^{-1}, which Zhang et al reported was due to the chemical bonding and molecular interaction between the $-NH_2$ in

chitosan and -OH group in hydroxyapatite, which aided in the conservation of the mechanical properties of the PHBV/chitosan/HA scaffolds.(178)

3.9.1.9. Crystal structure analysis

X-ray Diffraction (XRD) analysis is a valuable technique for characterising the crystallographic structure of mineralised electrospun scaffolds by providing insights into the composition, crystalline phases, crystallinity and orientation of mineral components within the scaffold. The system consists of an X-ray source that interacts with the sample's crystal lattice, resulting in the diffraction patterns collected by the detector. The diffraction intensity is plotted against the scanning range of 2θ angle). Each peak in the pattern corresponds to a specific crystal plane and lattice spacing of the mineral phases in the sample. Lin et al in their study, analysed the crystals formed by 10x SBF on chitosan-coated PLA nanofibres and observed the coating to be dicalcium phosphate dehydrates and apatite using XRD data.(179)

Raman spectroscopy is another powerful, non-destructive technique used to study molecular vibrations in materials, providing information about their composition, structure and chemical bonding. It involves emitting a monochromatic light (usually laser light) onto the sample, making the different molecules in the scaffold vibrate differently. Each vibrational mode is specific to a distinct mineral phase, which helps identify it. The intensity of the peaks recorded provides information about the composition and crystallinity of the deposited mineral. Chen et al were able to characterise the composition and structure of the minerals deposited on PLLA scaffolds after incubation in SBF for different periods as carbonated hydroxyapatite using valuable tools.(158) Selected Area Electron Diffraction (SAED) is another similar technique performed in a TEM to characterise the crystallographic structure while providing information about the arrangement of atoms within the minerals, allowing the identification of crystal phases, orientations, and crystallinity. Li et al were able to identify the lattice spacing of hydroxyapatite to be 0.283nm, which is designated to 211 in the crystallographic plane according to the brightest diffraction ring observed using this technique.(154) In another study, Li et al were able to observe the preferential growth orientation of hydroxyapatite deposited on keratin-containing PLLA scaffolds along the c-axis.(170)

3.9.2. Physicochemical characterisation

Mineral content quantification

One of the earlier techniques to quantify mineral content on polymeric scaffolds was introduced by Madurantakam et al in their study using Alizarin Red stain to visualise calcium deposits. This dye binds explicitly to calcium ions, forming a red complex. The staining intensity was correlated with the amount of mineralisation in the scaffold.(180)

Mineral ash is the weight of the inorganic residue remaining after completely combusting a mineralised scaffold at high temperatures, often expressed in percentage. This is a technique to quantify the mineral content, and there are several ways to determine it based on the type of material used. Andric et al., in their research, employed the use of ceramic crucibles placed in a furnace. The PLLA/gelatin scaffolds used in this study were heated until 700°C for 24 h. After cooling down, the mineral ash weight was recorded, and the average mineral deposition percentage was calculated as a ratio of mineral ash weight to the sample's original weight.[76,](182) Thermogravimetric analysis or TGA can also be used to measure the mineral content of the mineralised scaffolds as reported by Liu et al in their study where the authors heated mineralised poly (PHB/PEG urethane) samples at 800°C under an N_2 atmosphere. The copolymer completely degraded at ~450 °C, leaving behind the deposited minerals, which can be quantified. However, the authors compared this to the degradation of the pure minerals precipitated from the mineralising solution (SBF) in the absence of the electrospun scaffold, which also experienced a loss of weight when heated, leaving a residue of 78%. Therefore, residual weight from all the mineralised samples was corrected accordingly with equation (1).(168)

$$Mineral\ content\ on\ mineralized\ fiber\ mat\ (wt\ \%) = 100 \times fiber\ mat\ residue\ (wt\ \%)\ /\ pure\ minerals\ residue\ (wt\ \%)$$ Equation(1)(168)

Kim et al have also used this technique to quantify the mineral residue after heating the mineralised PCL scaffold at 700°C, which resulted in a 2-step degradation process due to the HA component.(148) In one study, the composite content of PHBV/pearl powder was measured from the thermogram at 600°C), which showed two-step degradation.(183) Lao et al used a calcium kit to quantify the mineral content deposited on collagen-coated PLGA scaffolds in their study. The calcium assay kit involves the extraction of the calcium deposits from a scaffold by shaking it in 0.6N HCl for 4h at 4°C. The lysates were then added into a Ca

reagent working solution, and absorbance was measured under a UV-Vis spectrophotometer at 610 nm to measure the calcium content.(171)

3.9.3. Mechanical characterisation

Incorporation of hydroxyapatite in the polymer matrix can reinforce the nanofibres with increased stiffness and strength, resulting in improved resistance to deformation and higher load-bearing capacity. However, in some cases, the weak molecular interactions between the hydroxyapatite particles and the polymer matrix can result in the deterioration of its mechanical properties, as seen in the study conducted by Chen et al. TEM analysis of the PDLLA nanofibres incorporated with HA showed that increased content of HA resulted in its agglomeration that consequently formed defect phases in the matrix, thereby depleting the strengthening effects of the inorganic phase in polymeric matrices.(184) Addressing the same issue, Souza et al have incorporated lauryl chloride functionalised octacalcium phosphate/hydroxyapatite into PLLA fibres, which enhanced mineralisation until 40% mineral phase. The authors reported that the inclusion of functionalised octacalcium phosphates with laurate produced improvements in the tensile strength and young's modulus showing enhanced adhesion between inorganic particles and the PLLA matrix.(185)

Whited et al fabricated porous PLLA scaffolds using a three-step water-soluble PEO fibre inclusion, dissolution, and mineralisation process. The PEO fibre included in the PLLA scaffold was dissolved at various percentages of content (0%, 25%, 50% and 75%) and mineralised in 10x SBF for 6h. The resulting mineralised scaffolds were mechanically tested for analysing uniaxial tensile properties. The mineralisation of the PLLA scaffolds resulted in a decreased elastic modulus for the 0% PEO scaffolds while increasing significantly for the scaffolds with 50% PEO content. A trend of decreased tensile strength and young's modulus with an increase in PEO content was observed, and the authors postulated that this is majorly due to the increase in pore size and porosity and decreased inter-fibre bonding, thereby deeming the scaffolds more suitable for filling bone voids rather than mechanical load bearing applications.(186)

In order to avoid the loss of mechanical properties experienced by the scaffold due to the highly porous structure of the minerals caused by the relatively large grain size of the mineral phase and their random orientation, Liu et al used a modified version of the 10x SBF solution to mineralise PLGA scaffolds immobilised with chitosan and heparin with controlled surface coating. The authors hypothesised that modifying the ionic concentration of HCO_3^- should

modify the mechanical properties of the scaffold, i.e., by increasing the deposition of HCO_3^-, a negatively charged species on the fibre surface, heterogeneous nucleation of calcium phosphate can be increased that subsequently produces a thick mineral coating with smaller grain size. The resulting mineralised nanofibres showed increased modulus with increasing mineral content and decreased toughness, indicating that the scaffolds have become more brittle upon mineralisation. Despite this increase in stiffness, no changes in the yield stress were seen, indicating that the mineral coating did not change the stress at which permanent deformation began. The non-modified 10x SBF mineralised scaffold showed 100 MPa of modulus, whereas the modified 10xSBF scaffolds showed 500 MPa due to a drastic reduction in grain size.(187) Lipner et al used the modified and non-modified 10xSBF to mineralise PLGA scaffolds by using a syringe pump that added the mineralising solution at a constant rate to a vial containing the PLGA scaffolds that resulted in linear gradients in mineral content. This technique was previously described by Li et al to produce dense and platelike mineral deposits. Upon conducting uniaxial tensile tests of the gradient scaffolds, the strain was higher on the low mineral content than on the high mineral content ends. The elastic modulus increased with an increase in mineral content, and the scaffolds with dense mineral coating showed rapid stiffening compared to those with platelike minerals. The authors developed a mathematical model to compare these experimental results to theoretical estimates to measure how effective the stiffening was. The results of these comparisons suggested that the minerals deposited by 10 x SBF were weaker and not well connected to the scaffold as compared to the minerals deposited by the modified 10x SBF, which showed stiffening that was nearly an order of magnitude higher than non-modified 10x SBF.(188),(189)

Lipner et al then conducted another study to understand how mineral stiffening and toughening occur without strengthening the fibres. To test this hypothesis, PLGA scaffolds with aligned nanofibres were tested in tension at several off-axis angles while simultaneously testing PLGA layered scaffolds in a peel test configuration. In a previous study conducted by Kolluru et al, the authors reported that the deposition of minerals on nanofibres stiffens the scaffold without stiffening or strengthening the individual nanofibres, suggesting that the mineral crystals form structural crosslinks between adjacent nanofibres, which Lipner et al have termed as mobile minerals in their study while conducting tensile tests at various angles. Peel tests revealed that the toughness increased with mineralisation time up to a peak value and then decreased until it reached the baseline value of non-mineralised scaffolds. These results were also supported by the theoretical predictions that the authors derived from mathematical modelling of mineral growth kinetics along with fracture energetics that suggested that the toughness increased until

mineral mobility was diminished by steric hindrance. The authors suggested that these results could be used to identify design principles for mineralised electrospun scaffolds and their toughening mechanisms.(190),(191) Xie et al in their study, demonstrated the effects of mineralisation on polydopamine-coated PCL scaffolds with aligned nanofibres incubated in SBF for 24 and 48hr and the consequent changes in their mechanical properties. The authors reported that the elastic modulus of the mineralised scaffolds increased dramatically from 86 MPa for the PCL samples to 459 MPa for 24 hrs of mineralisation and 768 MPa for 48 hrs of mineralised PCL/PDA samples. A similar trend was observed for toughness and ultimate tensile strength, indicating that mineralisation mediated by the polydopamine coating greatly enhanced the scaffold's mechanical properties.(192)

Apart from tensile strength, compression studies also provide invaluable information about the mechanical properties of mineralised scaffolds. Compressive strength is usually measured for bone-mimicking scaffolds and tensile strength for ligament and tendon scaffolds; however, there is no specific limitation. Luo et al. measured the compressive modulus of mineralised PCL/silk fibroin scaffolds, which showed higher compressive modulus compared to the non-mineralised scaffolds. This improvement was attributed to the crosslinked apatite formed on the fibres.(106)

3.9.4. Degradation testing

Jaiswal et al have studied the effect of mineralisation on the degradation properties of PLLA/gelatin mineralised scaffold. The PLLA/gelatin scaffolds were mineralised using the alternate soaking process with 0.5 M $CaCl_2$ and 0.3M Na_2HPO_4. Upon conducting a degradation test in 30 mL PBS until 8 weeks, the authors reported that the mineralised scaffolds with HA coating underwent a slower degradation than the non-mineralised PLLA/gelatin scaffolds explained by the binding of gelatin caused by HA particles. The addition of gelatin to PLLA usually accelerates its degradation due to the presence of carboxyl and amine groups. In order to avoid this, scaffolds containing gelatin or collagen are crosslinked using various techniques, but they come with a certain toxicity level. The authors of this study have reported that HA coating instead of crosslinking can be employed to slow the degradation rate of the electrospun scaffold. FTIR analyses confirmed that gelatin did not leach out of the mineralised scaffold even after incubation in PBS for 14 days.(174,193) However, Gautam et al in their study, reported that PCL/gelatin scaffolds with and without HA nanoparticles incorporated during electrospinning showed similar degradation rates after incubating in PBS for 8

weeks.(194) The usefulness of a mineral coating in slowing down degradation was also investigated by Barati et al employing PLA nanofibres mineralised in a modified SBF that contained organic acids such as citric acid, hydroxycitric acid, tartaric acid, malic acid, ascorbic acid and salicylic acid. The difference in the degradation of apatite was found to be directly proportional to the incubation time of the nanofibres in SBF, which in turn affected the crystallinity of the apatite, i.e., the scaffolds with higher apatite content and lower crystallinity experienced the slowest mass loss and this case, it was the scaffold treated with hydroxycitric acid.(195) One interesting study by Zhang et al investigated the dissolution of the mineral deposits from SBF in deionised water and Hank's balanced salt solution. PLLA/gelatin electrospun scaffolds were incubated in 5x SBF for 6, 12, 18 and 24 days, and the resulting mineral deposits were found to be sheet-like DCPA and spherical HA. When incubated in deionised water for 3 days, the 6-day SBF incubated samples lost almost all of the minerals, but the other samples were observed to retain the spherical HA deposits. However, in Hank's balanced salt solution, after 3 days and loss of all minerals, the samples started redepositing again owing to the ionic concentration of the incubation solution. For the rest of the samples, more and more minerals were seen to be deposited until 7 days, and these were classified as HA components with EDX analysis. Further, the authors also investigated the effects of these mineral dissolutions on the cell behaviour of MC3T3-E1, which were cultured in a growth medium along with the scaffold but without direct contact. They reported that the effects of the remineralised ions were insignificant for cell proliferation. However, all the samples affected the osteogenic differentiation due to higher Ca^{2+} concentration overall.(196)

3.9.5. Biological characterisation

Mineralised electrospun scaffolds offer exciting prospects for tissue regeneration, but before their full potential can be harnessed, a comprehensive understanding of the biological characteristics of these structures is imperative. The various biological aspects of mineralised electrospun scaffolds are commonly studied by cell adhesion, proliferation, osteogenic differentiation and angiogenesis, and this also aids in determining their biocompatibility. Table 3.4 shows the different types of analyses found in the literature investigating cell culture responses on mineralised electrospun scaffolds.

Table 3.4 Cell lines and their assays used for characterising mineralised scaffolds

Cell activity	Stain/assay	Cell types used and references	Ref
Cell viability/cytotoxicity	MTS/MTT assay PrestoBlue Alamar blue stain XTT assay	hFOB (Human foetal osteoblasts)	(197)
		NIH 3T3	(149)
		L929 mouse fibroblasts	(79)
		ADSC (adipose-derived stem cells)	(80)
		Human osteoblasts	(194)
		UMR-106 (rat osteosarcoma cell lines)	(54)
		NHDF (human dermal fibroblasts)	(152)
Osteogenic induction	ALP stain	Human osteosarcoma cells	(198)
		rBMSCs (Rat bone-marrow-derived mesenchymal stem cells)	(31)
		UMR-106 (rat osteosarcoma cell lines)	(54)
		SHED (stem cells from human exfoliated deciduous teeth)	(185)
Cell migration and distribution	CMFDA	hFOB (Human foetal osteoblasts)	(197)
Cell proliferation	CCK-8 assay	MC3T3-E1 (mouse osteoblast cells)	(71)
Osteocalcin expression	ELISA RT-PCR	hBMSCs (Human bone marrow-derived stromal cells)	(57)
		MC3T3-E1 (mouse osteoblast cells)	(16)
Calcium deposit identification	Von kossa staining	BMSCs (Bone Marrow mesenchymal stem cells)	(171)

These data are essential to ensure that the scaffold material does not provoke any adverse reactions or cause inflammation when implanted. Zhang et al in their study analysed the biocompatibility of mineralised PHBV/PAA scaffold by culturing human foetal osteoblasts (hFOB) to investigate its *in vitro* responses for 15 days. The cells were checked for alkaline phosphatase (ALP) activity, which is a marker for bone formation ability of osteoblast, by catalysing the hydrolysis of colourless organic phosphate ester substrate, p-nitro phenyl phosphate (pNPP), to a yellow product p-nitrophenol and phosphate. The cultured scaffolds were also tested for cytotoxicity using an MTS assay to assess the initial adhesion and viability of cells, which is critical for long-term stability and growth. The cells showed good adhesion,

proliferation and further osteogenic mineralisation on the mineralised scaffolds compared to the non-mineralised scaffolds owing to the osteo-inductive ability of the apatite layer. The cultured scaffolds were also tested using 5-chloromethylfluorescein diacetate (CMFDA) fluorescent dye for detecting the synthesis of bone matrix proteins in the deeper layers of the scaffold, and the morphology of the cells showed cuboidal appearances suggesting osteogenesis.(197) Chahal et al have also reported similar results on mineralised PVA scaffolds containing hydroxyethyl cellulose and cultured with human osteosarcoma cells. When analysed with MTS assay, the cells showed good proliferation with an increase in time on the CaP-coated scaffolds.(198),(199)

Osteoblast differentiation can also be evaluated at the cellular and molecular level, as shown in a study by Abudhahir et al where PCL scaffolds containing copper and wollastonite were cultured with mouse mesenchymal cells and osteogenic marker genes such as alkaline phosphate (ALP), type 1 collagen and major bone-specific transcription factor (Runx2). The calcium and silicon ions released from the wollastonite were reported to have acted as an induction signal for osteoblastic differentiation and showed increased mineralisation. The scaffolds were also tested for protein absorption by incubating in foetal bovine serum (FBS) for 48 hrs, which showed that the scaffolds with wollastonite showed the highest amount of protein absorption due to its increased crystallinity. This is a vital evaluation since proteins are essential for cell signalling and establishing interaction between the scaffold and cells at the target implant site.(200) Jing et al studied another protein called bone morphogenetic protein 2 (BMP2) along with the ones mentioned above using RT-PCR by culturing bone marrow stromal cells and reported a similar effect on mineralised PPY/PLLA fibres.(99) Taylor et al had also previously reported similar results with their trabecular scaffold of PDLA/PLLA/gelatin, mineralised using electrodeposition of SBF and cultured with human bone marrow-derived stromal cells. The ELISA test for osteocalcin protein showed a 30% increase in mineralised scaffolds than the non-mineralised scaffolds.(57)

Several studies have also employed *in vivo* testing to evaluate the effects of mineralised scaffolds. Ivanova et al have tested their mineralised carboxymethyl chitosan scaffolds in rat calvarial critical-sized defects on both parietal bones in the cranium. Eighteen male Sprague-Dawley rats were investigated in the study and divided into three groups of implantations: the control group, the non-mineralised group, and the mineralised group. After micro-CT scanning and histological evaluations with Hematoxylin and Eosin (H&E) staining and Masson's Trichrome staining, the scaffolds with HA coating showed new bone formation throughout the

area of the defect after 12 weeks as compared to the non-mineralised and control groups that showed incomplete defect repair. The authors also reported that the histological staining showed extensive collagen and bone regeneration due to the Ca^{2+} sensing receptor signalling activation.(172) Zheng et al have investigated the ability of ectopic osteogenesis *in vivo* while subcutaneously implanting their mineralised PCL/PDA scaffolds layered with collagen and chondroitin sulphate for 3 months in 15 male BLAB/c mice. The scaffolds were also cultured with MC3T3-E1 cells in subcutaneous incisions for 7 days before implantation. After histological analysis using Alizarin Red stain, H&E stain and Masson's Trichrome stain, the authors reported that the apatite-coated scaffolds showed a continuous bone-like matrix, which was confirmed to be ectopic bone from Toluidine Blue staining, indicating its great potential for artificial bone-repair scaffold.(16) Vaquette et al conducted a study using a mineralised PCL electrospun scaffold to correlate the investigations of *in vitro* cell culture observations to that of *in vivo* bone formation in a rat subcutaneous model. The mineralisation enhanced ALP activity in ovine osteoblasts, regardless of culture conditions and consequent osteogenesis. Upon subcutaneous implantation, the mineralised samples cultured in osteogenic media demonstrated a progressive increase in ectopic bone formation over time. In contrast, non-coated samples exhibited a delayed phase before bone formation occurred, from 4 to 8 weeks post-implantation. Histological and immunohistochemical analyses revealed the presence of bone formation throughout the scaffolds after 8 weeks of implantation, both in the coated and non-coated specimens. Markers such as ALP, osteocalcin, and collagen 1 were identified at the sites of bone formation and within the bone tissues. Additionally, vascularisation near the bone tissues indicated that the newly formed bone received sufficient oxygen and nutrients. This difference demonstrated that even though the CaP coating was significant *in vitro* for enhancing ALP activity and osteogenesis, it did necessarily navigate *in vivo* bone formation because of the insufficient release of calcium and phosphate ions to form new bone tissue. This suggests that there is no correlation between *in vitro* expression of osteogenic markers and *in vivo* bone formation, and these results were found concurrent with another critical study conducted by Chai et al. (201,202)

Hemocompatibility refers to the ability of a biomaterial to interact with erythrocytes without inducing adverse reactions such as clotting, haemolysis or activation of the coagulation cascade. In their study employing mineralised PLGA/silk fibroin scaffolds, Gao et al. investigated its hemocompatibility using human red blood cells, which showed no haemolytic phenomenon. The fraction of haemolysis was calculated using the equation –

$$Hemolysis\ \% = \left(\frac{D_t - D_{nc}}{D_{pc} - D_{nc}}\right) \times 100$$ Equation(107)

where D_t, D_{pc}, and D_{nc} are the absorbance of the sample, positive and negative control, respectively.(107) Similar results were also reported by Jaiswal et al in their study about mineralised gelatin-coated PLLA scaffolds that showed haemolysis under the permissible limit of 5%. The authors also investigated the adhesion, aggregation and activation of platelets in this study and reported that the mineralised scaffolds promoted the activation of platelets more effectively than the non-mineralised scaffolds, implying faster bone regeneration.(174)

In vitro, analysis of vascularisation also provides vital information on a scaffold's bioactivity and can be assessed by the ions released from it that can promote angiogenesis. Many studies have shown that magnesium ions can improve the expression of Vascular Endothelial Growth Factor (VEGF) in human umbilical endothelial cells. Zhang et al incorporated whitlockite, a rare phosphate mineral, into PCL nanofibres to induce VEGF by releasing magnesium ions from whitlockite. Further, subcutaneous implantation tested the scaffolds in vivo for their vascularisation ability. After 14 days, the neovascularisation was found to be enhanced in the whitlockite-containing PCL scaffolds as compared to the pristine ones.(203)

3.10. Conclusions

To conclude, the mineralisation of electrospun scaffolds emerges as a significant breakthrough in tissue engineering, offering a versatile avenue for crafting biomimetic frameworks that elevate tissue regeneration outcomes. This review explores various mineralisation techniques, each one showing distinct advantages based on scaffold synthesis. Adding minerals to the scaffolds gives important biochemical cues to cells and makes the scaffolds mechanically stronger. The strategies for achieving mineralisation include using simulated body fluid, alternate soaking method, supersaturated solutions, electrodeposition, electrospraying and polymer-induced mineralisation. The scaffold's properties that can be modified to enhance mineralisation include hydrophilicity, fibre diameter, electroactivity, hydroxyapatite nucleation, surface roughness, and porosity. Further, the scaffold can also be functionalised chemical methods such as hydrolysis and aminolysis or physico-chemical methods such as plasma treatment. The attempts to manipulate scaffold properties for directed mineralisation showcase its potential in shaping scaffold bioactivity and structural integrity, amplifying their efficacy as regenerative constructs. However, characterising the mineralised scaffolds remains pivotal in understanding the complex interactions between scaffold geometry, mineral content, and cellular reactivity. Moving forward, the invention of imaging techniques through

interdisciplinary approaches promises to illuminate the three-dimensional structures of these scaffolds. By combining insights from mineralisation methodologies, scaffold modifications, and characterisation techniques, this review pinpoints the potential of mineralised electrospun scaffolds in inspiring the next phase of tissue engineering, assisting in novel prospects for advancing the frontiers of regenerative medicine.

While significant strides have been made in understanding the influence of various fabrication parameters and mineral sources on scaffold properties, several avenues of exploration remain uncharted. Future directions for research in this area encompass a deeper investigation into the dynamic interplay between scaffold architecture, mineralisation techniques, and the resultant cellular responses. Researchers are investigating novel surface modification techniques to enhance mineralisation and improve the mechanical properties of the electrospun scaffolds. For instance, recent studies have explored the use of biomimetic peptides and inorganic nanoparticles to promote gradient mineral deposition. Other ongoing studies focus on developing controlled delivery approaches for incorporating growth factors and bioactive molecules into mineralised scaffolds for enhanced regenerative capabilities.

Additionally, integrating advanced imaging methods can provide real-time insights into the mineralisation process within electrospun fibres. In the realm of three-dimensional mineralised scaffolds, the characterisation challenge becomes pronounced due to the limitations of traditional techniques. Methods such as Fourier-transform infrared spectroscopy (FTIR) and X-ray diffraction (XRD), while valuable for material analysis, often necessitate flat or powdered samples, rendering their application to complex 3D scaffolds less straightforward. As these scaffolds inherently possess intricate architectures and topographies, alternative characterisation strategies are needed to probe their internal structures, mineralisation gradients, and spatial distributions accurately. The development of innovative imaging techniques and the adaptation of existing methods to accommodate three-dimensional samples hold the potential to unlock a deeper understanding of these multifaceted biomaterials. Furthermore, the potential synergy between mineralised scaffolds and emerging biotechnologies, such as stem cell therapies and gene editing techniques, opens new avenues for orchestrating enhanced tissue regeneration in the years ahead.

3.11. REFERENCES

1. Teo WE, Ramakrishna S. A review on electrospinning design and nanofibre assemblies. Nanotechnology. 2006 Jul 28;17(14):R89–106.

2. Wang X, Ding B, Li B. Biomimetic electrospun nanofibrous structures for tissue engineering. Materials Today. 2013 Jun 1;16(6):229–41.

3. Narayanan N, Jiang C, Uzunalli G, Thankappan SK, Laurencin CT, Deng M. Polymeric Electrospinning for Musculoskeletal Regenerative Engineering. Regen Eng Transl Med. 2016 Jun 1;2(2):69–84.

4. Holzwarth JM, Ma PX. Biomimetic nanofibrous scaffolds for bone tissue engineering. Biomaterials. 2011 Dec 1;32(36):9622–9.

5. Anjum S, Rahman F, Pandey P, Arya DK, Alam M, Rajinikanth PS, et al. Electrospun Biomimetic Nanofibrous Scaffolds: A Promising Prospect for Bone Tissue Engineering and Regenerative Medicine. Int J Mol Sci. 2022 Aug 16;23(16):9206.

6. Wu X, Walsh K, Hoff BL, Camci-Unal G. Mineralization of Biomaterials for Bone Tissue Engineering. Bioengineering (Basel). 2020 Oct 20;7(4):132.

7. Jiang N, He J, Zhang W, Li D, Lv Y. Directed differentiation of BMSCs on structural/compositional gradient nanofibrous scaffolds for ligament-bone osteointegration. Materials Science and Engineering: C. 2020 May 1;110:110711.

8. Li W, Yang X, Feng S, Yang S, Zeng R, Tu M. The fabrication of biomineralized fiber-aligned PLGA scaffolds and their effect on enhancing osteogenic differentiation of UCMSC cells. J Mater Sci: Mater Med. 2018 Jul 19;29(8):117.

9. Kung FC, Lin CC, Lai WFT. Osteogenesis of human adipose-derived stem cells on hydroxyapatite-mineralized poly(lactic acid) nanofiber sheets. Materials Science and Engineering: C. 2014 Dec 1;45:578–88.

10. Karaman O, Kumar A, Moeinzadeh S, He X, Cui T, Jabbari E. Effect of surface modification of nanofibres with glutamic acid peptide on calcium phosphate nucleation and osteogenic differentiation of marrow stromal cells. Journal of Tissue Engineering and Regenerative Medicine. 2016;10(2):E132–46.

11. Yunos DM, Ahmad Z, Boccaccini AR. Fabrication and characterization of electrospun poly-DL-lactide (PDLLA) fibrous coatings on 45S5 Bioglass® substrates for bone tissue engineering applications. Journal of Chemical Technology & Biotechnology. 2010;85(6):768–74.

12. Yunos D, Ahmad Z, Salih V, Boccaccini A. Stratified scaffolds for osteochondral tissue engineering applications: Electrospun PDLLA nanofibre coated Bioglass®-derived foams. J Biomater Appl. 2013 Jan 1;27(5):537–51.

13. Andric T, Sampson AC, Freeman JW. Fabrication and characterization of electrospun osteon mimicking scaffolds for bone tissue engineering. Materials Science and Engineering: C. 2011 Jan 1;31(1):2–8.

14. Bian T, Zhao K, Meng Q, Tang Y, Jiao H, Luo J. The construction and performance of multi-level hierarchical hydroxyapatite (HA)/collagen composite implant based on biomimetic bone Haversian motif. Materials & Design. 2019 Jan 15;162:60–9.

15. Masoudi Rad M, Nouri Khorasani S, Ghasemi-Mobarakeh L, Prabhakaran MP, Foroughi MR, Kharaziha M, et al. Fabrication and characterization of two-layered nanofibrous membrane for guided bone and tissue regeneration application. Materials Science and Engineering: C. 2017 Nov 1;80:75–87.

16. Zheng J, Rahman N, Li L, Zhang J, Tan H, Xue Y, et al. Biofunctionalization of electrospun fiber membranes by LbL-collagen/chondroitin sulfate nanocoating followed by mineralization for bone regeneration. Materials Science and Engineering: C. 2021 Sep 1;128:112295.

17. Mohan N, Wilson J, Joseph D, Vaikkath D, Nair PD. Biomimetic fiber assembled gradient hydrogel to engineer glycosaminoglycan enriched and mineralized cartilage: An in vitro study. Journal of Biomedical Materials Research Part A. 2015;103(12):3896–906.

18. Rajzer I, Menaszek E, Kwiatkowski R, Planell JA, Castano O. Electrospun gelatin/poly(ε-caprolactone) fibrous scaffold modified with calcium phosphate for bone tissue engineering. Materials Science and Engineering: C. 2014 Nov 1;44:183–90.

19. Pathmanapan S, Sekar M, Pandurangan AK, Anandasadagopan SK. Fabrication of Mesoporous Silica Nanoparticle–Incorporated Coaxial Nanofiber for Evaluating the In Vitro Osteogenic Potential. Appl Biochem Biotechnol [Internet]. 2021 Nov 11 [cited 2022 Jan 7]; Available from: https://doi.org/10.1007/s12010-021-03741-3

20. He Y, Tian M, Li X, Hou J, Chen S, Yang G, et al. A Hierarchical-Structured Mineralized Nanofiber Scaffold with Osteoimmunomodulatory and Osteoinductive Functions for Enhanced Alveolar Bone Regeneration. Advanced Healthcare Materials. n/a(n/a):2102236.

21. Xie J, Blough ER, Wang CH. Submicron bioactive glass tubes for bone tissue engineering. Acta Biomaterialia. 2012 Feb 1;8(2):811–9.

22. Kang MS, Kim JH, Singh RK, Jang JH, Kim HW. Therapeutic-designed electrospun bone scaffolds: Mesoporous bioactive nanocarriers in hollow fiber composites to sequentially deliver dual growth factors. Acta Biomaterialia. 2015 Apr 1;16:103–16.

23. Singh RK, Jin GZ, Mahapatra C, Patel KD, Chrzanowski W, Kim HW. Mesoporous Silica-Layered Biopolymer Hybrid Nanofibrous Scaffold: A Novel Nanobiomatrix Platform for Therapeutics Delivery and Bone Regeneration. ACS Appl Mater Interfaces. 2015 Apr 22;7(15):8088–98.

24. Han X, Wang D, Chen X, Lin H, Qu F. One-pot synthesis of macro-mesoporous bioactive glasses/polylactic acid for bone tissue engineering. Materials Science and Engineering: C. 2014 Oct 1;43:367–74.

25. Samavedi S, Olsen Horton C, Guelcher SA, Goldstein AS, Whittington AR. Fabrication of a model continuously graded co-electrospun mesh for regeneration of the ligament–bone interface. Acta Biomaterialia. 2011 Dec 1;7(12):4131–8.

26. Torricelli P, Gioffrè M, Fiorani A, Panzavolta S, Gualandi C, Fini M, et al. Co-electrospun gelatin-poly(l-lactic acid) scaffolds: Modulation of mechanical properties and chondrocyte response as a function of composition. Materials Science and Engineering: C. 2014 Mar 1;36:130–8.

27. Chen X, Wang W, Cheng S, Dong B, Li CY. Mimicking Bone Nanostructure by Combining Block Copolymer Self-Assembly and 1D Crystal Nucleation. ACS Nano. 2013 Sep 24;7(9):8251–7.

28. Jing X, Mi HY, Wang XC, Peng XF, Turng LS. Shish-Kebab-Structured Poly(ε-Caprolactone) Nanofibers Hierarchically Decorated with Chitosan–Poly(ε-Caprolactone) Copolymers for Bone Tissue Engineering. ACS Appl Mater Interfaces. 2015 Apr 1;7(12):6955–65.

29. Jing X, Jin E, Mi HY, Li WJ, Peng XF, Turng LS. Hierarchically decorated electrospun poly($$ \varepsilon $$-caprolactone)/nanohydroxyapatite composite nanofibers for bone tissue engineering. J Mater Sci. 2015 Jun 1;50(12):4174–86.

30. Xu T, Yang H, Yang D, Yu ZZ. Polylactic Acid Nanofiber Scaffold Decorated with Chitosan Islandlike Topography for Bone Tissue Engineering. ACS Appl Mater Interfaces. 2017 Jun 28;9(25):21094–104.

31. Liu L, Shang Y, Li C, Jiao Y, Qiu Y, Wang C, et al. Hierarchical Nanostructured Electrospun Membrane with Periosteum-Mimic Microenvironment for Enhanced Bone Regeneration. Advanced Healthcare Materials. 2021;10(21):2101195.

32. Kokubo T, Ito S, Shigematsu M, Sanka S, Yamamuro T. Fatigue and life-time of bioactive glass-ceramic A-W containing apatite and wollastonite. J Mater Sci. 1987 Nov;22(11):4067–70.

33. Kim HM, Kishimoto K, Miyaji F, Kokubo T, Yao T, Suetsugu Y, et al. Composition and structure of the apatite formed on PET substrates in SBF modified with various ionic activity products. Journal of Biomedical Materials Research. 1999;46(2):228–35.

34. Oyane A, Kim HM, Furuya T, Kokubo T, Miyazaki T, Nakamura T. Preparation and assessment of revised simulated body fluids. Journal of Biomedical Materials Research Part A. 2003;65A(2):188–95.

35. Kokubo T, Takadama H. How useful is SBF in predicting in vivo bone bioactivity? Biomaterials. 2006 May 1;27(15):2907–15.

36. 14:00-17:00. ISO. [cited 2023 Aug 14]. ISO 23317:2007. Available from: https://www.iso.org/standard/41446.html

37. Yilmaz B, Pazarceviren AE, Tezcaner A, Evis Z. Historical development of simulated body fluids used in biomedical applications: A review. Microchemical Journal. 2020 Jun 1;155:104713.

38. Li X, Xie J, Yuan X, Xia Y. Coating Electrospun Poly(ε-caprolactone) Fibers with Gelatin and Calcium Phosphate and Their Use as Biomimetic Scaffolds for Bone Tissue Engineering. Langmuir. 2008 Dec 16;24(24):14145–50.

39. Cai Q, Xu Q, Feng Q, Cao X, Yang X, Deng X. Biomineralization of electrospun poly(l-lactic acid)/gelatin composite fibrous scaffold by using a supersaturated simulated body fluid with continuous CO2 bubbling. Applied Surface Science. 2011 Sep 15;257(23):10109–18.

40. Bohner M, Lemaitre J. Can bioactivity be tested in vitro with SBF solution? Biomaterials. 2009 Apr 1;30(12):2175–9.

41. Pan H, Zhao X, Darvell BW, Lu WW. Apatite-formation ability – Predictor of "bioactivity"? Acta Biomaterialia. 2010 Nov 1;6(11):4181–8.

42. Yang D, Yu K, Ai Y, Zhen H, Nie J, Kennedy JF. The mineralization of electrospun chitosan/poly(vinyl alcohol) nanofibrous membranes. Carbohydrate Polymers. 2011 Mar 17;84(3):990–6.

43. Yang D, Jin Y, Zhou Y, Ma G, Chen X, Lu F, et al. In Situ Mineralization of Hydroxyapatite on Electrospun Chitosan-Based Nanofibrous Scaffolds. Macromolecular Bioscience. 2008;8(3):239–46.

44. Liu L, He D, Wang GS, Yu SH. Bioinspired Crystallization of CaCO3 Coatings on Electrospun Cellulose Acetate Fiber Scaffolds and Corresponding CaCO3 Microtube Networks. Langmuir. 2011 Jun 7;27(11):7199–206.

45. Ravichandran R, Venugopal JR, Sundarrajan S, Mukherjee S, Ramakrishna S. Precipitation of nanohydroxyapatite on PLLA/PBLG/Collagen nanofibrous structures for the differentiation of adipose derived stem cells to osteogenic lineage. Biomaterials. 2012 Jan 1;33(3):846–55.

46. Gandhimathi C, Venugopal J, Ravichandran R, Sundarrajan S, Suganya S, Ramakrishna S. Mimicking Nanofibrous Hybrid Bone Substitute for Mesenchymal Stem Cells Differentiation into Osteogenesis. Macromolecular Bioscience. 2013;13(6):696–706.

47. Gandhimathi C, Venugopal JR, Tham AY, Ramakrishna S, Kumar SD. Biomimetic hybrid nanofibrous substrates for mesenchymal stem cells differentiation into osteogenic cells. Materials Science and Engineering: C. 2015 Apr 1;49:776–85.

48. Arafat MT, Tronci G, Yin J, Wood DJ, Russell SJ. Biomimetic wet-stable fibres via wet spinning and diacid-based crosslinking of collagen triple helices. Polymer. 2015 Oct 23;77:102–12.

49. Liao S, Murugan R, Chan CK, Ramakrishna S. Processing nanoengineered scaffolds through electrospinning and mineralization suitable for biomimetic bone tissue engineering. Journal of the Mechanical Behavior of Biomedical Materials. 2008 Jul 1;1(3):252–60.

50. Rajzer I, Menaszek E, Kwiatkowski R, Chrzanowski W. Bioactive nanocomposite PLDL/nano-hydroxyapatite electrospun membranes for bone tissue engineering. J Mater Sci: Mater Med. 2014 May 1;25(5):1239–47.

51. Rajzer I, Kwiatkowski R, Piekarczyk W, Biniaś W, Janicki J. Carbon nanofibers produced from modified electrospun PAN/hydroxyapatite precursors as scaffolds for bone tissue engineering. Materials Science and Engineering: C. 2012 Dec 1;32(8):2562–9.

52. Zhao J, Zhao Y, Guan Q, Tang G, Zhao Y, Yuan X, et al. Crosslinking of electrospun fibrous gelatin scaffolds for apatite mineralization. Journal of Applied Polymer Science. 2011;119(2):786–93.

53. Van Hong Thien D, Ho MH, Hsiao SW, Li CH. Wet chemical process to enhance osteoconductivity of electrospun chitosan nanofibers. J Mater Sci. 2015 Feb 1;50(4):1575–85.

54. Van Hong Thien D, Hsiao SW, Ho MH, Li CH, Shih JL. Electrospun chitosan/hydroxyapatite nanofibers for bone tissue engineering. J Mater Sci. 2013 Feb 1;48(4):1640–5.

55. He C, Jin X, Ma PX. Calcium phosphate deposition rate, structure and osteoconductivity on electrospun poly(l-lactic acid) matrix using electrodeposition or simulated body fluid incubation. Acta Biomaterialia. 2014 Jan 1;10(1):419–27.

56. He C, Xiao G, Jin X, Sun C, Ma PX. Electrodeposition on Nanofibrous Polymer Scaffolds: Rapid Mineralization, Tunable Calcium Phosphate Composition and Topography. Advanced Functional Materials. 2010;20(20):3568–76.

57. Taylor BL, Perez X, Ciprano J, Freeman COU, Goldstein A, Freeman J. Three-Dimensional Porous Trabecular Scaffold Exhibits Osteoconductive Behaviors In Vitro. Regen Eng Transl Med. 2020 Sep;6(3):241–50.

58. Nedjari S, Hébraud A, Eap S, Siegwald S, Mélart C, Benkirane-Jessel N, et al. Electrostatic template-assisted deposition of microparticles on electrospun nanofibers: towards microstructured functional biochips for screening applications. RSC Adv. 2015 Oct 1;5(102):83600–7.

59. Du Z, Zhao Z, Liu H, Liu X, Zhang X, Huang Y, et al. Macroporous scaffolds developed from CaSiO3 nanofibers regulating bone regeneration via controlled calcination. Materials Science and Engineering: C. 2020 Aug 1;113:111005.

60. Datta P, Dhara S, Chatterjee J. Hydrogels and electrospun nanofibrous scaffolds of N-methylene phosphonic chitosan as bioinspired osteoconductive materials for bone grafting. Carbohydrate Polymers. 2012 Jan 15;87(2):1354–62.

61. Datta P, Chatterjee J, Dhara S. Electrospun nanofibers of a phosphorylated polymer—A bioinspired approach for bone graft applications. Colloids and Surfaces B: Biointerfaces. 2012 Jun 1;94:177–83.

62. Jie Y, Cai Z, Li S, Xie Z, Ma M, Huang X. Hydroxyapatite nucleation and growth on collagen electrospun fibers controlled with different mineralization conditions and phosvitin. Macromol Res. 2017 Sep 1;25(9):905–12.

63. Liang H, Sheng F, Zhou B, Pei Y, Li B, Li J. Phosphoprotein/chitosan electrospun nanofibrous scaffold for biomineralization. International Journal of Biological Macromolecules. 2017 Sep 1;102:218–24.

64. Choi MO, Kim YJ. Fabrication of gelatin/calcium phosphate composite nanofibrous membranes by biomimetic mineralization. International Journal of Biological Macromolecules. 2012 Jun 1;50(5):1188–94.

65. Kim YJ, Choi MO. Effect of mineralisation condition on characteristics of nanocomposite membranes. Materials Technology. 2013 Nov 1;28(6):324–31.

66. Choi MO, Kim YJ. Effect of poly(3-hydroxybutyrate-co-3-hydroxyvalerate)/gelatin ratios on the characteristics of biomimetic composite nanofibrous scaffolds. Colloid Polym Sci. 2018 May 1;296(5):917–26.

67. Suslu A, Albayrak AZ, Urkmez AS, Bayir E, Cocen U. Effect of surfactant types on the biocompatibility of electrospun HAp/PHBV composite nanofibers. J Mater Sci: Mater Med. 2014 Dec 1;25(12):2677–89.

68. Pant HR, Risal P, Park CH, Tijing LD, Jeong YJ, Kim CS. Synthesis, characterization, and mineralization of polyamide-6/calcium lactate composite nanofibers for bone tissue engineering. Colloids and Surfaces B: Biointerfaces. 2013 Feb 1;102:152–7.

69. Hwang TI, Kim JI, Joshi MK, Park CH, Kim CS. Simultaneous regeneration of calcium lactate and cellulose into PCL nanofiber for biomedical application. Carbohydrate Polymers. 2019 May 15;212:21–9.

70. Pant HR, Kim HJ, Bhatt LR, Joshi MK, Kim EK, Kim JI, et al. Chitin butyrate coated electrospun nylon-6 fibers for biomedical applications. Applied Surface Science. 2013 Nov 15;285:538–44.

71. Liao N, Joshi MK, Tiwari AP, Park CH, Kim CS. Fabrication, characterization and biomedical application of two-nozzle electrospun polycaprolactone/zein-calcium lactate composite nonwoven mat. Journal of the Mechanical Behavior of Biomedical Materials. 2016 Jul 1;60:312–23.

72. Silva Nykänen VP, Puska MA, Nykänen A, Ruokolainen J. Synthesis and biomimetic mineralization of l-proline substituted polyphosphazenes as bulk and nanofiber. Journal of Polymer Science Part B: Polymer Physics. 2013;51(17):1318–27.

73. Ngiam M, Liao S, Patil AJ, Cheng Z, Chan CK, Ramakrishna S. The fabrication of nano-hydroxyapatite on PLGA and PLGA/collagen nanofibrous composite scaffolds and their effects in osteoblastic behavior for bone tissue engineering. Bone. 2009 Jul 1;45(1):4–16.

74. Choubar EG, Nasirtabrizi MH, Salimi F, Sohrabi-gilani N, Sadeghianamryan A. Fabrication and in vitro characterization of novel co-electrospun polycaprolactone/collagen/polyvinylpyrrolidone nanofibrous scaffolds for bone tissue engineering applications. Journal of Materials Research. 2022 Dec 1;37(23):4140–52.

75. Li M, Liu W, Sun J, Xianyu Y, Wang J, Zhang W, et al. Culturing Primary Human Osteoblasts on Electrospun Poly(lactic-co-glycolic acid) and Poly(lactic-co-glycolic acid)/Nanohydroxyapatite Scaffolds for Bone Tissue Engineering. ACS Appl Mater Interfaces. 2013 Jul 10;5(13):5921–6.

76. Mohammadalipour M, Behzad T, Karbasi S, Mohammadalipour Z. Optimization and characterization of polyhydroxybutyrate/lignin electro-spun scaffolds for tissue engineering applications. International Journal of Biological Macromolecules. 2022 Oct 1;218:317–34.

77. Xu H, Shen M, Shang H, Xu W, Zhang S, Yang HR, et al. Osteoconductive and Antibacterial Poly(lactic acid) Fibrous Membranes Impregnated with Biobased Nanocarbons for Biodegradable Bone Regenerative Scaffolds. Ind Eng Chem Res. 2021 Aug 18;60(32):12021–31.

78. Deng L, Li Y, Zhang H. In vitro and in vivo assessment of glucose cross-linked gelatin/zein nanofibrous scaffolds for cranial bone defects regeneration. Journal of Biomedical Materials Research Part B: Applied Biomaterials. 2020;108(4):1505–17.

79. Yao C, Li Y, Wu F. Zein nanofibrous membranes as templates for biomineralization of hydroxyapatite crystallites. Polymer Composites. 2013;34(7):1163–71.

80. Zhang CY, Zhang W, Mao LB, Zhao Y, Yu SH. Biomimetic mineralization of zein/calcium phosphate nanocomposite nanofibrous mats for bone tissue scaffolds. CrystEngComm. 2014 Sep 23;16(40):9513–9.

81. Parvathi K, Krishnan AG, Anitha A, Jayakumar R, Nair MB. Poly(L-lactic acid) nanofibers containing Cissus quadrangularis induced osteogenic differentiation in vitro. International Journal of Biological Macromolecules. 2018 Apr 15;110:514–21.

82. Chang W, Mu X, Zhu X, Ma G, Li C, Xu F, et al. Biomimetic composite scaffolds based mineralization of hydroxyapatite on electrospun calcium-containing poly(vinyl alcohol) nanofibers. Materials Science and Engineering: C. 2013 Oct 1;33(7):4369–76.

83. Enayati MS, Behzad T, Sajkiewicz P, Rafienia M, Bagheri R, Ghasemi-Mobarakeh L, et al. Development of electrospun poly (vinyl alcohol)-based bionanocomposite scaffolds for bone tissue engineering. J Biomed Mater Res. 2018 Apr;106(4):1111–20.

84. Si J, Cui Z, Wang Q, Liu Q, Liu C. Biomimetic composite scaffolds based on mineralization of hydroxyapatite on electrospun poly(ε-caprolactone)/nanocellulose fibers. Carbohydrate Polymers. 2016 Jun 5;143:270–8.

85. Kim HW, Song JH, Kim HE. Nanofiber Generation of Gelatin–Hydroxyapatite Biomimetics for Guided Tissue Regeneration. Advanced Functional Materials. 2005;15(12):1988–94.

86. de Souza Araújo IJ, Ferreira JA, Daghrery A, Ribeiro JS, Castilho M, Puppin-Rontani RM, et al. Self-assembling peptide-laden electrospun scaffolds for guided mineralized tissue regeneration. Dental Materials. 2022 Nov 1;38(11):1749–62.

87. Gharaei R, Tronci G, Goswami P, Davies RPW, Kirkham J, Russell SJ. Biomimetic peptide enriched nonwoven scaffolds promote calcium phosphate mineralisation. RSC Adv. 2020 Jul 30;10(47):28332–42.

88. Ohkawa K, Hayashi S, Kameyama N, Yamamoto H, Yamaguchi M, Kimoto S, et al. Synthesis of Collagen-Like Sequential Polypeptides Containing O-Phospho-L-Hydroxyproline and Preparation of Electrospun Composite Fibers for Possible Dental Application. Macromolecular Bioscience. 2009;9(1):79–92.

89. Rodríguez K, Renneckar S, Gatenholm P. Biomimetic Calcium Phosphate Crystal Mineralization on Electrospun Cellulose-Based Scaffolds. ACS Appl Mater Interfaces. 2011 Mar 23;3(3):681–9.

90. Yamaguchi K, Prabakaran M, Ke M, Gang X, Chung IM, Um IC, et al. Highly dispersed nanoscale hydroxyapatite on cellulose nanofibers for bone regeneration. Materials Letters. 2016 Apr 1;168:56–61.

91. Taylor BL, Limaye A, Yarborough J, Freeman JW. Investigating processing techniques for bovine gelatin electrospun scaffolds for bone tissue regeneration. Journal of Biomedical Materials Research Part B: Applied Biomaterials. 2017;105(5):1131–40.

92. Dehkordi AN, Shafiei SS, Chehelgerdi M, Sabouni F, Sharifi E, Makvandi P, et al. Highly effective electrospun polycaprolactone/ layered double hydroxide nanofibrous scaffold for bone tissue engineering. Journal of Drug Delivery Science and Technology. 2022 Oct 1;76:103827.

93. Nitya G, Nair GT, Mony U, Chennazhi KP, Nair SV. In vitro evaluation of electrospun PCL/nanoclay composite scaffold for bone tissue engineering. J Mater Sci: Mater Med. 2012 Jul 1;23(7):1749–61.

94. baradaran T, Shafiei SS, Mohammadi S, Moztarzadeh F. Poly (ε-caprolactone)/layered double hydroxide microspheres-aggregated nanocomposite scaffold for osteogenic differentiation of mesenchymal stem cell. Materials Today Communications. 2020 Jun 1;23:100913.

95. Zhang H, Liu J, Yao Z, Yang J, Pan L, Chen Z. Biomimetic mineralization of electrospun poly(lactic-co-glycolic acid)/multi-walled carbon nanotubes composite scaffolds in vitro. Materials Letters. 2009 Nov 15;63(27):2313–6.

96. Tiwari AP, Joshi MK, Lee J, Maharjan B, Ko SW, Park CH, et al. Heterogeneous electrospun polycaprolactone/polyethylene glycol membranes with improved wettability, biocompatibility, and mineralization. Colloids and Surfaces A: Physicochemical and Engineering Aspects. 2017 May 5;520:105–13.

97. Rajzer I, Rom M, Menaszek E, Fabia J, Kwiatkowski R. Conductive Polyaniline Patterns on Electrospun Polycaprolactone/Hydroxyapatite Scaffolds for Bone Tissue Engineering. Materials. 2021 Sep;14(17):4837.

98. Jeong JO, Jeong SI, Lim YM, Park JS. Effective BMP-2 Release and Mineralization on a Graphene Oxide/Polyvinylpyrrolidone Hydrogel Forming Poly (ε-Caprolactone) Nanofibrous Scaffolds. Materials. 2022 Jan;15(23):8642.

99. Jing W, Huang Y, Wei P, Cai Q, Yang X, Zhong W. Roles of electrical stimulation in promoting osteogenic differentiation of BMSCs on conductive fibers. Journal of Biomedical Materials Research Part A. 2019;107(7):1443–54.

100. Ko SW, Lee JY, Rezk AI, Park CH, Kim CS. In-situ cellulose-framework templates mediated monodispersed silver nanoparticles via facile UV-light photocatalytic activity for anti-microbial functionalization. Carbohydrate Polymers. 2021 Oct 1;269:118255.

101. Ashraf R, Sofi HS, Akram T, Rather HA, Abdal-hay A, Shabir N, et al. Fabrication of multifunctional cellulose/TiO2/Ag composite nanofibers scaffold with antibacterial and bioactivity properties for future tissue engineering applications. Journal of Biomedical Materials Research Part A. 2020;108(4):947–62.

102. Wang D, Jang J, Kim K, Kim J, Park CB. “Tree to Bone”: Lignin/Polycaprolactone Nanofibers for Hydroxyapatite Biomineralization. Biomacromolecules. 2019 Jul 8;20(7):2684–93.

103. Shanmugavel S, Reddy VJ, Ramakrishna S, Lakshmi B, Dev VG. Precipitation of hydroxyapatite on electrospun polycaprolactone/aloe vera/silk fibroin nanofibrous scaffolds for bone tissue engineering. J Biomater Appl. 2014 Jul 1;29(1):46–58.

104. Paşcu EI, Stokes J, McGuinness GB. Electrospun composites of PHBV, silk fibroin and nano-hydroxyapatite for bone tissue engineering. Materials Science and Engineering: C. 2013 Dec 1;33(8):4905–16.

105. Panda N, Bissoyi A, Pramanik K, Biswas A. Directing osteogenesis of stem cells with hydroxyapatite precipitated electrospun eri-tasar silk fibroin nanofibrous scaffold. J Biomater Sci Polym Ed. 2014;25(13):1440–57.

106. Luo J, Zhang H, zhu J, Cui X, Gao J, Wang X, et al. 3-D mineralized silk fibroin/polycaprolactone composite scaffold modified with polyglutamate conjugated

with BMP-2 peptide for bone tissue engineering. Colloids and Surfaces B: Biointerfaces. 2018 Mar 1;163:369–78.

107. Gao Y, Shao W, Qian W, He J, Zhou Y, Qi K, et al. Biomineralized poly (l-lactic-co-glycolic acid)-tussah silk fibroin nanofiber fabric with hierarchical architecture as a scaffold for bone tissue engineering. Materials Science and Engineering: C. 2018 Mar 1;84:195–207.

108. Lee JY, Chung J, Chung WJ, Kim G. Fabrication and in vitro biocompatibilities of fibrous biocomposites consisting of PCL and M13 bacteriophage-conjugated alginate for bone tissue engineering. J Mater Chem B. 2016 Jan 20;4(4):656–65.

109. Junka R, Zhou X, Wang W, Yu X. Albumin-Coated Polycaprolactone (PCL)–Decellularized Extracellular Matrix (dECM) Scaffold for Bone Regeneration. ACS Applied Bio Materials [Internet]. 2022 Nov 14 [cited 2023 Mar 14]; Available from: https://pubs.acs.org/doi/full/10.1021/acsabm.2c00686

110. Cheng G, Xie C, Cheng Y, Gong C, Li Z, Dong X, et al. Enhanced mineralization of the nanofibers-incorporated aerogels increases mechanical properties of scaffold and promotes bone formation. Materials Today Advances. 2022 Dec 1;16:100318.

111. Pangon A, Saesoo S, Saengkrit N, Ruktanonchai U, Intasanta V. Hydroxyapatite-hybridized chitosan/chitin whisker bionanocomposite fibers for bone tissue engineering applications. Carbohydrate Polymers. 2016 Jun 25;144:419–27.

112. Davarpanah Jazi R, Rafienia M, Salehi Rozve H, Karamian E, Sattary M. Fabrication and characterization of electrospun poly lactic-co-glycolic acid/zeolite nanocomposite scaffolds using bone tissue engineering. Journal of Bioactive and Compatible Polymers. 2018 Jan 1;33(1):63–78.

113. Ghorbani F, Zamanian A, Aidun A. Conductive electrospun polyurethane-polyaniline scaffolds coated with poly(vinyl alcohol)-GPTMS under oxygen plasma surface modification. Materials Today Communications. 2020 Mar 1;22:100752.

114. Zheng X, Ke X, Yu P, Wang D, Pan S, Yang J, et al. A facile strategy to construct silk fibroin based GTR membranes with appropriate mechanical performance and enhanced osteogenic capacity. J Mater Chem B. 2020 Nov 25;8(45):10407–15.

115. Gao C, Gao Q, Li Y, Rahaman MN, Teramoto A, Abe K. Preparation and in vitro characterization of electrospun PVA scaffolds coated with bioactive glass for bone regeneration. Journal of Biomedical Materials Research Part A. 2012;100A(5):1324–34.

116. Gao C, Gao Q, Li Y, Rahaman MN, Teramoto A, Abe K. In vitro evaluation of electrospun gelatin-bioactive glass hybrid scaffolds for bone regeneration. Journal of Applied Polymer Science. 2013;127(4):2588–99.

117. Ghorbani F, Zamanian A, Aidun A. Bioinspired polydopamine coating-assisted electrospun polyurethane-graphene oxide nanofibers for bone tissue engineering application. Journal of Applied Polymer Science. 2019;136(24):47656.

118. Dhand C, Ong ST, Dwivedi N, Diaz SM, Venugopal JR, Navaneethan B, et al. Bio-inspired in situ crosslinking and mineralization of electrospun collagen scaffolds for bone tissue engineering. Biomaterials. 2016 Oct 1;104:323–38.

119. Cui W, Li X, Chen J, Zhou S, Weng J. In Situ Growth Kinetics of Hydroxyapatite on Electrospun Poly(dl-lactide) Fibers with Gelatin Grafted. Crystal Growth & Design. 2008 Dec 3;8(12):4576–82.

120. Zou B, Liu Y, Luo X, Chen F, Guo X, Li X. Electrospun fibrous scaffolds with continuous gradations in mineral contents and biological cues for manipulating cellular behaviors. Acta Biomaterialia. 2012 Apr 1;8(4):1576–85.

121. Zou B, Chen X, Zhi W, Liu Y, Cui W, Hu S, et al. Promoted healing of femoral defects with in situ grown fibrous composites of hydroxyapatite and poly(DL-lactide). Journal of Biomedical Materials Research Part A. 2012;100A(6):1407–18.

122. Lu Y, Wan Y, Gan D, Zhang Q, Luo H, Deng X, et al. Enwrapping Polydopamine on Doxorubicin-Loaded Lamellar Hydroxyapatite/Poly(lactic-co-glycolic acid) Composite Fibers for Inhibiting Bone Tumor Recurrence and Enhancing Bone Regeneration. ACS Appl Bio Mater. 2021 Aug 16;4(8):6036–45.

123. Furtos G, Rivero G, Rapuntean S, Abraham GA. Amoxicillin-loaded electrospun nanocomposite membranes for dental applications. Journal of Biomedical Materials Research Part B: Applied Biomaterials. 2017;105(5):966–76.

124. Serio F, Miola M, Vernè E, Pisignano D, Boccaccini AR, Liverani L. Electrospun Filaments Embedding Bioactive Glass Particles with Ion Release and Enhanced Mineralization. Nanomaterials. 2019 Feb;9(2):182.

125. Wang D, Xuan L, Zhong H, Gong Y, Shi X, Ye F, et al. Incorporation of well-dispersed calcium phosphate nanoparticles into PLGA electrospun nanofibers to enhance the osteogenic induction potential. RSC Advances. 2017;7(39):23982–93.

126. Shi M, Xuan L, Zhang Y, Wang D, Ye F, Shi X, et al. Synergistic effects of thermal treatment and encapsulation of calcium phosphate nanoparticles on enhancing dimensional stability and osteogenic induction potential of free-standing PLGA electrospun membranes. Colloids and Surfaces B: Biointerfaces. 2019 Nov 1;183:110437.

127. Weng L, Teusink MJ, Shuler FD, Parecki V, Xie J. Highly controlled coating of strontium-doped hydroxyapatite on electrospun poly(ε-caprolactone) fibers. Journal of Biomedical Materials Research Part B: Applied Biomaterials. 2017;105(4):753–63.

128. Obata A, Hotta T, Wakita T, Ota Y, Kasuga T. Electrospun microfiber meshes of silicon-doped vaterite/poly(lactic acid) hybrid for guided bone regeneration. Acta Biomaterialia. 2010 Apr 1;6(4):1248–57.

129. Wakita T, Obata A, Poologasundarampillai G, Jones JR, Kasuga T. Preparation of electrospun siloxane-poly(lactic acid)-vaterite hybrid fibrous membranes for guided bone regeneration. Composites Science and Technology. 2010 Nov 15;70(13):1889–93.

130. Konyali R, Deliormanli AM. Preparation and mineralization of 13-93 bioactive glass-containing electrospun poly-epsilon-caprolactone composite nanofibrous mats. J Thermoplast Compos Mater. 2019 May;32(5):690–709.

131. Deliormanlı AM. Preparation, in vitro mineralization and osteoblast cell response of electrospun 13–93 bioactive glass nanofibers. Materials Science and Engineering: C. 2015 Aug 1;53:262–71.

132. Kim S, Ko JW, Park CB. Bio-inspired mineralization of CO2 gas to hollow CaCO3 microspheres and bone hydroxyapatite/polymer composites. J Mater Chem. 2011 Jul 19;21(30):11070–3.

133. Cao Z, Wang D, Lyu L, Gong Y, Li Y. Fabrication and characterization of PCL/CaCO3 electrospun composite membrane for bone repair. RSC Adv. 2016 Jan 26;6(13):10641–9.

134. Sambudi NS, Park SB, Cho K. Enhancing the mechanical properties of electrospun chitosan/poly(vinyl alcohol) fibers by mineralization with calcium carbonate. J Mater Sci. 2016 Aug 1;51(16):7742–53.

135. Rezk AI, Hwang TI, Kim JY, Lee JY, Park CH, Kim CS. Functional composite nanofibers loaded with β-TCP and SIM as a control drug delivery system. Materials Letters. 2019 Apr 1;240:25–9.

136. Elsayed NA, Zada S, Allam NK. Mineralization of electrospun gelatin/CaCO3 composites: A new approach for dental applications. Mater Sci Eng C-Mater Biol Appl. 2019 Jul;100:655–64.

137. McCool JM, Rodriguez IA, Sell SA, Han Y, Bowlin GL. A preliminary study on amelogenin-loaded electrospun scaffolds. Journal of Bioactive and Compatible Polymers. 2014 Jan 1;29(1):32–49.

138. Serafim A, Cecoltan S, Lungu A, Vasile E, Iovu H, Stancu IC. Electrospun fish gelatin fibrous scaffolds with improved bio-interactions due to carboxylated nanodiamond loading. RSC Adv. 2015 Nov 5;5(116):95467–77.

139. Moosavifar MJ, Moztarzadeh F, Azami M. Preparation of Mineralized Electrospun Fibers as a Biomimetic Nanocomposite. International Journal of Polymeric Materials and Polymeric Biomaterials. 2014 Jul 24;63(11):576–82.

140. Zhao X, Zhou L, Li Q, Zou Q, Du C. Biomimetic mineralization of carboxymethyl chitosan nanofibers with improved osteogenic activity in vitro and in vivo. Carbohydrate Polymers. 2018 Sep 1;195:225–34.

141. Nirmala R, Nam KT, Navamathavan R, Park SJ, Kim HY. Hydroxyapatite Mineralization on the Calcium Chloride Blended Polyurethane Nanofiber via Biomimetic Method. Nanoscale Res Lett. 2011 Dec;6(1):1–8.

142. Afza S, Esfahani H, Nourian A, Ghaani MR. A novel approach to bio-mineralization of electrospun PCL scaffolds by protein and hydroxyapatite nanoparticles; molecular dynamics simulation and in-vitro evaluation. European Polymer Journal. 2023 Jan 3;182:111739.

143. Lee JH, Park JH, El-Fiqi A, Kim JH, Yun YR, Jang JH, et al. Biointerface control of electrospun fiber scaffolds for bone regeneration: Engineered protein link to mineralized surface. Acta Biomaterialia. 2014 Jun 1;10(6):2750–61.

144. Zhu J, Tang D, Lu Z, Xin Z, Song J, Meng J, et al. Ultrafast bone-like apatite formation on highly porous poly(l-lactic acid)-hydroxyapatite fibres. Materials Science and Engineering: C. 2020 Nov 1;116:111168.

145. Rodríguez K, Sundberg J, Gatenholm P, Renneckar S. Electrospun nanofibrous cellulose scaffolds with controlled microarchitecture. Carbohydrate Polymers. 2014 Jan 16;100:143–9.

146. Lee S, Joshi MK, Tiwari AP, Maharjan B, Kim KS, Yun YH, et al. Lactic acid assisted fabrication of bioactive three-dimensional PLLA/β-TCP fibrous scaffold for biomedical application. Chemical Engineering Journal. 2018 Sep 1;347:771–81.

147. Sun B, Li J, Liu W, Aqeel BM, El-Hamshary H, Al-Deyab SS, et al. Fabrication and characterization of mineralized P(LLA-CL)/SF three-dimensional nanoyarn scaffolds. Iran Polym J. 2015 Jan 1;24(1):29–40.

148. Kim M, Kim G. Physical and biological activities of newly designed, macro-pore-structure-controlled 3D fibrous poly(ε-caprolactone)/hydroxyapatite composite scaffolds. RSC Adv. 2015 Mar 13;5(34):26954–64.

149. Mi HY, Jing X, Salick MR, Cordie TM, Peng XF, Turng LS. Morphology, mechanical properties, and mineralization of rigid thermoplastic polyurethane/hydroxyapatite scaffolds for bone tissue applications: effects of fabrication approaches and hydroxyapatite size. J Mater Sci. 2014 Mar 1;49(5):2324–37.

150. Lyu LX, Huang NP, Yang Y. Accelerating and increasing nano-scaled pore formation on electrospun poly(3-hydroxybutyrate-co-3-hydroxyvalerate) fibers. Journal of Biomaterials Science, Polymer Edition. 2016 Jul 23;27(11):1155–69.

151. Luickx N, Van den Vreken N, D'Oosterlinck W, Van der Schueren L, Declercq H, De Clerck K, et al. Optimization of the activation and nucleation steps in the precipitation of a calcium phosphate primer layer on electrospun poly(ε-caprolactone). Journal of Biomedical Materials Research Part A. 2015;103(2):511–24.

152. Savelyeva MS, Abalymov AA, Lyubun GP, Vidyasheva IV, Yashchenok AM, Douglas TEL, et al. Vaterite coatings on electrospun polymeric fibers for biomedical applications. Journal of Biomedical Materials Research Part A. 2017;105(1):94–103.

153. Luickx N, Van Den Vreken N, Segaert J, Declercq H, Cornelissen M, Verbeeck R. Optimization of the time efficient calcium phosphate coating on electrospun poly(d,l-lactide). Journal of Biomedical Materials Research Part A. 2015;103(8):2720–30.

154. Li K, Wang J, Liu X, Xiong X, Liu H. Biomimetic growth of hydroxyapatite on phosphorylated electrospun cellulose nanofibers. Carbohydrate Polymers. 2012 Nov 6;90(4):1573–81.

155. Ha YM, Amna T, Kim MH, Kim HC, Hassan MS, Khil MS. Novel silicificated PVAc/POSS composite nanofibrous mat via facile electrospinning technique: Potential scaffold for hard tissue engineering. Colloids and Surfaces B: Biointerfaces. 2013 Feb 1;102:795–802.

156. Wu M, Wang Q, Liu X, Liu H. Biomimetic synthesis and characterization of carbon nanofiber/hydroxyapatite composite scaffolds. Carbon. 2013 Jan 1;51:335–45.

157. Samadian H, Mobasheri H, Azami M, Faridi-Majidi R. Osteoconductive and electroactive carbon nanofibers/hydroxyapatite nanocomposite tailored for bone tissue engineering: in vitro and in vivo studies. Sci Rep. 2020 Sep 9;10(1):14853.

158. Chen J, Chu B, Hsiao BS. Mineralization of hydroxyapatite in electrospun nanofibrous poly(L-lactic acid) scaffolds. Journal of Biomedical Materials Research Part A. 2006;79A(2):307–17.

159. Yu HS, Jang JH, Kim TI, Lee HH, Kim HW. Apatite-mineralized polycaprolactone nanofibrous web as a bone tissue regeneration substrate. Journal of Biomedical Materials Research Part A. 2009;88A(3):747–54.

160. Joshi MK, Tiwari AP, Pant HR, Shrestha BK, Kim HJ, Park CH, et al. In Situ Generation of Cellulose Nanocrystals in Polycaprolactone Nanofibers: Effects on Crystallinity, Mechanical Strength, Biocompatibility, and Biomimetic Mineralization. ACS Appl Mater Interfaces. 2015 Sep 9;7(35):19672–83.

161. Joshi MK, Pant HR, Tiwari AP, Maharjan B, Liao N, kim HJ, et al. Three-dimensional cellulose sponge: Fabrication, characterization, biomimetic mineralization, and in vitro cell infiltration. Carbohydrate Polymers. 2016 Jan 20;136:154–62.

162. Joshi MK, Tiwari AP, Maharjan B, Won KS, Kim HJ, Park CH, et al. Cellulose reinforced nylon-6 nanofibrous membrane: Fabrication strategies, physicochemical characterizations, wicking properties and biomimetic mineralization. Carbohydrate Polymers. 2016 Aug 20;147:104–13.

163. Kim SE, Tiwari AP. Three dimensional polycaprolactone/cellulose scaffold containing calcium-based particles: a new platform for bone regeneration. Carbohydr Polym. 2020 Dec 15;250:116880.

164. Niemczyk-Soczynska B, Gradys A, Sajkiewicz P. Hydrophilic Surface Functionalization of Electrospun Nanofibrous Scaffolds in Tissue Engineering. Polymers. 2020 Nov;12(11):2636.

165. Cui W, Li X, Xie C, Zhuang H, Zhou S, Weng J. Hydroxyapatite nucleation and growth mechanism on electrospun fibers functionalized with different chemical groups and their combinations. Biomaterials. 2010 Jun 1;31(17):4620–9.

166. Zou B, Li X, Zhuang H, Cui W, Zou J, Chen J. Degradation behaviors of electrospun fibrous composites of hydroxyapatite and chemically modified poly(dl-lactide). Polymer Degradation and Stability. 2011 Jan 1;96(1):114–22.

167. Cui W, Li X, Xie C, Chen J, Zou J, Zhou S, et al. Controllable growth of hydroxyapatite on electrospun poly(dl-lactide) fibers grafted with chitosan as potential tissue engineering scaffolds. Polymer. 2010 May 14;51(11):2320–8.

168. Liu KL, Choo ESG, Wong SY, Li X, He CB, Wang J, et al. Designing Poly[(R)-3-hydroxybutyrate]-Based Polyurethane Block Copolymers for Electrospun Nanofiber Scaffolds with Improved Mechanical Properties and Enhanced Mineralization Capability. J Phys Chem B. 2010 Jun 10;114(22):7489–98.

169. Raic A, Friedrich F, Kratzer D, Bieback K, Lahann J, Lee-Thedieck C. Potential of electrospun cationic BSA fibers to guide osteogenic MSC differentiation via surface charge and fibrous topography. Sci Rep. 2019 Dec 27;9(1):20003.

170. Li JS, Li Y, Liu X, Zhang J, Zhang Y. Strategy to introduce an hydroxyapatite–keratin nanocomposite into a fibrous membrane for bone tissue engineering. J Mater Chem B. 2012 Dec 20;1(4):432–7.

171. Lao L, Zhu Y, Zhang Y, Gao Z, Zhou F, Chen L, et al. Mineralization of Collagen-Coated Electrospun Poly(lactide-co-glycolide) Nanofibrous Mesh to Enhance Growth and Differentiation of Osteoblasts and Bone Marrow Mesenchymal Stem Cells. Advanced Engineering Materials. 2012;14(4):B123–37.

172. Ivanova AA, Syromotina DS, Shkarina S, Shkarin R, Cecilia A, Weinhardt V, et al. Effect of low-temperature plasma treatment of electrospun polycaprolactone fibrous scaffolds on calcium carbonate mineralisation. RSC Adv. 2018;8(68):39106–14.

173. Meng ZX, Li HF, Sun ZZ, Zheng W, Zheng YF. Fabrication of mineralized electrospun PLGA and PLGA/gelatin nanofibers and their potential in bone tissue engineering. Materials Science and Engineering: C. 2013 Mar 1;33(2):699–706.

174. Jaiswal AK, Chandra V, Bhonde RR, Soni VP, Bellare JR. Mineralization of nanohydroxyapatite on electrospun poly(l-lactic acid)/gelatin by an alternate soaking process: A biomimetic scaffold for bone regeneration. Journal of Bioactive and Compatible Polymers. 2012 Jul 1;27(4):356–74.

175. Sani IS, Rezaei M, Khoshfetrat AB, Razzaghi D. Preparation and characterization of polycaprolactone/chitosan-g-polycaprolactone/hydroxyapatite electrospun

nanocomposite scaffolds for bone tissue engineering. Int J Biol Macromol. 2021 Jul 1;182:1638–49.

176. Dorozhkin SV. Calcium Orthophosphates in Nature, Biology and Medicine. Materials. 2009 Jun;2(2):399–498.

177. Fu S, Yang L, Fan J, Wen Q, Lin S, Wang B, et al. In vitro mineralization of hydroxyapatite on electrospun poly(ε-caprolactone)–poly(ethylene glycol)–poly(ε-caprolactone) fibrous scaffolds for tissue engineering application. Colloids and Surfaces B: Biointerfaces. 2013 Jul 1;107:167–73.

178. Zhang S, Prabhakaran MP, Qin X, Ramakrishna S. Biocomposite scaffolds for bone regeneration: Role of chitosan and hydroxyapatite within poly-3-hydroxybutyrate-co-3-hydroxyvalerate on mechanical properties and in vitro evaluation. Journal of the Mechanical Behavior of Biomedical Materials. 2015 Nov 1;51:88–98.

179. Lin CC, Fu SJ, Lin YC, Yang IK, Gu Y. Chitosan-coated electrospun PLA fibers for rapid mineralization of calcium phosphate. International Journal of Biological Macromolecules. 2014 Jul 1;68:39–47.

180. Madurantakam PA, Rodriguez IA, Cost CP, Viswanathan R, Simpson DG, Beckman MJ, et al. Multiple factor interactions in biomimetic mineralization of electrospun scaffolds. Biomaterials. 2009 Oct 1;30(29):5456–64.

181. Andric T, Wright LD, Taylor BL, Freeman JW. Fabrication and characterization of three-dimensional electrospun scaffolds for bone tissue engineering. Journal of Biomedical Materials Research Part A. 2012;100A(8):2097–105.

182. Andric T, Taylor BL, Whittington AR, Freeman JW. Fabrication and Characterization of Three-Dimensional Electrospun Scaffolds for Bone Tissue Engineering. Regen Eng Transl Med. 2015 Dec 1;1(1):32–41.

183. Electrospun composites of PHBV/pearl powder for bone repairing. Progress in Natural Science: Materials International. 2015 Aug 1;25(4):327–33.

184. Chen J, Li X, Cui W, Xie C, Zou J, Zou B. In situ grown fibrous composites of poly(dl-lactide) and hydroxyapatite as potential tissue engineering scaffolds. Polymer. 2010 Dec 10;51(26):6268–77.

185. Souza DC de, Abreu H de LV de, Oliveira PV de, Capelo LP, Passos-Bueno MR, Catalani LH. A fast degrading PLLA composite with a high content of functionalized octacalcium phosphate mineral phase induces stem cells differentiation. Journal of the Mechanical Behavior of Biomedical Materials. 2019 May 1;93:93–104.

186. Whited BM, Whitney JR, Hofmann MC, Xu Y, Rylander MN. Pre-osteoblast infiltration and differentiation in highly porous apatite-coated PLLA electrospun scaffolds. Biomaterials. 2011 Mar 1;32(9):2294–304.

187. Liu W, Yeh YC, Lipner J, Xie J, Sung HW, Thomopoulos S, et al. Enhancing the Stiffness of Electrospun Nanofiber Scaffolds with a Controlled Surface Coating and Mineralization. Langmuir. 2011 Aug 2;27(15):9088–93.

188. Li X, Xie J, Lipner J, Yuan X, Thomopoulos S, Xia Y. Nanofiber Scaffolds with Gradations in Mineral Content for Mimicking the Tendon-to-Bone Insertion Site. Nano Lett. 2009 Jul 8;9(7):2763–8.

189. Lipner J, Liu W, Liu Y, Boyle J, Genin GM, Xia Y, et al. The mechanics of PLGA nanofiber scaffolds with biomimetic gradients in mineral for tendon-to-bone repair. Journal of the Mechanical Behavior of Biomedical Materials. 2014 Dec 1;40:59–68.

190. Lipner J, Boyle JJ, Xia Y, Birman V, Genin GM, Thomopoulos S. Toughening of fibrous scaffolds by mobile mineral deposits. Acta Biomater. 2017 Aug;58:492–501.

191. Kolluru PV, Lipner J, Liu W, Xia Y, Thomopoulos S, Genin GM, et al. Strong and tough mineralized PLGA nanofibers for tendon-to-bone scaffolds. Acta Biomaterialia. 2013 Dec 1;9(12):9442–50.

192. Xie J, Zhong S, Ma B, Shuler FD, Lim CT. Controlled biomineralization of electrospun poly(ε-caprolactone) fibers to enhance their mechanical properties. Acta Biomaterialia. 2013 Mar 1;9(3):5698–707.

193. Jaiswal AK, Kadam SS, Soni VP, Bellare JR. Improved functionalization of electrospun PLLA/gelatin scaffold by alternate soaking method for bone tissue engineering. Applied Surface Science. 2013 Mar 1;268:477–88.

194. Gautam S, Sharma C, Purohit SD, Singh H, Dinda AK, Potdar PD, et al. Gelatin-polycaprolactone-nanohydroxyapatite electrospun nanocomposite scaffold for bone tissue engineering. Materials Science and Engineering: C. 2021 Feb 1;119:111588.

195. Barati D, Walters JD, Pajoum Shariati SR, Moeinzadeh S, Jabbari E. Effect of Organic Acids on Calcium Phosphate Nucleation and Osteogenic Differentiation of Human Mesenchymal Stem Cells on Peptide Functionalized Nanofibers. Langmuir. 2015 May 12;31(18):5130–40.

196. Zhang C, Cao M, Lan J, Wei P, Cai Q, Yang X. Regulating proliferation and differentiation of osteoblasts on poly(l-lactide)/gelatin composite nanofibers via timed biomineralization. Journal of Biomedical Materials Research Part A. 2016;104(8):1968–80.

197. Zhang S, Jiang G, Prabhakaran MP, Qin X, Ramakrishna S. Evaluation of electrospun biomimetic substrate surface-decorated with nanohydroxyapatite precipitation for osteoblasts behavior. Materials Science and Engineering: C. 2017 Oct 1;79:687–96.

198. Chahal S, Hussain FSJ, Kumar A, Yusoff MM, Rasad MSBA. Electrospun hydroxyethyl cellulose nanofibers functionalized with calcium phosphate coating for bone tissue engineering. RSC Adv. 2015 Mar 23;5(37):29497–504.

199. Chahal S, Hussain FSJ, Yusoff MM, Abdull Rasad MSB, Kumar A. Nanohydroxyapatite-coated hydroxyethyl cellulose/poly (vinyl) alcohol electrospun scaffolds and their cellular response. International Journal of Polymeric Materials and Polymeric Biomaterials. 2017 Feb 11;66(3):115–22.

200. Abudhahir M, Saleem A, Paramita P, Kumar SD, Tze-Wen C, Selvamurugan N, et al. Polycaprolactone fibrous electrospun scaffolds reinforced with copper doped wollastonite for bone tissue engineering applications. J Biomed Mater Res Part B. 2021 May;109(5):654–64.

201. Vaquette C, Ivanovski S, Hamlet SM, Hutmacher DW. Effect of culture conditions and calcium phosphate coating on ectopic bone formation. Biomaterials. 2013 Jul 1;34(22):5538–51.

202. Chai YC, Roberts SJ, Desmet E, Kerckhofs G, Van Gastel N, Geris L, et al. Mechanisms of ectopic bone formation by human osteoprogenitor cells on CaP biomaterial carriers. Biomaterials. 2012 Apr;33(11):3127–42.

203. Zhang X, Liu W, Liu J, Hu Y, Dai H. Poly-ε-caprolactone/Whitlockite Electrospun Bionic Membrane with an Osteogenic–Angiogenic Coupling Effect for Periosteal Regeneration. ACS Biomater Sci Eng. 2021 Jul 12;7(7):3321–31.

Chapter 4: Gradient Mineralisation of Fascicle-Inspired Electrospun Bundles for Enthesis Regeneration

Amirdhavarshini Padmanabhan[a], Maria Letizia Focarete[a], Luca Cristofolini[b]

[a]Department of Chemistry, "G.Ciamician", University of Bologna, Italy
[b]Department of Industrial Engineering, University of Bologna, Italy

Keywords: Electrospun scaffolds; gradient mineralisation; enthesis; ligament and tendon regeneration

MANUSCRIPT IN PREPARATION

4.1. Abstract

Entheses, the sites of tendon and ligament attachment to bone, are crucial for musculoskeletal function as they transmit forces from muscle to bones or between bones, enabling joint movement and stability. They also play a vital role in energy storage and dissipation, essential for shock absorption during athletic activities. Injuries to the entheses are common and can lead to chronic pain and disability due to suboptimal repair. Regenerative therapies for entheseal injuries are limited, and there is a need for new strategies to promote healing and restore function. We have developed a novel approach to enthesis regeneration using gradient mineralised PLLA/collagen electrospun bundles with aligned nanofibres. These bundles mimic the hierarchical structure of native fascicles seen in ligaments and tendons. To mimic the mineral gradient found in native entheses the bundles were soaked in calcium and phosphate solutions alternatively and this method was fine-tuned to deposit minerals in a gradient. Images from Scanning electron microscopy showed a uniform coating of mineral deposits on the mineralised bundle with varying degrees of mineralisation. Energy dispersive spectroscopy showed the elemental composition of the mineral deposits ranged from 1.22-1.29, similar to hydroxyapatite's (1.67). Thermogravimetric analysis confirmed increased mineral content residue across the gradient regions (0.75-11.67%). DSC analysis showed that while some thermal properties, such as the glass transition temperature (64°C), appear unaltered, others, such as the enthalpy of melting (12.91-10.06 J/g) and crystallisation (11.9-9.39 J/g) and the degree of crystallinity (0.008-0.009%) have shown noticeable difference upon mineralisation. Uniaxial tensile testing showed that the bundles with gradient mineralisation on two extremities had Young's modulus of 445.1±55.3 MPa (average on the entire bundle) and the bundles with gradient mineralisation on one extremity had 403.2±33.44 MPa (average on the entire bundle), making them ideal candidates for optimal repair of tendon and ligament enthesis.

4.2. Introduction

The enthesis is a specialised, fibrocartilaginous zone where tendons/ligaments (T/L) attach to the bone. It plays a crucial role in the musculoskeletal system by acting as the connective interface between T/L and bone, facilitating force transmission between them while also providing stability to the joints. (1) The enthesis is not merely a junction of two different tissues, i.e., bone and tendon/ligament, but a functionally graded interface essential for distributing stress and shock absorption during repetitive movements. This functional gradation

allows for the effective dissipation of forces, reducing the risk of stress concentrations that could lead to injury. Clinically, injuries and degenerative conditions affecting the entheses are common, and they result in chronic pain, inflammation and significant loss of function. These injuries are usually caused by mechanical overloading, overuse, or systemic diseases. (2)

The enthesis's complex structure and unique biomechanical properties pose significant challenges in repair and regeneration following injury or degeneration. (3) Traditional treatments, often involving surgical interventions and physiotherapy, have limitations in restoring the native structure and functionality of the enthesis, leading to suboptimal recovery and a risk of re-injury. These limitations highlight the need for innovative approaches in tissue engineering and regenerative medicine to mimic the enthesis's unique architecture and biomechanical properties for full recovery. (4)

In tissue engineering, some recent approaches have provided promising results to guide new tissue growth while fully restoring its functions. (5) These recent advancements in scaffold design mimic the complex and unique structure of the native enthesis characterised by gradual changes in composition, structure, and mechanical and chemical properties. (6) Electrospinning has emerged as an essential technique in designing these innovative nanofibrous scaffolds that can be tailored to achieve functional gradation of mechanical properties and biological signals needed to regenerate the enthesis. It uses an electric field to produce nanofibers from a polymer solution collected on a grounded metal collector to form a nanofibrous mesh. The resulting scaffolds have high porosity and an interconnected fibrous structure similar to the natural extracellular matrix. (7)

Gradient mineralisation techniques significantly advance scaffold design, especially for fascicle-inspired bundles in enthesis regeneration. These techniques allow for the precise control of mineral deposition within a scaffold, creating spatially varied mineral profiles that closely mimic the natural gradation seen in tissues like the enthesis.(8) By controlling factors like mineral concentration, pH, and immersion time, it's possible to transition from mineral-rich to mineral-poor areas within the scaffold gradually. The rationale behind replicating this gradient *in vitro* is to mimic the enthesis's biomechanical microenvironment and provide cellular cues for new tissue development. (9)

Initially, some studies have incorporated the use of simulated body fluid at different formulations and concentrations to create a gradient in mineralisation that also resulted in a variation in the morphology of the mineral deposits. (10) Following that, some studies also developed a mineral gradient by continuously feeding the mineralisation solution into a container with the scaffold inside. (11,12),(13) Samavedi et al. have fabricated a graded mesh

containing nano-hydroxyapatite/PCL and poly(ester urethane) urea elastomer to mimic the ligament-bone interface to capture its intricate mechanical and chemical gradients. Tensile tests of these graded meshes showed a gradient of tensile modulus along its length, and the gradient was found to be more pronounced upon treatment with 5x SBF for 2h. (14,15) Jiang et al. investigated an electrospun scaffold with a gradient distribution of BMP-2/hydroxyapatite nanoparticles, and fibre orientation changing from random to aligned was investigated for its potential to induce interfacial tissue regeneration. Biomimetic mineralisation of this scaffold using 5x SBF to create a second mineral gradient on the surface. The resulting mineral deposits were analysed to be phosphate deposits gradually distributed along the nanofiber surface and calcium deposits localised to the region with a high content of hydroxyapatite nanoparticles, specifically in the region with random fibre orientation. (16) Kim et al., in their study, incorporated different ratios of hydroxyapatite (20, 40 and 60 wt%) into gelatin nanofibers to develop a bone interface scaffold with a compositional gradient from lower to higher ratios of hydroxyapatite/gelatin. The authors used hydroxyapatite formulation, which was achieved by combining aqueous solutions of calcium nitrate and ammonium hydrogen phosphate, separately dissolved with gelatin powder and mixed dropwise while keeping a constant pH of 10 at 40 °C). The resulting electrospun scaffolds contained increasing amounts of apatite formation with an increase in the ratio of hydroxyapatite/gelatin in the nanofibers. This nanocomposite was layered from a lower to a higher ratio of hydroxyapatite to form a compositional gradient, and the authors believed that this strategy would eliminate the limitations experienced in depositing apatite crystals post-electrospinning. (17) Another strategy to induce gradient mineralisation is surface modification of electrospun scaffold with gelatin grafts. By varying the grafting concentration at different places on the scaffold, it is possible to control the nucleation and growth of HA on the fibres. Cui et al. and Zou et al. in their studies have employed gelatin grafting on PDLLA nanofibers to induce the formation of nonstoichiometric nanostructured HA.(18,19) Paik et al fabricated electrospun PCL/tricalcium composite (TCP) matrix scaffolds with a high content of TCO at the bottom and nearly zero content at the top of the matrix. However, the authors reported that in this method, the mechanical properties were reduced due to presence of composite in the fibres.(20)

Our research aimed to develop a gradient mineralised fascicle-inspired electrospun bundle to enhance enthesis regeneration with a simple and effective mineralisation process that can be adapted to any scaffold design to create a mineral gradient.

4.3. Materials and methods

4.3.1. Materials

Poly (L-lactic acid) (PLLA) (Lacea H.100-E, M_w= 8.4 x 10^4 g/mol^{-1}, PDI=1.7) was purchased from Mitsui Fine Chemicals (Dusseldorf, Germany). Collagen (COLL) (Type I) was kindly provided by Kensey Nash Corporation d/b/a DSM Biomedical (Exton, USA). Trifluoroethanol (TFE), 1,1,1,3,3,3-Hexafluoro-2-propanol (HFIP), N-(3-dimethylaminopropyl)-N′-ethylcarbodiimide hydrochloride (EDC), N-hydroxysuccinimide (NHS), sodium hydroxide (NaOH), calcium chloride ($CaCl_2$) and disodium hydrogen phosphate (Na_2HPO_4) were purchased from Sigma Aldrich.

4.3.2. Electrospinning

Electrospinning of poly (lactic acid) (PLLA) and collagen (COLL) to produce hierarchical bundles was carried out using a method previously outlined by Sensini et al.(21). The process involved the blending of PLLA and COLL into a polymer solution at 75:25 (w/w) ratio. This blend was dissolved in a solvent mixture comprising equal volumes of TFE and HFIP, achieving a concentration of 20% (w/v). This solution was loaded into four glass syringes, which were evenly aligned on a syringe pump to ensure consistent distribution. Each syringe was connected to a blunt-ended stainless-steel needle (0.51 mm inner diameter) via PTFE tubing. These needles were positioned on a sliding stand, maintaining a distance of 20 cm from a rapidly rotating cylindrical drum collector.

The electrospinning process involved pumping the solution at a rate of 0.5 mL per hour under a voltage of 22 kV for 2 hours at room temperature, with the relative humidity between 20% and 30%. Fibres produced during this process were collected on the drum, rotating at 2500 rpm (equating to a peripheral speed of 19.6 meters per second), resulting in a mat of uniaxially oriented nanofibers. The mat was cut along the drum's circumference into smaller strips to form the bundles. These strips were manually rolled into bundles, with diameters ranging from 550-650μm) length 220mm. Care was taken to remove these bundles from the drum collector without additional cutting, preserving their ring-like shapes.

4.3.3. Crosslinking

The PLLA/COLL bundles were crosslinked using a 95% ethanol solution containing EDC and NHS for 24 hrs at room temperature. Subsequently, the bundles were rinsed using phosphate-buffered saline (PBS) for 30 mins. This step was followed by an extensive rinse with distilled water for two hours to eliminate any unbound crosslinkers from the bundles. They were dried in a vacuum desiccator to achieve dry, crosslinked bundles.

4.3.4. Functionalisation with NaOH

The PLLA/COLL scaffold was first methodically segmented (Fig 4.1A). Initially, it was split into two halves. Following this division, each half was further subdivided into four distinct sections. These sections were organised to represent the various parts of the enthesis, starting with non-mineralised areas in the centre, progressing to the fibrocartilage, then to the calcified fibrocartilage, and ultimately culminating in the bone-like section at the extremities. The sectioned bundles were immersed in 0.1 M NaOH for 20 sec at room temperature (Fig 4.1B). The bundles were washed in distilled water and dried in a vacuum desiccator.

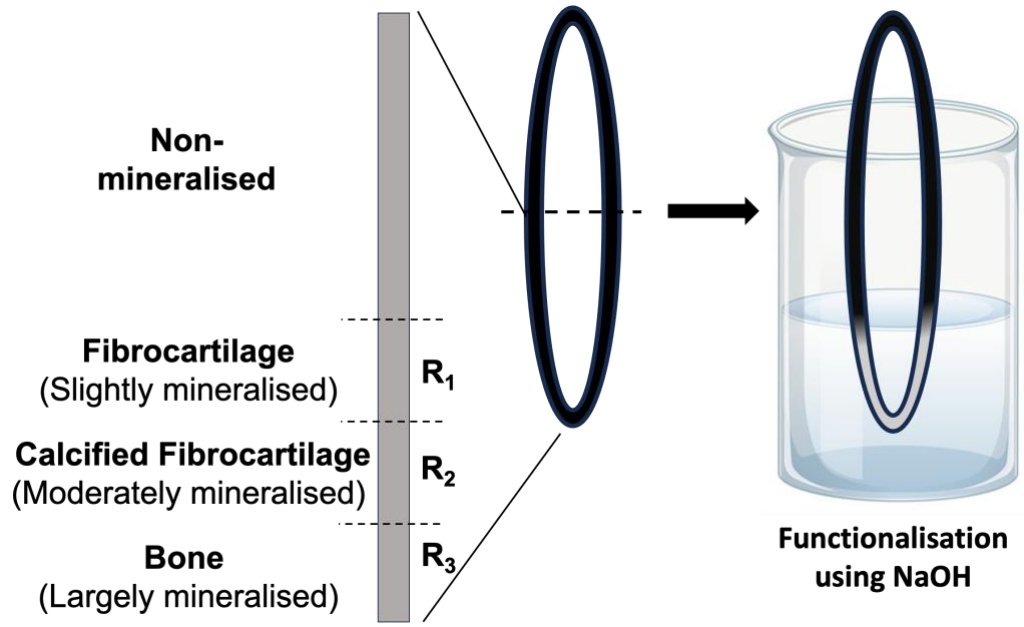

Figure 4.1. (A) Segmentation of the bundle scaffold to represent various parts of the enthesis; (B) Functionalisation of the segmented bundles using NaOH.

4.3.5. Mineral deposition using alternate soaking method

NaOH-treated PLLA/COLL bundles were mineralised using an alternate soaking technique (22) to create a gradient of mineral deposition across consecutive parts of the scaffold (Fig 4.2). This process entailed the following steps:

a. Cycle 1

- The bundles were first immersed in 0.5 M $CaCl_2$ solution and then in 0.3 M Na_2HPO_4 solution.
- Each immersion lasted for 30 mins.
- After each immersion, the bundles were washed in distilled water for 10 seconds.
- All the three regions (R_1, R_2, R_3) were immersed.

b. Cycle 2

- The bundles were again immersed sequentially in the $CaCl_2$ and Na_2HPO_4 solutions in this cycle.
- Each immersion in this cycle was shortened to 15 minutes.
- After each immersion, the bundles were washed in distilled water for 10 seconds.
- Only the R_2 and R_3 regions were immersed.

c. Cycle 3

- For the final cycle, the immersion time in each solution was further reduced to 7 minutes.
- After each immersion, the bundles were washed in distilled water for 10 seconds.
- This cycle focused exclusively on the R_3 region.

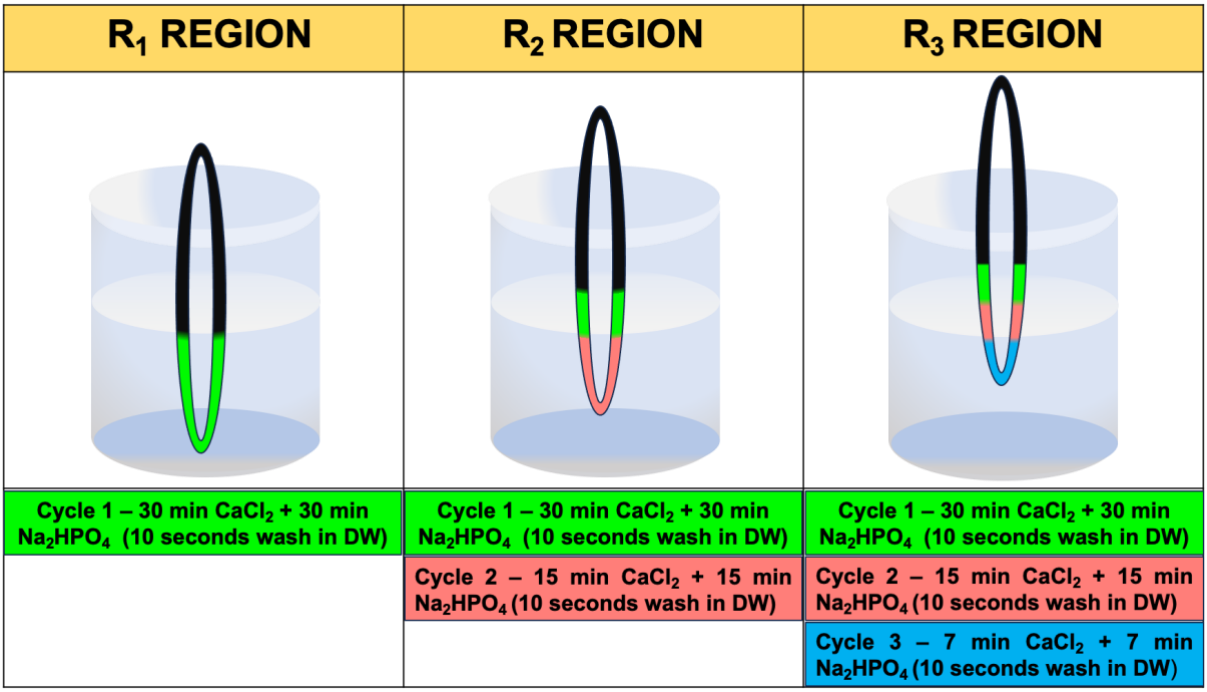

Figure 4.2. Gradient mineralisation using an alternate soaking method

4.4. Characterisation of mineralised bundles

4.4.1. Surface Morphology

The surface morphology of the PLLA/COLL bundles before and after mineralisation was investigated using the scanning electron microscope (SEM) model Phenom Pro-X, produced by PhenomWorld (Eindhoven, The Netherlands). A specimen of the respective bundles was cut, fixed on a stub, and placed under a sputter coater (Qurom, Laughton, UK) for metallisation with a gold-platinum alloy. The samples were visualised at 8000x and 15000x. The mineralised samples were also analysed using Energy Dispersive Spectroscopy (EDS) at different regions to identify the elemental composition of the mineral deposits.

4.4.2. Physicochemical analysis

Thermogravimetric analyses (TGA) and Differential Scanning Calorimetry (DSC) were performed on the non-mineralised bundle (NM) and bundles after gradient mineralisation at various regions (R_1, R_2 and R_3). TGA was performed with a TGA2950 analyser from TA Instruments by heating at 10°C/min in a nitrogen atmosphere until 900°C. DSC was performed with a TA Instruments Q100 DSC. The heating and cooling steps were carried out at a rate of

20°C/min and 10°C/min, respectively, in a nitrogen atmosphere from -60°C to 190°C. Glass transition temperature (T_g), crystallisation temperature (T_c) and melting temperature (T_m) were determined from the third cycle of heating. Crystallinity degree (χ_c) was calculated for the samples using equation 1:

$$\chi_c(\%) = \frac{\Delta H_m - \Delta H_c}{\Delta H_f \times W_{PLLA}} \times 100 \qquad \text{Equation (1)}$$

where,

- ΔH_m is the enthalpy of melting
- ΔH_c is the enthalpy of crystallisation
- ΔH_f is the heat of fusion of 100% crystallised poly (L-lactic) acid, which is 93.7 J/g (23)
- W_P is the weight fraction of poly (L-lactic) acid in the scaffold

4.4.3. Mechanical Properties

To evaluate their mechanical properties, uniaxial tensile tests were carried out on PLLA/COLL bundles before and after mineralisation. The testing utilised three types of mineralised bundles – Fully mineralised bundles (FM, consistent mineralisation throughout), gradually mineralised on both extremities (GM2, mimicking a ligament's enthesis), and gradually mineralised on one extremity (GM1, mimicking the tendon's enthesis) (Fig 4.3C). The non-mineralised samples were named NM. The bundles for the tensile test were folded into a double-ring configuration (Fig 4.3A-B). Therefore, the samples were mineralised after folding the bundles into the double ring configuration to differentiate the mineralised portions distinctly and facilitate easy handling. The bundles (n=5 specimens per treatment group) were immersed in saline solution for 2 mins before performing the tensile test. A material testing machine, Model 4465 Instron (Norwood, MA, USA), equipped with a ± 100 N load cell from Instron (Norwood, MA, USA), was used. Custom-made capstan grips to reduce stress concentrations at the sample ends as previously optimised (Sensini et al., 2019). The testing consisted of a monotonic ramp in displacement control, adjusting the actuator speed for each specimen to reach a strain rate of 10% s^{-1}. The procedure was consistent with the ASTM D1414 standard for determining the physical properties of O-rings. From the load-displacement curves, the following data were computed: yield stress (σ_Y), yield strain (ε_Y), Young's modulus (E), failure stress (σ_F), failure strain (ε_F), unit work to yield (L_Y), unit work to failure (L_F). The obtained results were then statistically evaluated using one-way ANOVA followed by Tukey's multiple comparisons in GraphPad Prism software.

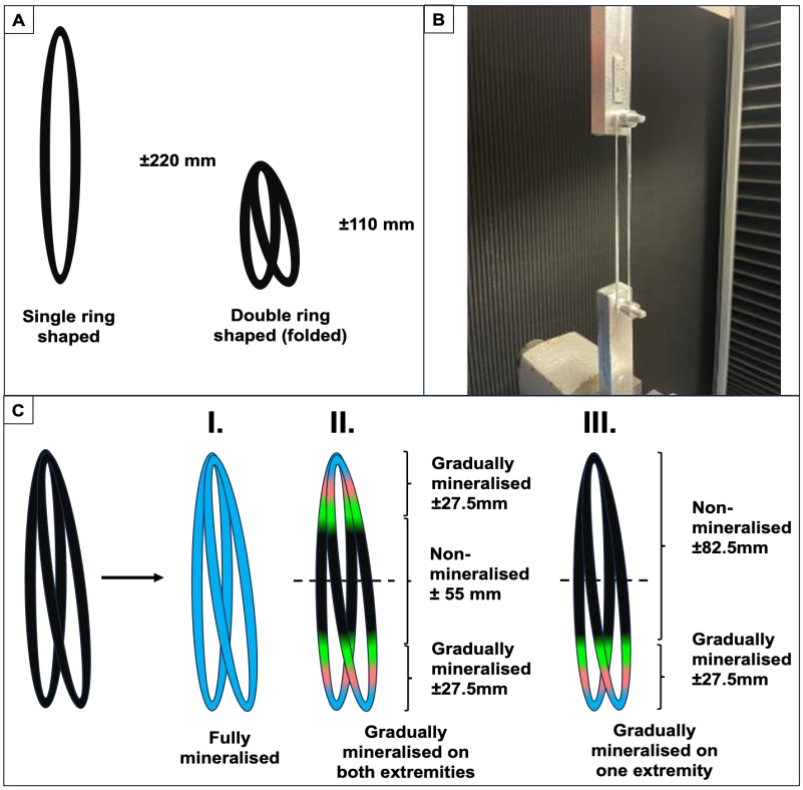

Figure 4.3. (A) Folding of the electrospun bundles into double ring configuration; (B) Loading of the bundles onto customised capstan grips; (C) Types of mineralised bundles used in tensile strength testing.

4.5. Results

4.5.1. Surface morphology

SEM images of the PLLA/COLL bundles before and after mineralisation were captured at 8000x and 15000x magnifications to visualise the mineral deposits at the different scaffold regions (R_1, R_2 and R_3). In the R_1 region designed to mimic the fibrocartilage part of an enthesis, a homogenous deposition of minerals was seen across the nanofibre length and the mineral crystals look isolated from each other (Fig 4.4B (I)). In the R_2 sample, an increase in mineral deposit was observed covering all of the nanofibre surface, and a few clusters were visible, but the scaffold's porosity appeared to be unaltered (Fig 4.4B (II)). In the R_3 sample, there was a further increase in mineral deposition, and the deposits appeared interconnected and densely packed (Fig 4.4B (III)).

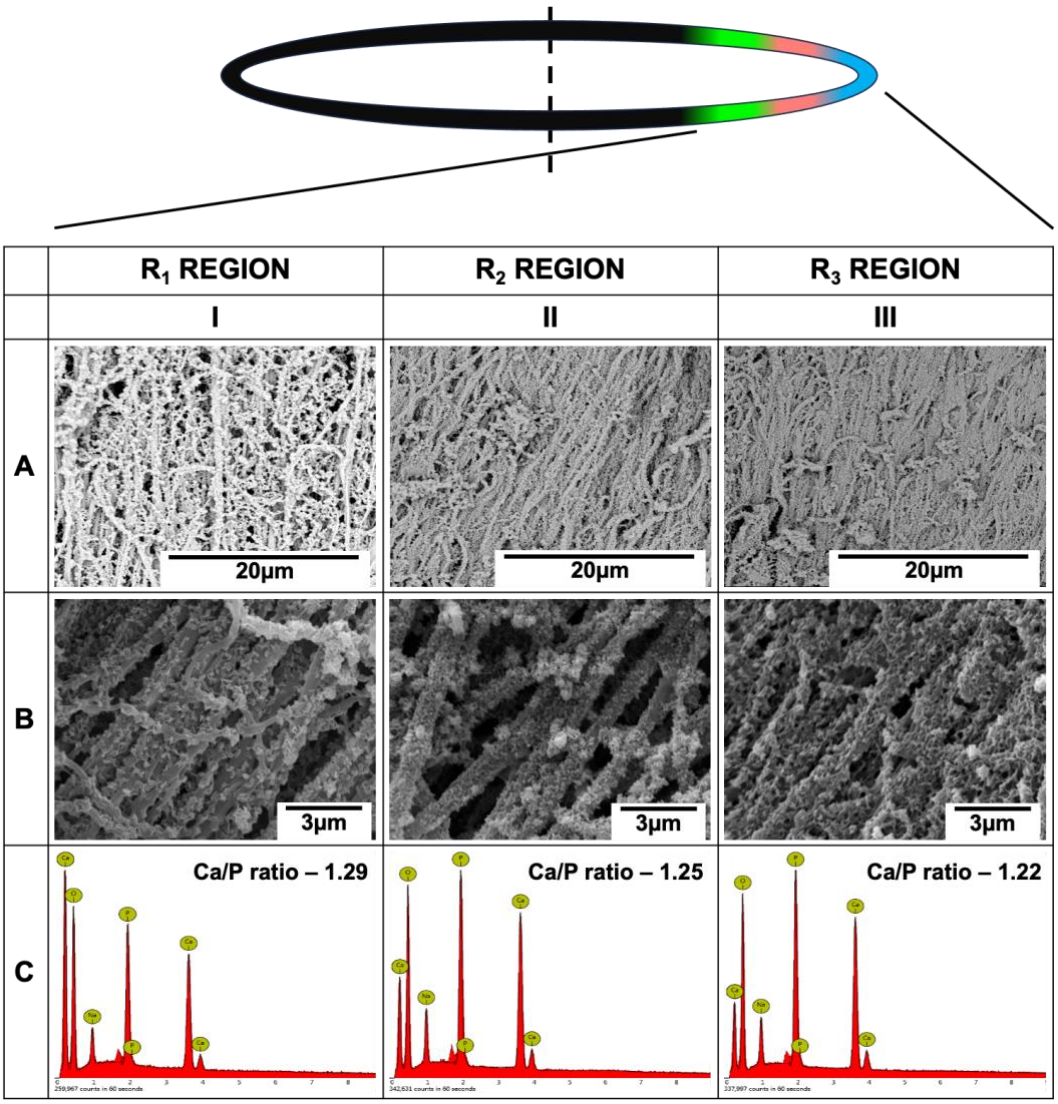

Figure 4.4. Morphological characterisation results of (I) R_1; (II) R_2; and (III) R_3 regions of the mineralised bundles - (A) & (B) SEM images (C) EDS graphs.

Energy dispersive spectroscopy (EDS) was used to analyse the elemental composition of the mineral deposits in the various regions of the mineralised bundle scaffold. The analysis showed that the deposits were primarily calcium phosphate (CaP), which is the primary component of hydroxyapatite (Fig 4.4C (I-III)). Across the regions R_1, R_2, and R_3, the calcium-to-phosphate ratios were in the range 1.22 – 1.29, indicative of a hydroxyapatite precursor (1.67). The results also suggest that the mineralisation process is efficient and uniform, as the Ca/P ratio remains relatively constant throughout the samples, suggesting that the mineralisation process is well-controlled and reproducible.

4.5.2. Physico-chemical analyses

The TGA graph (Fig 4.5) shows the thermal stability and composition of different regions of the gradually mineralised bundle samples by measuring the weight loss as a function of temperature as compared to the non-mineralised bundles. Table 4.1 shows the TGA data of non-mineralised and mineralised bundles, along with previously published values of PLLA and collagen (25). The non-mineralised sample had the lowest residue of 0.7523%. The consecutive regions of the gradually mineralised samples (R_1, R_2 and R_3) showed a steady increase in the residue of 5.619%, 6.802% and 11.67%, respectively. The degradation temperatures of R_1 (309°C), R_2 (313°C) and R_3 (311°C) were lower as compared to the non-mineralised sample (320°C). The Dm%, which measures sample weight loss when heated from room temperature to 150°C), were the lowest for non-mineralised regions (1.9%). It shows an increase for R_1 (3.4%) and R_3 (4.8%) regions while dropping for R_2 (2.8%).

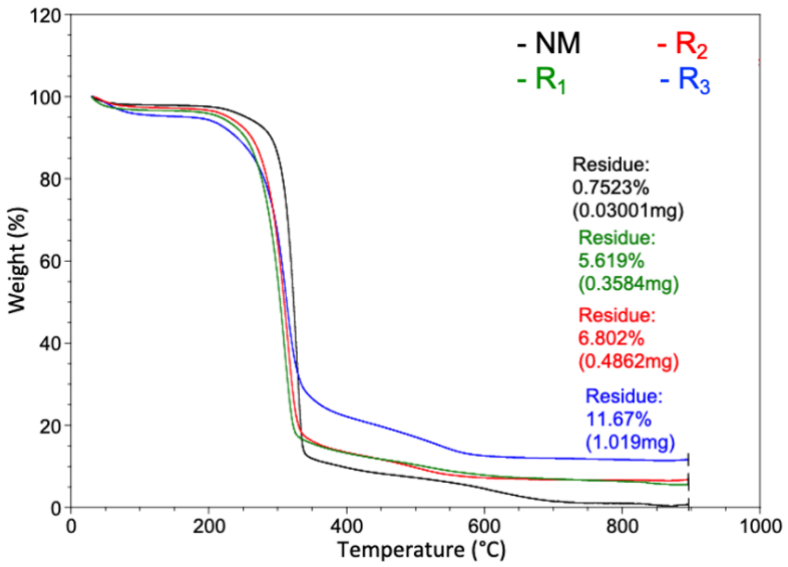

Figure 4.5. Thermogravimetric analysis of non-mineralised bundle (NM) and the mineralised bundle's R_1, R_2 and R_3 regions.

Table 4.1. TGA data

Sample	**D_m% (RT-150°C)**	**Degradation temperature (°C)**	**Residual weight % (at 900°C)**
Poly (L-lactic) acid	0	330	4.2
Collagen	7.3	319	27
NM	1.9	320	0.75
R_1	3.4	309	5.69
R_2	2.8	313	6.8
R_3	4.8	311	11.67

DSC graph (Fig 4.6) displays the endothermic and exothermic events as changes in heat flow. The transitions related to glass transition temperature (T_g), melting temperature (T_m), and crystallisation temperature (T_c) are observed for PLLA/COLL scaffold samples with varying degrees of mineralisation as compared to the non-mineralised scaffolds (Table 4.2). The T_g values are consistent across all samples. There's an increase in T_c values for R_1 and R_2 regions, followed by a decrease in R_3 compared to the non-mineralised CL samples. The T_m value decreases slightly in R_1 and R_3, with R_2 being almost the same as CL. The change in specific heat capacity (ΔC_p) values for the mineralised and non-mineralised samples were all in a same range. The enthalpy of crystallisation (ΔH_c) shows a steady decrease with an increase in mineral content in R_1 (11.37 J/g), R_2 (10.93 J/g) and R_3 (9.39 J/g) regions as compared to the non-mineralised sample (11.5 J/g). The enthalpy of melting (ΔH_m) also follows the same trend of steady decrease for mineralised samples R_1 (11.99 J/g), R_2 (11.54 J/g) and a big difference for R_2 (10.06 J/g). The degree of crystallinity was calculated using Equation 1, and they were in the range 0.008-0.009 % for all the mineralised samples and reduced compared to the non-mineralised (0.02).

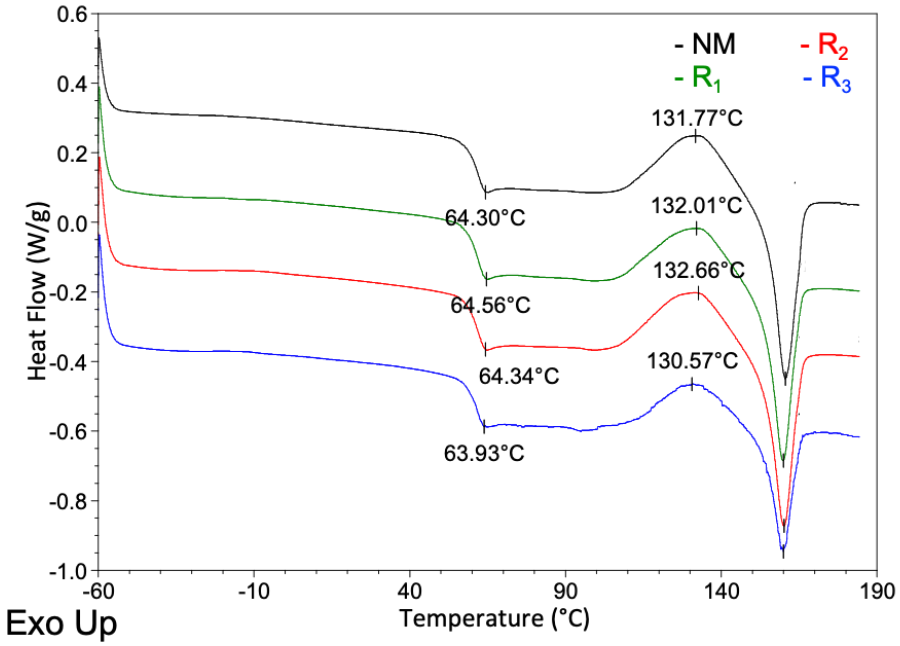

Figure 4.6. Differential scanning calorimetry curves of the non-mineralised bundle and the mineralised bundle's R_1, R_2 and R_3 regions.

Table 4.2. DSC data

Sample	**T_g (°C)**	**ΔC_p (J/g°C)**	**ΔH_c (J/g)**	**T_c (°C)**	**ΔH_m (J/g)**	**T_m (°C)**	**χ_c (%)**
Poly (L-lactic) acid	60	0.51	31	126	32	162	0.014
NM	64	0.47	11.5	131	12.91	160	0.02
R_1	64	0.50	11.37	132	11.99	159	0.008
R_2	64	0.48	10.93	132	11.54	160	0.008
R_3	64	0.49	9.39	130	10.06	159	0.009

4.5.3. Mechanical properties

All the stress-strain curves exhibited a non-linear ductile behaviour with an initial toe region. The toe region suggests an initial realignment of fibres under stress, as seen in T/L fascicles. (26,27) The highest yield stress was shown by GM2 bundles (9.9±0.7 MPa). GM1(9.5±1.0 MPa) and FM (9.8±1.9 MPa) bundles showed values lower than GM2, and the lowest values were seen in NM (7.1±0.4 MPa) bundles. All the values were found to be statistically significant. The failure stress values of the NM (10.7±0.3 MPa) and GM2(11.3±1.5 MPa) were in the same range, whereas the highest values were shown by FM (13.3±2.4 MPa) and GM1(13.2±1.5 MPa) bundles. Notably, there was no statistical significance for these values. The yield strain values of FM (3.7±0.6%) and GM1(3.7±0.4%) bundles were in the same range, while the values of GM2 (4.7±0.6%) and NM (5.0±0.3%) bundles had higher values with NM bundles showing the highest yield strain. The highest failure strain was seen in NM (26.6±7.0%) bundles and the lowest in GM2 (6.6±2.9%) while the values for FM (10.5±2.3%) and GM1 (10.4±4.4%) only showed a small difference. All the values were found to be statistically significant. The highest Young's modulus values were seen in GM2 (445.1±55.3 MPa) bundles and followed closely by FM (440.2±73.75 MPa) bundles. The NM (163.7±10.6 MPa) bundles showed the lowest Young's modulus value, while the GM1 bundles showed 403.2±33.44 MPa. Statistically significant differences were found between the values of NM and all the other categories. However, GM1, GM2 and FM did not differ significantly from each other (Table S1). The unit work to yield of FM (0.014±0.002 J/mm^3), GM1 (0.014±0.003 J/mm^3), and GM2 (0.014±0.002 J/mm^3) were all in the same range while the highest value was seen in NM (0.018±0.002 J/mm^3) bundles. The highest value for unit work to failure was seen

in NM (0.228±0.07 J/mm^3) bundles and the lowest value in GM2(0.037±0.04 J/mm^3) while the values for FM (0.095±0.03 J/mm^3) and GM1 (0.097±0.06 J/mm^3) were in the same range.

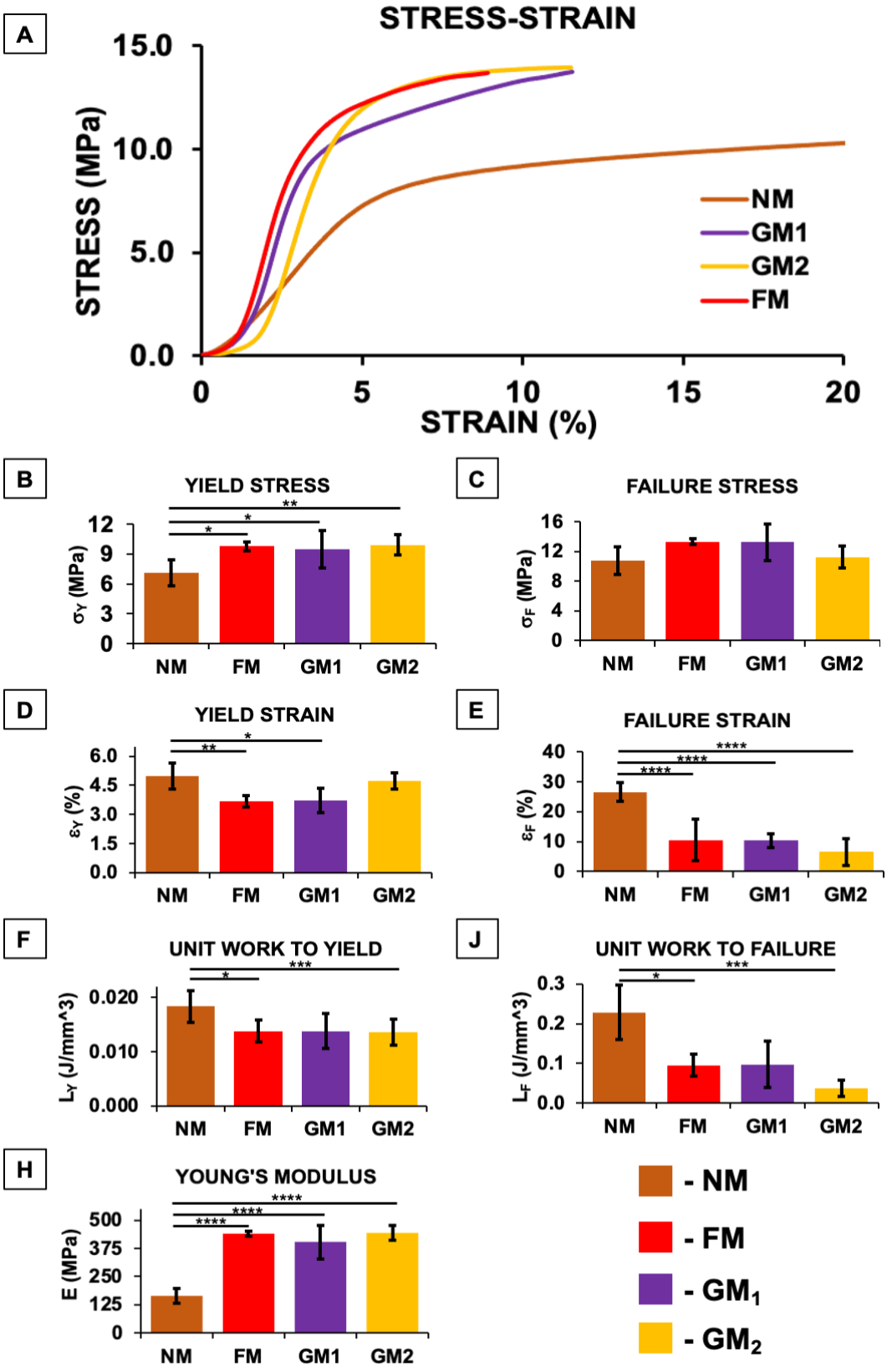

Figure 4.7. (A) Typical stress-strain curve derived for mineralised and non-mineralised bundles. Mechanical properties as calculated from the stress-strain data – (B) Yield stress; (C) Failure stress; (D) Yield strain; (E) Failure strain; (F) Unit work to yield; (J) Unit work to failure and (H) Young's modulus. The mean and standard deviation are plotted, and statistical significance is evaluated using one-way ANOVA followed by Tukey's multiple comparisons, plotted as *p≤0.05, **p≤0.01, ***p≤0.001, ****p≤0.0001.

4.6. Discussion

This study aimed to develop and characterise a gradient mineralised PLLA/COLL electrospun bundle to mimic the hierarchical structure and functional mineral gradation of the complex native enthesis, which can enhance the regeneration of the tendon and ligament. PLLA and COLL were blended at the ratio of 75:25 (w/w) in TFE and HFIP, resulting in a polymer solution of 20% (w/v) that was electrospun to fabricate a hierarchical fascicle-inspired bundle scaffold with aligned nanofibres. The diameter of the bundles was from 550-650μm, and the length was 220 mm. The bundles were then crosslinked using EDC/NHS to reduce collagen degradation. To functionalise the PLLA/COLL scaffolds, they were immersed in 0.1M NaOH for 20 seconds at room temperature. This served as to modify the scaffold surface by introducing functional groups through hydrolysis. (28) To create a gradient mineral deposit, the functionalised bundles were demarcated with three regions (R_1, R_2, and R_3) and then alternatively soaked in 0.5M $CaCl_2$ and 0.3M Na_2HPO_4 with decreasing immersion times and selective treatment of consecutive scaffold regions. These regions were also segmented to differentiate the fibrocartilage, calcified fibrocartilage and the bone regions of the native enthesis. When the scaffold was first immersed in 0.5M $CaCl_2$, the calcium ions adhered to the negatively charged sites on the scaffold introduced from the NaOH treatment. Following this, when immersed in 0.3M Na_2HPO_4, the interaction between calcium and phosphate ions induced the nucleation of calcium phosphate crystals. The first cycle could be considered as a nucleation cycle to create nucleation points for the consecutive cycles to form apatite growth. The mineralised bundles were characterised to evaluate their surface morphology, elemental composition, thermal properties and mechanical properties.

SEM images of the mineralised regions of the bundle were acquired in 8000x and 15000x. The images of the R_1 region showed homogenous mineral deposition along the nanofibre length with isolated mineral crystals with small grain sizes. Due to the distance between the mineral grains, the underlying nanofibers were still visible. This resembles the fibrocartilage matrix of

the enthesis, where mineralisation tends to be less dense. In the R_2 region, a homogenous growth of mineral coating with small clusters was observed. The nanofibres looked completely covered with mineral deposits, and the space between the nanofibers was reduced. The SEM images of the R_3 region showed an increased amount of mineral deposition with bigger clusters. The nanofibres appeared slightly fused due to the thick mineral coating, which gave the appearance of interconnected mineral networks between the nanofibres.

EDS analysis was used to identify the elemental composition of the mineral deposits in the different regions, and it revealed that they were primarily composed of calcium phosphate (CaP), the significant component of hydroxyapatite, a mineral found in natural bone. Across the regions R_1, R_2, and R_3, the Ca/P ratios ranged from 1.22-1.29. These values indicate the presence of hydroxyapatite precursors since the Ca/P ratio of hydroxyapatite is 1.67. This similarity suggests that the scaffold could provide appropriate cues to support bone cell attachment, proliferation and differentiation owing to the osteoconductive properties of hydroxyapatite. (10)

The TGA graph (Fig 4.5.) shows the thermal stability and composition of different regions of the gradually mineralised bundle samples by measuring the weight loss as a function of temperature as compared to the non-mineralised bundles. The residue percentages at the end of the analysis (at 900°C) indicate the non-volatile or non-combustible material remaining, which is the mineral content of the scaffolds. The increase in the amount of residue for mineralised samples suggests an increasing amount of inorganic or mineral content that does not volatilise at high temperatures. In this case, the non-mineralised sample, representing the control, showed the lowest residue of 0.7523%. The consecutive regions of the gradually mineralised samples (R_1, R_2 and R_3) showed a steady increase in the residue of 5.619%, 6.802% and 11.67%, respectively. These results suggest a successful gradation in mineral deposition, with the highest mineral content in the R3 region. The degradation temperatures of R_1 (309°C), R_2 (313°C), and R3 (311°C) were lower as compared to the non-mineralised sample, indicating a reduction in thermal stability due to mineralisation but does not show any specific trend of reduction in degradation temperature with increase in mineral content. This could suggest that while the mineralisation process does affect the degradation temperature, the effect is not linearly correlated with the amount of mineral content. A similar trend is also seen for the initial loss of mass (Dm%) that occurred within 150°C for the non-mineralised sample (1.9%), which then increased for the R_1 region (3.4%) and R3 (4.8%) but reduced for R_2 (2.8%). A similar

trend of results was reported by Gaharwar et al. in their study using nanoclay-enriched PCL electrospun scaffolds. (29)

From the DSC curves, it can be seen that the glass transition temperature before and after mineralisation of the PLLA/COLL scaffolds is constant, indicating that the degree of mineralisation did not alter the mobility of the polymer chains in the amorphous regions of the scaffold. On the other hand, the crystallisation temperatures increased from 131°C for non-mineralised and further to 132°C for R_1 and R_2 regions) before dropping to 130°C for R3 region. The initial increase in T_c could be due to the nucleating effect of the minerals, providing sites for PLLA to crystalise more easily. The decrease in T_c for R3 might indicate that minerals no longer act only as nucleating agents but may start to obstruct the crystallisation process, possibly due to the higher mineral content. The similar T_m observed for non-mineralised and mineralised samples could imply that the mineralisation process did not cause notable variation in the thermal stability of the crystalline regions of the scaffold. The enthalpies of crystallisation and melting also decreased with an increase in mineral content, indicating that the mineralisation process or the mineral deposits have restricted the polymer chains from crystallising. This aligns with the degree of crystallinity calculated for the mineralised samples (0.008-0.009%), which is lower than that of the non-mineralised sample (0.02%), indicating that the scaffold's overall crystallinity is reduced after mineralisation. A similar trend of results was reported by Gaharwar et al. in their study using nanoclay-enriched PCL electrospun scaffolds. (29)

All the stress-strain curves exhibited a non-linear ductile behaviour with an initial toe region in the tensile test. The toe region suggests an initial realignment of fibres under stress, as seen in T/L fascicles. The model of the tensile test was to analyse the mechanical properties of the bundles (n=5) that were gradually mineralised to mimic the enthesis of the tendon and ligament. The GM1 bundles were gradually mineralised on one extremity to mimic the enthesis of a tendon. In contrast, the GM2 bundles were gradually mineralised on both extremities to mimic the enthesis of a ligament. In this case, the non-mineralised (NM) and fully mineralised (FM) bundles can be considered as controls to measure the minimum and maximum limits of stiffness displayed by the PLLA/COLL bundles after NaOH treatment. The GM2 bundles showed higher yield stress (9.9±0.7 MPa) and Young's modulus values (445.1±55.3 MPa) with lower failure strain (6.6±2.9%), unit work to failure (0.037±0.04 J/mm3) and failure stress (11.3±1.5 MPa) values as compared to GM1. These results show that the GM2 bundles have increased stiffness and are more resistant to deformation, making them good candidates for the reconstruction of

the enthesis of a ligament. The GM1 bundles displayed yield stress (9.5±1.0 MPa), yield strain (3.7±0.4%)and Young's modulus (403.2±33.44 MPa) lesser than that of GM2 but showed a higher failure stress (13.2±1.5 MPa) and failure strain (10.4±4.4%) than GM2. These results suggest that the GM2 bundles are more resistant to tensile forces and can experience deformation without failure while balancing stiffness and elasticity, making them good candidates for the reconstruction of the enthesis of a tendon.

The fully mineralised bundles, even though hypothesised to display the maximum stiffness, showed lower Young's modulus than the GM2 bundles even though it was more brittle due to the closely packed network of minerals. The higher value for the GM2 bundles can be explained by the masking of the effect of the different degrees of mineralisation by the non-mineralised part, which was much more deformable and much less stiff than the mineralised regions. Statistically significant differences were only seen between the NM and the mineralised bundles, but no significant differences were seen amongst GM1, GM2 and FM bundles.

The investigation of the mechanical properties of the mineralised scaffolds has highlighted the role of mineral deposition in modulating the mechanical behaviour when put under stress. The yield and failure stress results of FM and NM scaffolds from the tensile test show that mineralisation enhances the mechanical strength of the scaffold. Similarly, the gradient-mineralised GM1 and GM2 samples also showed increased yield stresses compared to the NM samples, suggesting that even partial mineralisation contributes to the overall structural integrity of the bundles.

4.7. Conclusion

In conclusion, this study successfully developed and characterised gradient mineralised PLLA/COLL electrospun bundles to mimic the hierarchical structure and functional mineral gradation of the native enthesis for optimal tendon and ligament regeneration. The NaOH treatment of the PLLA/COLL bundles, followed by the alternate soaking in $CaCl_2$ and Na_2HPO_4, successfully created a gradient in mineral deposition across the scaffold regions (R_1, R_2 and R_3), as evidenced by SEM, EDS, and TGA analyses. The SEM images revealed a progressive increase in mineral deposition from R_1 to R_3, aligning with the mineral gradation observed from fibrocartilage to calcified regions in natural enthesis. The consistent glass transition temperature across all regions of the mineralised bundle indicated that the mineralisation did not adversely affect the mobility of polymer chains in the amorphous regions of the scaffold. However, the decrease in crystallisation temperatures and enthalpies with

increased mineral content suggested that the mineralisation process obstructed the polymer crystallisation, leading to a low degree of crystallinity in the mineralised samples. Tensile testing revealed that gradient mineralisation significantly enhanced the mechanical properties, with GM2 samples displaying higher stiffness and resistance to deformation, ideal for ligament enthesis reconstruction. In contrast, GM1 samples displayed a balance between stiffness and elasticity, more suited for tendon enthesis. These analyses highlight the importance of controlled mineral deposition in designing scaffolds for enthesis regeneration, offering a promising approach for advanced tissue engineering and regenerative therapies.

4.8. References

1. Kannus P. Structure of the tendon connective tissue. Scandinavian Journal of Medicine & Science in Sports. 2000;10(6):312–20.

2. Moffat KL, Wang INE, Rodeo SA, Lu HH. Orthopedic Interface Tissue Engineering for the Biological Fixation of Soft Tissue Grafts. Clinics in Sports Medicine. 2009 Jan 1;28(1):157–76.

3. Genin GM, Kent A, Birman V, Wopenka B, Pasteris JD, Marquez PJ, et al. Functional Grading of Mineral and Collagen in the Attachment of Tendon to Bone. Biophys J. 2009 Aug 19;97(4):976–85.

4. Calejo I, Costa-Almeida R, Reis RL, Gomes ME. Enthesis Tissue Engineering: Biological Requirements Meet at the Interface. Tissue Engineering Part B: Reviews. 2019 Aug;25(4):330–56.

5. Sensini A, Massafra G, Gotti C, Zucchelli A, Cristofolini L. Tissue Engineering for the Insertions of Tendons and Ligaments: An Overview of Electrospun Biomaterials and Structures. Front Bioeng Biotechnol. 2021 Mar 2;9:645544.

6. Patel S, Caldwell JM, Doty SB, Levine WN, Rodeo S, Soslowsky LJ, et al. Integrating soft and hard tissues via interface tissue engineering. Journal of Orthopaedic Research. 2018;36(4):1069–77.

7. Luo W, Wang Y, Han Q, Wang Z, Jiao J, Gong X, et al. Advanced strategies for constructing interfacial tissues of bone and tendon/ligament. J Tissue Eng. 2022 Jan 1;13:20417314221144714.

8. Zhu C, Qiu J, Thomopoulos S, Xia Y. Augmenting Tendon-to-Bone Repair with Functionally Graded Scaffolds. Advanced Healthcare Materials. 2021;10(9):2002269.

9. Smith L, Xia Y, Galatz LM, Genin GM, Thomopoulos S. Tissue-Engineering Strategies for the Tendon/Ligament-to-Bone Insertion. Connective Tissue Research. 2012 Apr 1;53(2):95–105.

10.Lipner J, Liu W, Liu Y, Boyle J, Genin GM, Xia Y, et al. The mechanics of PLGA nanofiber scaffolds with biomimetic gradients in mineral for tendon-to-bone repair. Journal of the Mechanical Behavior of Biomedical Materials. 2014 Dec 1;40:59–68.

11.Li X, Xie J, Lipner J, Yuan X, Thomopoulos S, Xia Y. Nanofiber Scaffolds with Gradations in Mineral Content for Mimicking the Tendon-to-Bone Insertion Site. Nano Lett. 2009 Jul 8;9(7):2763–8.

12.Liu W, Lipner J, Xie J, Manning CN, Thomopoulos S, Xia Y. Nanofiber Scaffolds with Gradients in Mineral Content for Spatial Control of Osteogenesis. ACS Appl Mater Interfaces. 2014 Feb 26;6(4):2842–9.

13.Kolluru PV, Lipner J, Liu W, Xia Y, Thomopoulos S, Genin GM, et al. Strong and tough mineralized PLGA nanofibers for tendon-to-bone scaffolds. Acta Biomaterialia. 2013 Dec 1;9(12):9442–50.

14.Samavedi S, Olsen Horton C, Guelcher SA, Goldstein AS, Whittington AR. Fabrication of a model continuously graded co-electrospun mesh for regeneration of the ligament–bone interface. Acta Biomaterialia. 2011 Dec 1;7(12):4131–8.

15.Samavedi S, Guelcher SA, Goldstein AS, Whittington AR. Response of bone marrow stromal cells to graded co-electrospun scaffolds and its implications for engineering the ligament-bone interface. Biomaterials. 2012 Nov 1;33(31):7727–35.

16.Jiang N, He J, Zhang W, Li D, Lv Y. Directed differentiation of BMSCs on structural/compositional gradient nanofibrous scaffolds for ligament-bone osteointegration. Materials Science and Engineering: C. 2020 May 1;110:110711.

17.Kim HW, Song JH, Kim HE. Nanofiber Generation of Gelatin–Hydroxyapatite Biomimetics for Guided Tissue Regeneration. Advanced Functional Materials. 2005;15(12):1988–94.

18.Cui W, Li X, Chen J, Zhou S, Weng J. In Situ Growth Kinetics of Hydroxyapatite on Electrospun Poly(dl-lactide) Fibers with Gelatin Grafted. Crystal Growth & Design. 2008 Dec 3;8(12):4576–82.

19.Zou B, Liu Y, Luo X, Chen F, Guo X, Li X. Electrospun fibrous scaffolds with continuous gradations in mineral contents and biological cues for manipulating cellular behaviors. Acta Biomaterialia. 2012 Apr 1;8(4):1576–85.

20.Paik DH, Jeong KY, Moon SK, Oh MJ, Ryu TK, Kim SE, et al. A facile method for preparation of polycaprolactone/tricalcium phosphate fibrous matrix with a gradient mineral content. Colloids and Surfaces A: Physicochemical and Engineering Aspects. 2013 Jul 20;429:134–41.

21.Sensini A, Gualandi C, Zucchelli A, Boyle LA, Kao AP, Reilly GC, et al. Tendon Fascicle-Inspired Nanofibrous Scaffold of Polylactic acid/Collagen with Enhanced 3D-Structure and Biomechanical Properties. Sci Rep. 2018 Nov 21;8(1):17167.

22.Taguchi T, Muraoka Y, Matsuyama H, Kishida A, Akashi M. Apatite coating on hydrophilic polymer-grafted poly(ethylene) films using an alternate soaking process. Biomaterials. 2000 Jan 1;22(1):53–8.

23.Fischer EW, Sterzel HJ, Wegner G. Investigation of the structure of solution grown crystals of lactide copolymers by means of chemical reactions. In: Fischer EW, Müller FH, Kausch HH, editors. Aktuelle Probleme der Polymer-Physik IV. Heidelberg: Steinkopff; 1973. p. 980–90. (Aktuelle Probleme der Polymer-Physik).

24.Sensini A, Gotti C, Belcari J, Zucchelli A, Focarete ML, Gualandi C, et al. Morphologically bioinspired hierarchical nylon 6,6 electrospun assembly recreating the structure and performance of tendons and ligaments. Medical Engineering & Physics. 2019 Sep 1;71:79–90.

25.Sensini A, Gualandi C, Cristofolini L, Tozzi G, Dicarlo M, Teti G, et al. Biofabrication of bundles of poly(lactic acid)-collagen blends mimicking the fascicles of the human Achille tendon. Biofabrication. 2017 Mar 8;9(1):015025.

26.Pioletti DP, Rakotomanana LR, Leyvraz PF. Strain rate effect on the mechanical behavior of the anterior cruciate ligament-bone complex. Med Eng Phys. 1999 Mar;21(2):95–100.

27.Black J, Hastings G. Handbook of Biomaterial Properties. Springer Science & Business Media; 2013. 607 p.

28.Chen J, Chu B, Hsiao BS. Mineralization of hydroxyapatite in electrospun nanofibrous poly(L-lactic acid) scaffolds. Journal of Biomedical Materials Research Part A. 2006;79A(2):307–17.

29.Gaharwar AK, Mukundan S, Karaca E, Dolatshahi-Pirouz A, Patel A, Rangarajan K, et al. Nanoclay-Enriched Poly(ε-caprolactone) Electrospun Scaffolds for Osteogenic Differentiation of Human Mesenchymal Stem Cells. Tissue Eng Part A. 2014 Aug 1;20(15–16):2088–101.

SUPPORTING INFORMATION

Table S1. Statistical significance of mechanical properties evaluated using one-way ANOVA followed by Tukey's multiple comparisons, which are plotted as *p≤0.05, **p≤0.01, ***p≤0.001, ****p≤0.0001

	Yield stress (MPa)	Failure stress (MPa)	Young's modulus (MPa)	Yield strain (%)	Failure strain (%)	Unit work to yield (J/mm^3)	Unit work to failure (J/mm^3)
NM vs FM	* p=0.0143	ns p=0.1469	**** p<0.0001	** p=0.0084	**** p<0.0001	ns p=0.9994	* p=0.0266
NM vs GM1	* p=0.0336	ns p=0.1684	**** p<0.0001	* p=0.0128	**** p<0.0001	ns p=0.9994	ns p=0.3830
NM vs GM2	** p=0.0095	ns p=0.9883	**** p<0.0001	ns p0.9523	**** p<0.0001	ns p=0.9993	*** p=0.0004
FM vs GM1	ns p=0.9943	ns p>0.9999	ns p=0.7191	ns p=0.9997	ns p>0.9999	ns p>0.9999	ns p=0.5978
FM vs GM2	ns p=0.9997	ns p=0.3231	ns p=0.9998	* p=0.0389	ns p=0.6003	ns p>0.9999	ns p=0.3638
GM1 vs GM2	ns p=0.9763	ns p=0.3608	ns p=0.6210	ns p=0.0575	ns p=0.6115	ns p>0.9999	* p=0.0245

Chapter 5 : Overall Conclusions

The motive of this PhD was to contribute to the field of ligament and tendon tissue engineering by developing an optimised hierarchical electrospun scaffold and addressing two primary objectives: sterilisation processes and gradient mineralisation for mimicking the enthesis interface. To achieve this, fascicle-inspired biomimetic electrospun bundles with uniaxially aligned nanofibres were fabricated from PLLA and collagen. To prevent the accelerated loss of collagen from the scaffolds, they were crosslinked using EDC/NHS.

The global tendon repair market is experiencing steady growth, with estimates suggesting a market size of USD 2.1 billion in 2021 and projections reaching USD 4.7 billion by 2032, reflecting a Compound Annual Growth Rate (CAGR) of around 7.5-8%. This upward trend is driven by several factors, including a rising geriatric population with increased susceptibility to tendon and ligament injuries, increased participation in sports activities leading to higher injury rates, and advancements in minimally invasive surgical procedures for tendon and ligament repair. The market has a demand for biocompatible materials and techniques that promote faster healing and better functional outcomes. Understanding these trends can inform the development of electrospun scaffolds with properties that cater to the evolving needs of the tendon repair market and address the growing demand for effective solutions in the orthopaedic field.

In the first part of this research, the effect of gamma irradiation on these PLLA/Collagen electrospun bundles was investigated. The bundles' morphological, physicochemical and mechanical properties were analysed before and after gamma-ray sterilisation at three doses – 5, 10 and 25 kGy. Despite 25 kGy being the gold standard for implantable devices, we found that this dose had detrimental effects on PLLA/Collagen bundles. Therefore, analysing the impact of gamma irradiation at three different doses aided us in identifying doses at which the scaffold properties were not affected significantly. Among the three irradiation doses, 5 kGy dose had the most negligible effect on the scaffold's properties.

In the next part, a literature review was conducted to understand the advances in the mineralisation of electrospun scaffolds. This review explored various mineralisation techniques, each showing distinct advantages based on scaffold synthesis. Adding minerals to the scaffolds gives important biochemical cues to cells and makes the scaffolds mechanically stronger. By combining insights from mineralisation methodologies, scaffold modifications, and characterisation techniques, this review pinpoints the potential of mineralised electrospun scaffolds to inspire the next phase of tissue engineering.

With the help of the information gathered from this review, a gradient mineralisation technique was developed to deposit minerals on the PLLA/Collagen scaffold, mimicking the natural

enthesis. These bundles were sequentially soaked in $CaCl_2$ and Na_2HPO_4 alternatively to create a gradient in mineral content across the regions of the scaffold. The morphological analyses showed successful deposition of minerals with a Ca/P ratio of 1.22-1.29, which is similar to hydroxyapatite (1.67), and physicochemical analyses showed an increase in mineral content from consecutive regions of the scaffold without adversely affecting the properties of the scaffold. The minerals on the bundles were deposited to mimic the enthesis of the tendon and ligament, i.e., gradient mineralisation on one extremity and two extremities, respectively. These mineralised scaffolds showed enhanced mechanical properties with balanced stiffness and elasticity, proving them ideal for enthesis reconstruction. Further work will have to be done to understand the effect of gradient mineralisation in manipulating biochemical cues and in vitro and in vivo studies are crucial to evaluate cell adhesion, proliferation, and differentiation within the scaffolds, mimicking the tendon and ligament regeneration process. The global tendon repair market is experiencing steady growth, with estimates suggesting a market size of USD 2.1 billion in 2021 and projections reaching USD 4.7 billion by 2032, reflecting a Compound Annual Growth Rate (CAGR) of around 7.5-8%. This upward trend is driven by several factors, including a rising geriatric population with increased susceptibility to tendon injuries, growing participation in sports activities leading to higher injury rates, and advancements in minimally invasive surgical procedures for tendon repair. The market is also witnessing a surge in demand for biocompatible materials and techniques that promote faster healing and better functional outcomes. Understanding these trends can inform the development of electrospun scaffolds with properties that cater to the evolving needs of the tendon repair market and address the growing demand for effective solutions in the orthopaedic field.